N°Ordre : 42336

IBCP of NAS of Ukraine

Sergei Mikhaylov

SYNTHESIS AND INVESTIGATION OF NANOSTRUCTURED CONDUCTING POLYMERS BASED NANOCOMPOSITES FOR AMMONIA AND AMINES DETECTION

THESIS

presented in order to obtain the PhD degree

In the Specialty
Optic, Lasers Physico-chemistry, Atmosphere
defended on 17 March 2017

Jury:

Pr. Sergii RIABOV: Institute of macromolecular chemistry, the NAS of Ukraine, **Reviewer**

Pr. Alexander PUD: Institute of Bioorganic Chemistry and Petrochemistry, National Academy of Sciences of Ukraine, 02160, Kyiv, Ukraine, **Examiner**

Pr. Patrice CODDEVILLE: Institut Mines-Télécom Lille Douai, Département Sciences de l'Atmosphère et Génie de l'Environnement, SAGE, Douai, France, **Examiner**

Dr. Stéphanie REYNAUD (HDR): Université de Pau et des Pays de l'Adour, IPREM – Equipe de Physique et Chimie des Polymères – UMR 5254, France, **Reviewer**

Invited Members:

Pr. Jean-Luc WOJKIEWICZ; Institut Mines-Télécom Lille Douai, Département Sciences de l'Atmosphère et Génie de l'Environnement, SAGE, Douai, France, **Examiner**

Dr. Nathalie REDON: Institut Mines-Télécom Lille Douai, Département Sciences de l'Atmosphère et Génie de l'Environnement, SAGE, Douai, France, **Examiner**

Institut Mines Télécom Lille Douai, Département Sciences de l'atmosphère et Génie de l'Environnement,
SAGE, F-59500 Douai, France
Institute of Bioorganic Chemistry and Petrochemistry, National Academy of Sciences of Ukraine,
02160, Kyiv, Ukraine

TABLE OF CONTENTS

LIST OF ABBREVIATIONS AND SYMBOLS

ADPA	Aminodiphenilamine
An	Aniline
APS	Ammonium persulfate
B	Benzenoid unit
BSA	Benzene sulfonic acid
CB	Chlorobenzene
CMC	Critical micelle concentration
CMOS	Complementary metal–oxide–semiconductor technology
CSA	Camphor sulfonic acid
DBSA	Dodecylbenzene sulphonic acid
DCAA	Dichloroacetic acid
DTA	Differential thermal analysis
EB	Emeraldine base
FTIR	Fourier transform infrared spectroscopy
HOMO	Highest occupied molecular orbital
ICP	Intrinsically conducting polymers
LSA	Lauryl sulfate
LUMO	Lowest unoccupied molecular orbital
MA	Methylamine
M_n	Mass-average molecular number
M_w	Mass-average molecular weight
M_w/M_n	Polydispersity
MWCNT	Multi-walled carbon nanotubes
NDSA	1.5-Naphtalenedisulfonic acid
NHE	Normal hydrogen electrode
NMP	N-methylpyrrolidone
NMR	Nuclear magnetic resonance
NSA	2-Naphtalenesulfonic acid
OCP	Open circuit potential
OD	Oxidation degree
PANI	Polyaniline
PBQI	*N*-phenyl-1,4-benzoquinonediimine

PC	Polycarbonate
PN	Pernigraniline
PPy	Polypyrrole
PTh	Polythiophene
PVDF	Polyvinylidene fluoride
Q	Quinoid unit
RH	Relative humidity
SAXS	Small-angle x-ray scattering
SDS	Sodium lauryl sulfate
SEM	Scanning electron microscopy
SHE	Standard hydrogen electrode
SR	Sensors response
TEM	Transmission electron microscopy
TG	Thermogravimetry
TMA	Trimethylamine
TSA	Toluene sulfonic acid
UV-Vis	Ultraviolet-visible
WAXS	Small-angle x-ray scattering
XRD	X-ray diffraction

INTRODUCTION

One of the main research areas of modern chemistry is the search and creation of new polymer materials with improved properties. In this regard, polyconjugated systems such as intrinsically conducting polymers (ICPs) attract the increasing attention due to a whole range of specific properties inherent to this class of polymers. In particular, these materials have high redox and catalytic activities, the ability to change the electrical conductivity in a wide range, electrochromic properties and photoactivity. All of this allows efficient use of conducting polymers in chemical current sources, non-volatile electronic memory, polymer LEDs, as well as for electromagnetic and corrosion protection. The new promising direction is the use of ICPs in the field of electronic gas sensor technologies. However, the great progress reached in groups of Stejskal (Czech Republic) [1, 2], Ćirić- Marjanović (Serbia) [3, 4], Sapurina (Russia) [5, 6] is primarily concerned with fundamental researches of the mechanism and influence of polymerization conditions on properties of a synthesized polymer, while a number of applied problems still remain unresolved.

Specifically, characteristics of pure polymer are often not able to fully satisfy the requirements put forward to them. That is why a direction of polymer functional characteristics improvement through the creation of nanocomposites where filler nanoparticles would interact with the polymer matrix at a molecular level is of great interest.

Context

The rapid development of industry inevitably leads to air pollution. Emissions of pollutants are often represented by a whole range of substances. The prominent place among them is taken by highly toxic ammonia and amines, which adversely affect human health. The solution of the problem of their concentrations control is creation of chemical sensors based on conducting polymers, such as polyaniline (PANI), which quickly responds to the presence of such substances by a change of its electrical resistance and other properties. This polymer possess numerous advantages compared to other polyconjugated ICPs, such as ease of changing the doping state and electrical conductivity, chemical and thermal stability, synthesis simplicity and low cost of monomer.

However, pure PANI has such drawbacks as poor mechanical and film-forming properties, insolubility in the majority of organic solvents, infusibility. An effective way to improve PANI properties is the creation of its composite materials with metal oxides nanoparticles. Such new materials have high specific surface area and very often demonstrate a synergetic effect, owing to emergence of specific physicochemical interactions at the polymer-nanoparticle interface.

At the same time, specificities of such nanocomposites formation and interconnection of starting synthesis parameters with resulting performances are still insufficiently studied and characterized, which hampers such materials wide use in different applications. In particular, there is no information concerning influence of dopants structure, metal oxides nanoparticles size and nature on kinetic parameters of nanocomposites formation, molecular characteristics of PANI phase, morphology, stability, electrical conductivity, sensing and other properties of hybrid materials. In this regard, obtaining and analysis of such information are of great importance from the viewpoint of the controlled formation of hybrid nanocomposite materials with predetermined properties.

Connection with academic programs, plans, themes

The work was performed in frames of the joint Ukrainian-French project of cotutelle thesis, based on existing agreement on international cooperation between the University of Lille 1 (France), the Atmospheric Sciences and Environmental Engineering department of Mines Douai (France) and Bioorganic and petrochemistry institute of National Academy of Sciences of Ukraine (BPCI of NAS of Ukraine, Ukraine) and in accordance with state research programs: “Synthesis and investigation of conducting polymers based hybrid nanocomposites with controlled structure and properties” (2010 – 2014, №0112U005144); “Formation, properties and interaction of conducting polymers’ nanocomposites and bioactive compounds in the heterophase systems” (2013 – 2017, №0113U003093); “Sensor devices for medicoenvironmental and industrial-technological needs: metrological support and trial operation" (2013 – 2017, №0115U002691).

The aim of the work was the determination of synthesis specifics of nanostructured composite materials based on conducting polymers and metal oxide nanoparticles, sensitive to ammonia and amines.

To achieve this goal the following **tasks** needed to be solved:

- To study features of the PANI phase formation at the surface of metal oxides nanoparticles by analyzing changes in RedOx potential and pH of the polymerization medium.
- To determine the impact of sulfonic acids-dopants and metal oxide nanoparticles TiO_2 (anatase, rutile) and SnO_2 on kinetics of aniline polymerization process and conduct a comparative analysis the morphology and properties of obtained materials.
- To study the influence of used dopants and inorganic phase (oxide nanoparticles) on conducting polymer phase molecular characteristics and state in synthesized nanocomposites.
- To show the connection of synthesized nanocomposites properties with their quantitative and qualitative composition, morphology and structure.
- To determine optimal polymer and nanoparticles ratio and conditions for the formation of nanocomposites with the best sensing characteristics for ammonia and amines detection.
- To determine the impact of dopant structure, content and nature of conducting polymers and nanoparticles on sensing and other properties of hybrid materials.
- To study the efficiency of chemically synthesized nanocomposites in comparison with mechanically mixed analogs.
- To characterize synthesized materials stability to ultraviolet (UV) irradiation.

The object of research is the process of formation of hybrid nanostructured composites based on conducting polymers and metal oxide nanoparticles.

The subject of research is the nanocomposite materials based on polyaniline and polypyrrole and metal oxide nanoparticles for ammonia and amines detection.

Research techniques used in the work include: potentiometry and pH monitoring on the synthesis stages, infra-red (IR) and ultraviolet-visible (UV-Vis) spectroscopy for the polymer phase content, oxidation degree and polymerization yield determination, scanning (SEM) and transmission (TEM) electron microscopies for materials structure and morphology investigations, thermogravimetry (TG) and differential thermal analysis (DTA) for thermal stability examinations, liquid chromatography with spectrophotometric registration for polyaniline molecular characteristics determination, electrical conductivity measurements and sensing properties investigation.

Scientific novelty of results:

- A new approach to the study of aniline polymerization kinetics using simultaneous monitoring of RedOx potential and pH of the reaction medium was developed.
- For the first time a linear correlation between the metal oxides nanoparticles content in the reaction medium and reciprocal values of the duration of individual stages of aniline polymerization was shown.
- The influence of sulfonic acids-dopants and hydrogen laurylsulfate, content and nature of metal oxides nanoparticles (TiO_2 rutile and anatase, SnO_2) on the kinetics of aniline chemical polymerization was shown for the first time. The aniline polymerization reaction rate constants values were estimated.
- For the first time the impact of dopant and oxide nanoparticles on the molecular weight, molecular weight distribution and oxidation degree of polyaniline in synthesized core-shell morphology nanocomposites was shown.
- For the first time the higher efficiency in sensing measurements of chemically synthesized nanocomposites compared to mechanically mixed analogs and pure polymers was shown.

- For the first time it was found that UV irradiation leads to photodegradation and changes in performance characteristics of synthesized materials.

The practical significance of results

Proposed approaches to the controlled formation of nanostructured composites based on ICPs and metal oxides with “core-shell” structure can serve as the basis of the production technology of materials with predetermined properties. Developed new hybrid electroconductive materials can be used as active layers in the production of chemoresistive sensors for ammonia and amines. Determined peculiarities of photochemical degradation of PANI nanocomposites with metal oxides should be considered when predicting the stability not only of sensing, but also photocatalytic properties.

Publications

The main scientific results of the thesis were presented in 12 papers, including 5 articles in peer-reviewed journals, 7 conference proceedings.

The thesis structure

The thesis consists of an introduction, 5 chapters, conclusions, list of references. In the *introduction* the actuality of chosen thesis topic is shown. The study goals and objectives the scientific novelty and results practical significance are formulated. The *first chapter* is devoted to a literature overview by the thesis topic and analysis of current trends in the approaches applied to the synthesis of PANI and its composites, as well as to hybrid materials application in chemoresistive sensors for ammonia and amines detection. The *second chapter* provides the information concerning synthesis techniques of pure polymer and hybrid organic-inorganic ICPs based materials with metal oxides nanoparticles. The main research methods of materials structure and morphology, thermal and photostability, conductivity, molecular characteristics, gas sensitivity to ammonia and amines are presented. In the *third chapter* the description and analysis of changes occurring during the aniline polymerization in the presence of metal oxides nanoparticles (TiO_2 and SnO_2) and different sulfonic acid-dopants and hydrogen laurylsulfate are given. The *fourth* *chapter* demonstrates the significant dependence of PANI phase molecular weight and molecular weight distribution, synthesized materials structure and morphology, electrical properties, thermal and photostability on the nature and content of dispersed nanoparticles of metal oxides in hybrid materials and used acid-dopant type. In the *fifth chapter*, sensing properties of synthesized materials depending on the nature of used dopant and oxide nanoparticles, polymer content and morphology on their sensitivity to ammonia and amines are considered.

1 STATE OF THE ART

1.1 Environmental considerations and health protection

The term “atmospheric pollution” relates to the components of the atmosphere appearing in abnormal concentrations due to natural and/or anthropogenic activity and adversely affecting living organisms or the environment [7]. The pollutants come into being due to direct human activity are classified as *primary*. After releasing into the air they begin to interact with each other and the environment in complex ways depending on temperature, humidity and other environmental conditions, forming the *secondary* pollutants [8]. For example, the sunlight absorption leads to radicals formation such as $^*OH$, $^*NO_3$, O_3, intermediate peroxy radicals (RO_2), R=H etc. [9].

The main air pollution sources in cities and rural areas are associated with transport (CO_X, suspended PM); industry and power plants, refineries (SO_X, NO_X, VOC); natural processes (volcanic eruptions, sea spray and wind-blown soil, dust storms) and agriculture which is the main source (> 93.7%) of NH_3 and amines [10, 11].

A significant portion of NH_3 emissions comes from livestock and poultry due to conversion of animals’ urea and excrements by enzyme and urease, which is excreted in products of vital activity. The other big portion refers to the use of commercial nitrogenous fertilizers and natural organic manures. In both cases, the nitrogen is converted to either ammonium (NH_4^+) under acidic/neutral pH or ammonia (NH_3) at higher pH levels [12].

Volatilized ammonia can travel on hundreds of kilometers from the site of origin. Thus, the US National Research Council (NRC, 2003) identified ammonia emissions as a major air quality concern not only at national, but also at global levels [13]. The NH_3 atmospheric deposition leads to eutrophication of surface waters and to increased algal growth and bloom that can deplete oxygen, affecting plants, fish and other life forms. Therefore, the changes in coastal ecosystem structure and functioning, resulting in decline of aquatic species, including those with commercial value are possible [12, 14].

In addition to its effects on water, plant, and soil systems, ammonia reacts with other compounds to form particulate matter, mainly PM2.5 or less (figure 1.1). The small size of the particles allows them to penetrate deep into the lungs causing to significant respiratory and cardiovascular problems [12, 15].

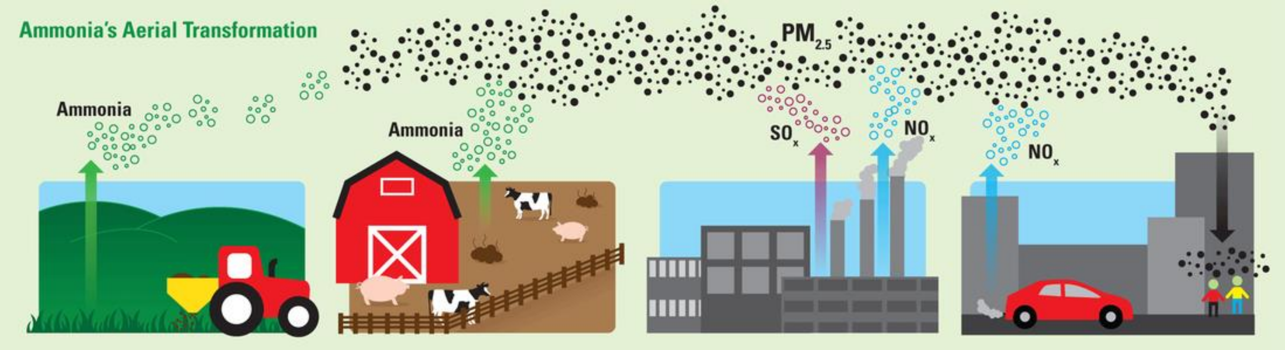

Figure 1.1 – Dangerous reaction. Ammonia (green) reacts with sulfur (red) and nitrogen (blue) oxides to produce tiny, dangerous particles [15].

The results of measurements obtained at 50 stations in Asia, Africa, South America and Europe evidence that global ammonia concentration varies from less than 1 to 20 ppb [16, 17]. At the same time, the local atmospheric concentrations, especially in agricultural areas, can be orders of magnitude higher. According to the data provided by authors [18], the concentration of 47 ppm was registered in pigpens. Moreover, right after the application of fertilizers the soils background ammonia concentrations can temporarily raise up to 3000 ppm [19]. In such agricultural settings rural residents can be continuously exposed to a wide range of concentrations from 280 ppb to 88 ppm [20]. These values are significantly higher than generally accepted standards in different countries (table 1.1) [21, 22].

Table 1.1 Ammonia concentration regulations at workplaces in different countries*

	Ukraine	EU	France	Germany	USA
TWA	25 ppm	20 ppm	10 ppm	20 ppm	25 ppm
STEL	–	50 ppm	20 ppm	–	35 ppm

*TWA – time weighted average; STEL – short time exposition limit.

The recent studies revealed also a link between breath gas composition and pathologies of a human body [23]. For example, ammonia, which is one of the products of nitrogen metabolism process, can be linked with liver dysfunctions [24]. If ammonia is not metabolized correctly, its blood level increase, often leading to hepatic encephalopathy, cognitive impairment, coma and, in extreme cases, even death [25]. Taking into account the intensive gaseous exchange between the blood and alveoli air in the lungs the authors [26, 27] demonstrated the possibility in principal to trace ammonia in exhaled air. Particularly, the typical concentrations range is 50 ppb – 3 ppm, depending on patients health status, metabolic activity, pharmaceutical use, diet and other factors [28]. Thus, the developing measurement techniques must be sensitive enough to ammonia while be free from interference from other breath constituents [23]. The latter is of great importance, since the exhaled human breath consists of more than 1000 different volatile compounds [29, 30], in particular, such amines as di- and trimethylamine that were found to be biomarkers for renal failure, including uremia [31, 32].

Besides, amines that are ammonia alkyl- or aryl-substituted derivatives even more hazardous class of chemicals [33]. They can cause skin and eyes irritation, dermatitis [34-36]. Many aromatic amines have carcinogenic [37, 38], mutagenic and/or hemotoxicant effects [39, 40]. In this regard, their wide industrial use in pesticides, rubber, medicaments, dyes and pigments production results in an increased risk of occupational exposure [41]. Due to the difference in physical properties they can be present in air as vapors and/or aerosols [42]. Therefore, the workers can be exposed during the manufacturing, transportation stages or during the application of amines-based agricultural chemicals [43, 44].

The World Health Organization (WHO) research revealed that air pollution kills more than 7 million people every year [45]. In this regard, it is very important not only to control the emissions of pollutants but also monitor their concentrations at workplaces. However, solving these tasks is impossible without development of new approaches to pollutants measurement. Thus, creation of compact devices that can quickly measure and timely alert about exceeding the threshold is of great interest.

1.2 Methods of ammonia/amines concentrations determination

The high toxicity of ammonia and amines at high concentrations for human health, coupled with their low permissible level concentrations and often requirement for in situ automated analysis, led to the development of many analytical techniques based on different physical and chemical principles. Some of most important techniques are described shortly below.

1.2.1 Chromatographic method

The chromatographic techniques coupled with different detectors became one of the most common analytical methods nowadays. The chromatography operating principle is based on fractional distillation of complex mixtures. The investigated sample is solvated in a fluid/gas (mobile phase) which contacts with stationary liquid/solid phase [9]. The difference in affinities of mixture components to the stationary phase makes the components to elute one by one at different time [46] simplifying the quantitative determination. The majority of used detectors ionize the sample followed by separation either by mass, charge or ion shape. The most popular solutions are flame ionization detector [47, 48], electron capture detector [49], mass spectrometer [8, 50], ionization mass spectrometer [51] or combinations of these methods [52].

The chromatography technique has quite long history and is a proven by time, which made it de facto the normalized method, often used for verification of results obtained by other methods. Its main advantages are the high precision and sensitivity. Thus, Ruzsanyi et al. [53] reported about possibility of ammonia determination even at low-ppt range. At the same time, chromatography based techniques have numerous disadvantages, such as expensive, bulky and quite sophisticated equipment; the need for pre-collection with potential of contamination or loss of sample; the sufficient separation of complex amines often needs pre-derivatization [54]. Also, the increase of manual operations number causes the loss of low-molecular-weight fraction and decrease in measurement accuracy [47, 50].

1.2.2 Colorimetric sensor arrays

The one more method for quick and selective recognition of a wide range of substances is colorimetric sensor arrays. This approach utilizes colorimetric arrays obtained by simple printing with chemoresponsive dyes (e.g. metalloporphyrin dyes) [55] on various inert solid supports (silica gel, acid-free paper, nylon, PVDF etc.) [56-58] and allows visual identification of a wide range of ligating (alcohols, amines, ethers, phosphines, phosphites, thioethers and thiols) and even weakly ligating (arenes, halocarbons and ketones) vapors [55]. The working principle of the colorimetric sensor array is based on dyes ability to change color, in either reflected or absorbed light, upon intermolecular interactions between ammonia/amines and dye, including Brönsted and Lewis acid–base, hydrogen bonding, dipolar, and π–π interactions [59, 60]. The generated characteristic olfactory-like pattern is unique to a given odorant and can be quantified by digital imaging. The system is limited by the amount of known “odor fingerprints” rather than by number of receptors. Hence, the different receptors are need not be highly specific for one analyte [61]. Thus, Suslick et al. [56] reported about possibility of amines detection at sub-ppm range.

However, the arrays are disposable and are not meant for reuse, especially after exposure to high analyte concentrations [56], plus the large number of chemically diverse dyes into the sensor array usually reduces the functionality [60]. Additionally, the array can be applied for mixture identification but not the components of the mixture simultaneously. Even the slight changes in the mixture composition can confuse the system [61].

1.2.3 Laser photoacoustic spectroscopy

An attractive technique for gas sensing is laser photoacoustic spectroscopy. This analytic tool is based on the effect of sound waves formation upon light absorption by ammonia/amines molecules. The molecules that received the additional energy become excited for some period of time. The accompanied by collisions return to lower energy level increases the ammonia/amines gas temperature due to energy transfer into translation. If the laser beam is modulated (in frequency or amplitude) the temperature will change periodically, giving rise to a periodical pressure change which can be observed as an acoustic signal with a sensitive microphone (figure 1.2).

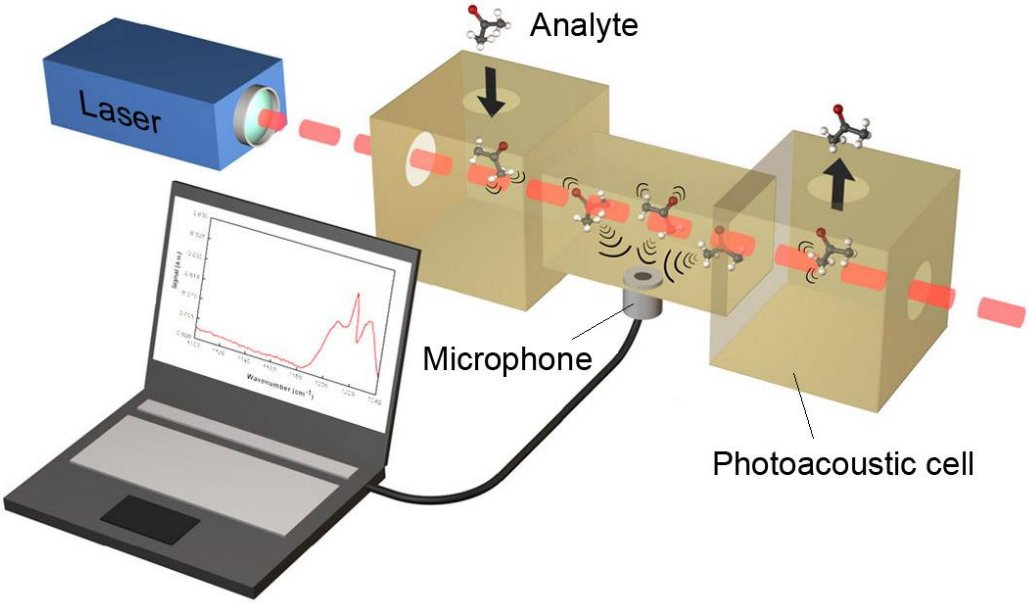

Figure 1.2 – The scheme of photoacoustic cell.

The technique allows to reach high selectivity due to possibility of operation at approximately 120 discrete wavelengths between 9 and 11 μm [62, 63] and high sensitivity which is proportional to the laser power [63, 64]. Thus, Hibbard and Killard [28] reported about possibility of low-ppb ammonia detection, using Nephrolux^{TM} CO_2 laser.

However, the power requirements and size of traditional tabletop CO_2 lasers used in photoacoustic gas detection systems [62], possible radiation source noise and amplitude fluctuations [64] leading to increase of background noise [65] narrows the scope of possible applications of such devices.

1.2.4 Chemical sensors

Sensors based solutions allow rapid local real-time detection and are a promising and cheap alternative to time-consuming laboratory techniques. The key ability of such devices is a possibility to reversibly change their characteristics depending on atmosphere composition. Thus, quite simple conversion of chemical changes into electrically measurable response signal can be effectively used for ammonia/amines concentrations determination. The used to date systems include electrochemical sensors [66-68] and number of chemical sensors represented by optical [69, 70], piezoelectric sensors [71-76], transistors/diodes [77-80] and chemiresistors. The latter can be metal oxides based and polymer based.

The operation principle of metal oxide sensors (ZnO, SnO_2, TiO_2, Fe_2O_3; NiO, CoO) is based on the gas adsorption trapping the charge carriers in the semiconductor conduction band. The resulted electrical conductivity changes are function of surface coverage. The main advantages are fast responses, short recovery times and possibility to be integrated directly into the measurement circuit (CMOS technology). The main disadvantages are high operating temperatures (200 – 500°C), resulting in high power consumption, complex and expensive equipment for production, dependence of the sensitivity and selectivity on operating temperature and grain size. Additionally the sulfur and ethanol poisoning of sensor is possible [81, 82]. At the same time, Dhivya and Sridharan [83]reported about fabrication of thin-film metal oxide sensor by reactive dc magnetron sputtering technique, capable for low-ppm ammonia detection even at room temperature.

Intrinsically conducting polymers (ICP), such as polypyrrole (PPy), polyaniline (PANI), polythiophene (PTh) (figure 1.3) and their derivatives have been used as the active layers of gas sensors since early 1980s [75] due to high sensitivity, relative ease of synthesis and ambient temperature gases detection [84]. However, despite big potential of applicability in the sensors the PTh has many disadvantages inherent only to this polymer, such as need of non-aqueous media for polymerization with thorough parameters control, problems with the regioregularity and comparatively higher price.

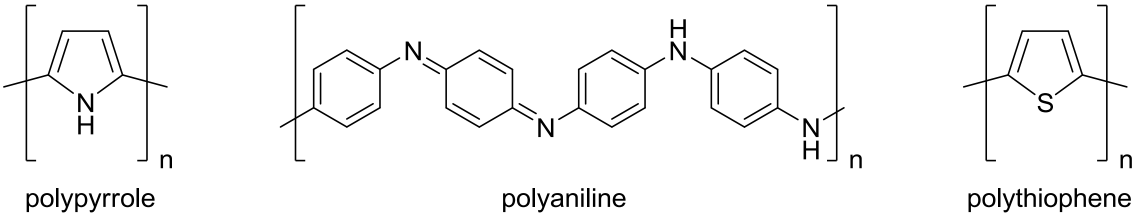

Figure 1.3 – The molecular structure of intrinsically conducting polymers.

That is why the other conducting polymers representatives, namely PANI and PPy are used significantly more often [85, 86]. At the same time, the polypyrrole active layers demonstrate low sensitivity and high response time, coupled with incomplete desorption of gas molecules, i.e. incomplete sensor response reversibility [87]. Therefore, despite the comparable levels of environment stability and price, significantly more studies are devoted to PANI. The comparison of best results obtained by using different techniques and approaches for ammonia detection is given in table 1.2.

Table 1.2 The comparison of different techniques capable for ammonia detection

Sensor technique	Advantages	Disadvantages	Response time	Detection limit	Ref.
Chromatography	High precision	Expensive and bulky equipment	Not real-time detection	14 ppt	[53]
Colorimetric arrays	High selectivity	Disposable, recognize only known odors	12 s	Sub-ppm	[56, 60]
Laser photoacoustic spectoscopy	High selectivity and sensitivity	Expensive, special power source requirements	120 s	1 ppb	[28]
Metal oxide sensors	Fast response and recovery times, cheap	Expensive equipment for sensors production	12 s	Low ppm	[83]
Pure conducting polymers	Operate at room temperature, low production cost	Sensitive to temperature and humidity	300 s	Low ppb	[88]

It worth to note, that term PANI in literature is generally related to one of the possible chemical structures with intermediate oxidation degree named emeraldine form (figure 1.4).

This intermediate emeraldine form contains both quinoid diimine and benzenoid diamine units. Despite of other conducting polymers it gives the additional possibility to control the level of electrical conductivity by doping. This process represents the reaction of emeraldine base neutralization by protonic acid, giving the emeraldine salt with higher conductivity (figure 1.5). The advantage of doping compare to oxidation/reduction reactions used in case of PPy or PTh is that polymers

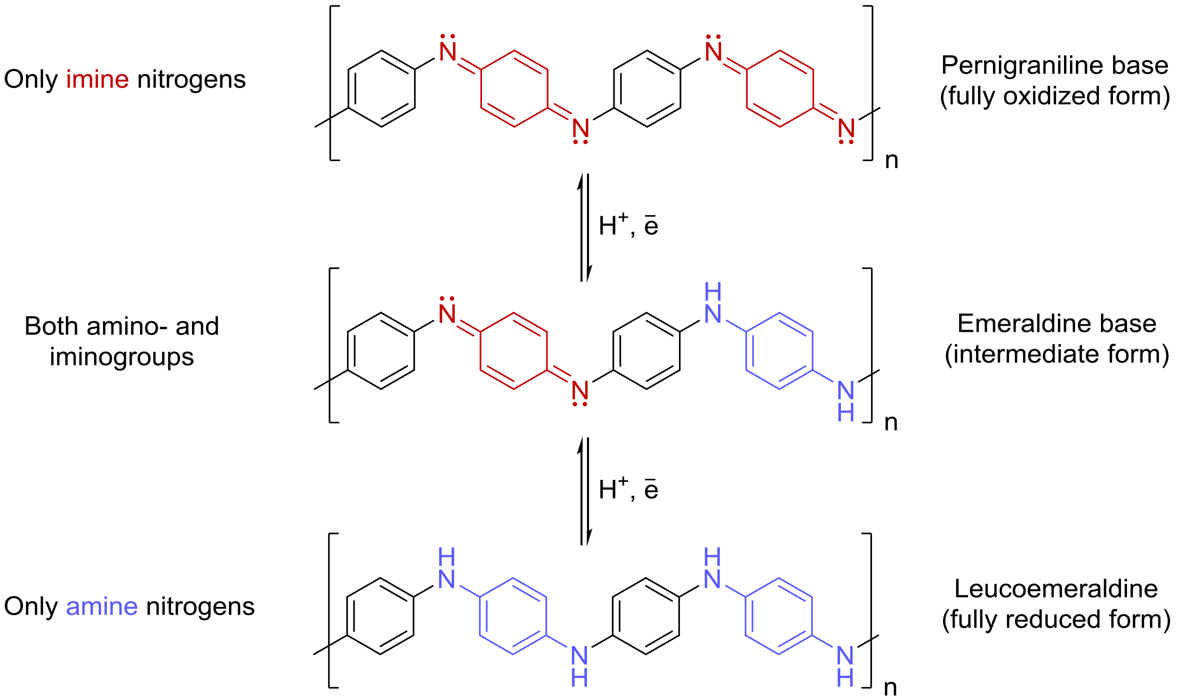

Figure 1.4 – Different polyaniline forms and their interconversions.

in extreme degrees of oxidation are not stable. In turn, it reflects on the constancy of their conductivity level. At the same time, PANI in its emeraldine salt form is very stable. It is also worth to note, that doping reaction is reversible and therefore can be used in sensor applications.

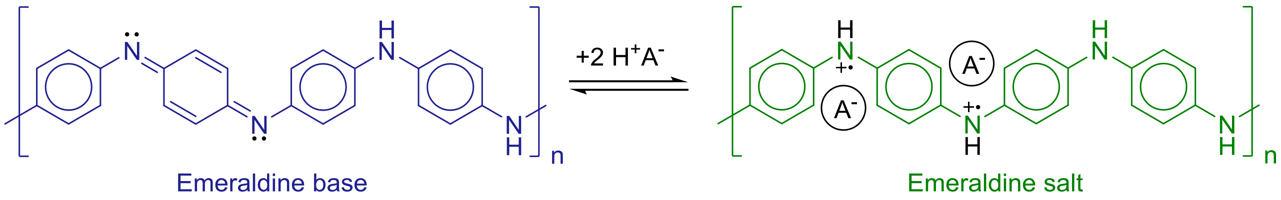

Figure 1.5 – The process of emeraldine base protonation/deprotonation.

Conducting polymers are usually obtained through chemical or electrochemical syntheses in the presence of different dopants, and their molecular chain structure can be modified conveniently by copolymerization or structural derivations. At the same time, synthesized materials properties strongly depend on preparation conditions and methods [89, 90]. Probably, this variability is caused by the interaction and interference of factors having different nature and thus affecting PANI synthesis kinetics and resulting properties in unexpected ways. That is why the comprehensive understanding of PANI polymerization mechanism is of critical importance for the progress in new materials development.

1.3 The use of PANI based conducting polymer materials in sensor technology

1.3.1 PANI polymerization mechanism

Despite the mechanism of PANI oxidative polymerization was studied during the last three decades by many authors [3, 91-96] the consensus on this issue still does not exist. The main reason is the necessity to take into account a number of different factors [5]. The [oxidant] : [polymer] : [acid] ratio, nature and concentration of dopant, type of oxidant, solvent, temperature, stirring mode, presence of nanoparticles – all of these factors are interfere and strongly influence resulted polymer structure and properties. The particular importance has the high acidity of polymerization medium and oxidant choice [5]. The common oxidant is ammonium peroxydisulfate (APS) due to high oxidation potential, good solubility in water and high polymerization yields achieved at [APS]:[aniline] ratio 1.25:1 [93, 97]. In this connection it seems appropriate to give the mechanism which is most probable in synthesis conditions used in this work.

The initiation phase in acidic conditions (pH<2) begins from aniline two-electron oxidation with ammonium peroxydisulfate. The reaction proceeds slowly, as the concentration of more reactive aniline is significantly lower than anilinium cations which are dominant monomer species under this conditions [3] (figure 1.6). The process is accompanied by temperature, acidity and open circuit potential (OCP) increase of the reaction mixture during the whole induction period [5, 98].

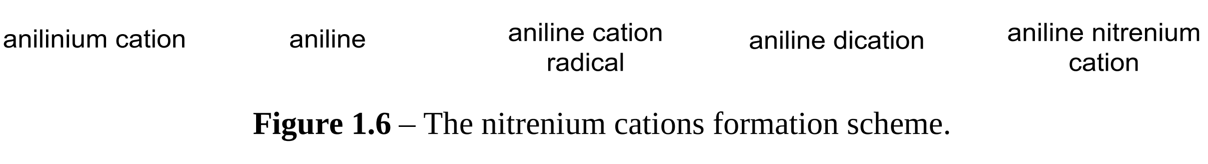

Figure 1.6 – The nitrenium cations formation scheme.

The dimerization starts from electrophilic aromatic substitution reaction between aniline nitrenium cations and aniline molecules, resulting in formation of protonated 4-aminodiphenilamine (4-ADPA). The latter is more oxidizable than anilinium cation and undergoes rapid two-electron oxidation with APS to yield deprotonated *N*-phenyl-1,4-benzoquinonediimine (PBQI) [4, 99] (figure 1.7).

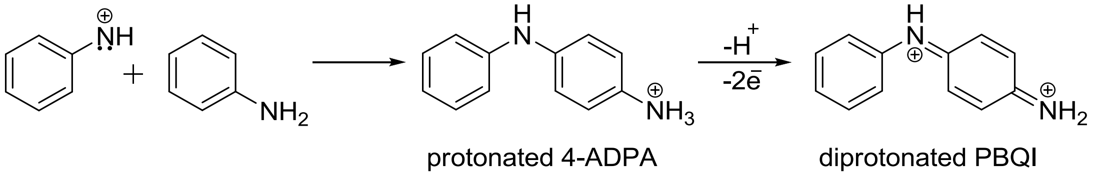

Figure 1.7 – The dimerization reaction.

The substantial oxidation potential increase upon formation of *N*-phenyl-1,4-benzoquinonediimine protonated form leads to autoacceleration in reaction kinetics. The H_2PBQI undergoes redox (electron transfer) process with aniline/anilinium cation [95, 99] leading to the formation of cation radicals with their further recombination (figure 1.8) [3, 100].

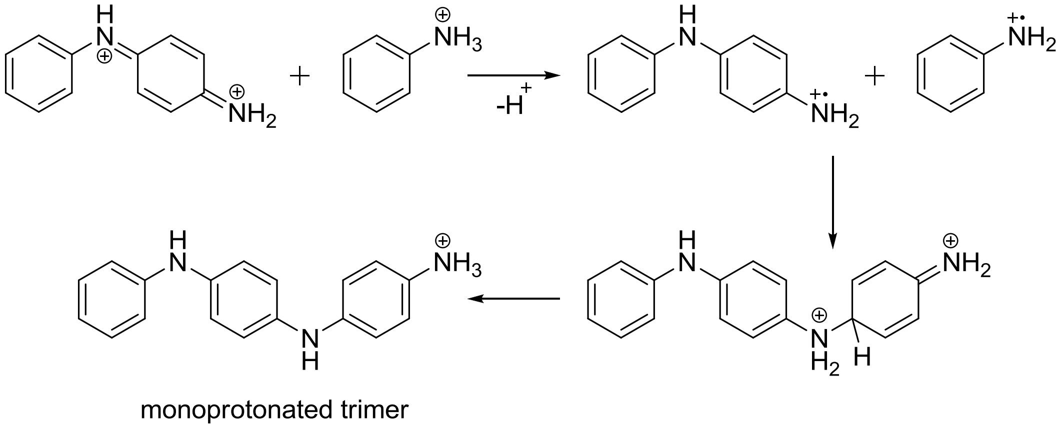

Figure 1.8 – The trimerization process.

The monoprotonated aniline trimer is more oxidizable compared to anilinium cation or monoprotonated 4-ADPA and undergoes rapid two-electron oxidation with APS, giving at first protonated forms of half-oxidized aniline trimer and then nitrenium trication [4, 99] (figure 1.9).

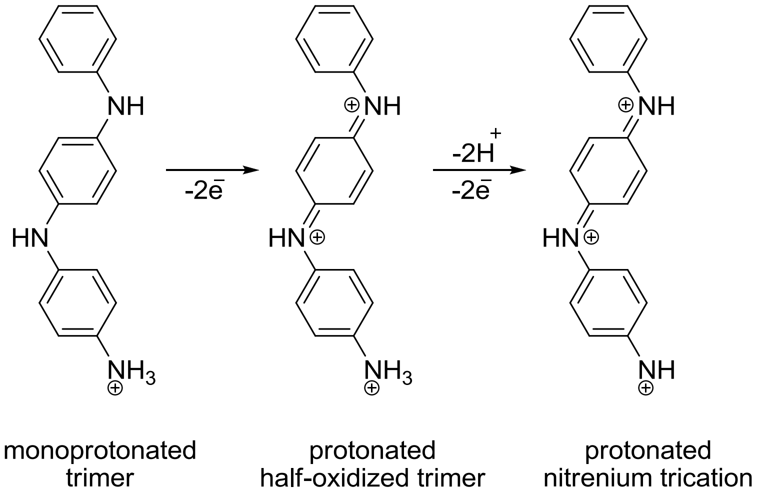

Figure 1.9 – Aniline nitrenium trication formation.

The further chain growth leads to sharp oligoanilines concentration increase. At certain point it becomes more favorable for APS to oxidize the monoprotonated oligoanilines than to generate nitrenium cations from aniline/anilinium cations. The protonated oligoanilines, being oxidants and electrophiles at the same time, easily oxidize and incorporate anilinium cations into the growing polymer chain [3, 100]. The reaction continues till the exhaustion of reagents, resulting in PANI emeraldine salt formation (figure 1.10).

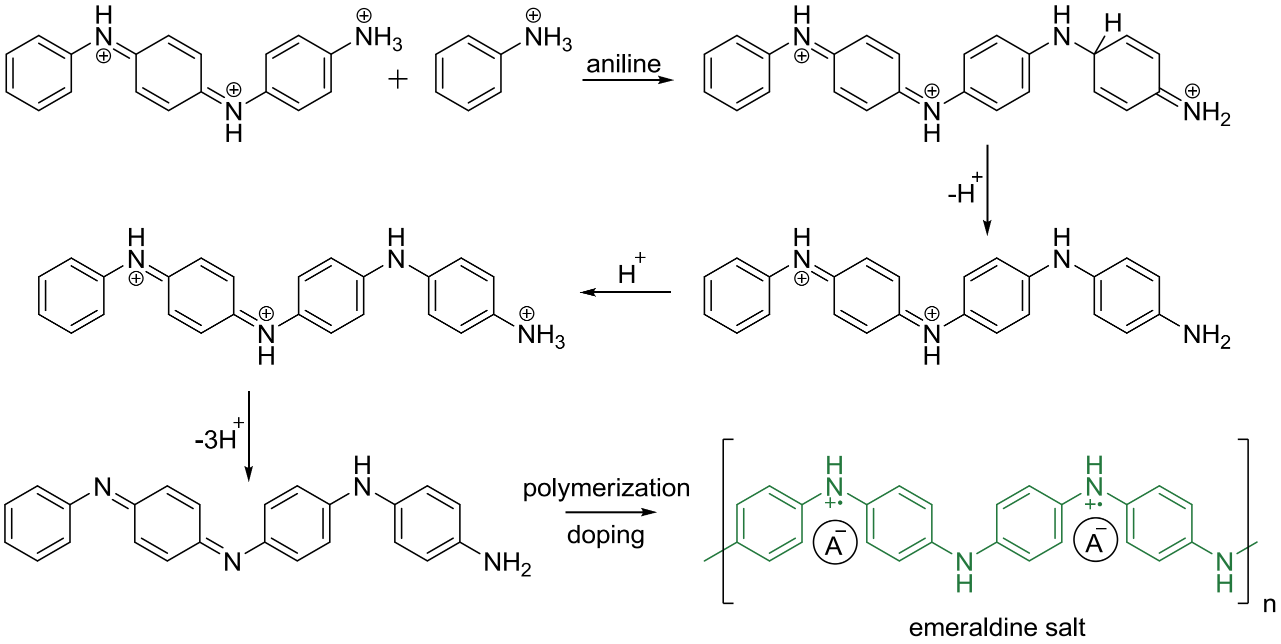

Figure 1.10 – The PANI chain growing reaction.

The in situ control of the polymerization process is usually performed by the measurements of open circuit potential. The MacDiarmid and Wei groups used OCP time dependence as auxiliary tool providing additional information concerning current PANI redox state and helped to shade more light on aniline polymerization, particularly on its separate stages [101, 102] their duration and aniline polymerization rate [98, 102, 103].

1.3.2 The polyaniline self-assembly process

The materials structuring at nano-scale level usually yields improved strength and conductivity, reactivity or appearing of novel properties [104-108]. In this regard, the interest in controllable nanostructures self-assembling during synthesis without any templates is well understandable.

Despite the number of studies devoted to the influence of PANI synthesis conditions on the resulting polymer structure [1, 3-6, 99, 109, 110] the self-assembly mechanism is still a subject of scientific debates. The most popular explanations include micellar and phenazine theories. The former one claims that polymerization proceeds at the micelle/water interface, where the micelle is formed by anilinium cations [111-113]. According to the latter, the π-π stacking of phenazine-like polymerization by-products produce columnar aggregates and serve as nuclei for the new linear chains [5, 114, 115].

The recent multi-layer theory is an attempt to combine aforementioned theories. It is based on the assumption that PANI forms only three intrinsic morphologies (nanofibrils, nanogranules, nanosheets) depending on synthesis conditions. Their self-assembly process driven by stacking, hydrogen bonding and charge-charge repulsion from protonation, gives rise to growth, agglomeration and curling behaviors, thus generating complex structures [116].

The use of template agents such as nanoparticles usually accelerates the polymerization due to increase of the reagents contact surface and inhibiting the supramolecular structures formation to different degree. The chemisorption of PANI macromolecules coupled with possibility of hydrogen, donor-acceptor, ionic or covalent bonds formation in system particle-polymer [98] suppresses the intrinsic PANI crystalline structure growth. The polymer chains tethers to nanoparticles surface and the formation of core-shell structure can be observed [117, 118]. The factors of starting pH and oxidant nature are no less important as those ones predetermining the resulted morphology and composite properties [5, 6, 93]. In this regard the monitoring of polymerization parameters is crucial when a given type of nanostructures is desirable.

1.3.3 Polyaniline properties

Similarly to other conducting polymers pure PANI has a rigid structure originating from π-electron delocalization along the polymer chain as well as due to interchain hydrogen bonding [119]. As the more rigid chains are sterically more favorable for aggregation, it leads to additional reinforcement due to multiple associations between successive repeat units along aligned chain sections. Altogether it results in formation of non-melting and insoluble in nearly all solvents of practical interest structure with poor mechanical properties [120, 121].

One of the possible solutions to overcome processability problems is the use of aniline derivatives. The presence of substituent groups (e.g. alkyl, alkoxy, sulfonated) induces distortions in the chain, weakening the π-electron conjugation and increasing the chain flexibility. At the same time, improved solubility is accompanied by a simultaneous electrical conductivity and polymer molecular weight decrease [121].

Based on general considerations, the PANI chains shortening should increase the number of interchain contacts, hindering the electrons hopping and, thus, reducing overall conductivity. The authors [122] show the possibility of significant PANI molecular weight increase in sub-zero temperatures syntheses. At the same time, the later studies [1] demonstrate the independence of molecular weight and polyaniline electrical conductivity. This phenomenon was explained by PANI tendency to form “compact coil” structures when the polymer chain length reaches certain point. The charge transfer between such structures is limited and doesn’t depend on polymer molecular weight. The discovered solution is the introduction of secondary dopant that changes PANI conformation to “expanded coil” structure. The secondary dopant influences only the conformation, while the electronic, optical, magnetic and other properties changes are induced by primary dopants [123]. In this regard the common approach to PANI processability improvement is the use of functionalized protonic acids (e.g. DBSA, CSA etc.) acting as dopants and rendering the PANI salt complex soluble in nonpolar or weakly polar organic solvents [124, 125].

At the same time, from a practical point of view, the more perspective way is the formation of PANI composites with different materials such as insulating polymers, inorganic semiconductors, carbon nanotubes, metal clusters or magnetic substances [89, 120]. This approach is one of the most effective methods allowing remarkable characteristics improvement without need of complicated procedures as the resulted materials very often combine properties from both the parent organic and inorganic class of materials [126]. Furthermore, the synergetic effect can appear in some of the cases, depending on used hybrid material preparation method [127].

1.3.4 Formation and properties of polyaniline composites

The two most common ways for the composites preparation include PANI blending with the inert matrix (usually insulating polymer) and aniline polymerization in the presence of dispersed particles of different size and nature in the reaction medium.

The blending can be performed in the solution as well as melt processing can be used. The solution route is based on imparting solubility to initially insoluble polyaniline by influencing its aromatic structure or charge delocalization [128]. The known approaches utilize substituted PANI forms [129-132], doping with functionalized protonic acids [124, 125, 133] or dissolving in amide solvents [134-136]. During the melt blending the mechanical mixture of ICP with thermoplastic polymer is processed by compression molding, injection or extrusion [89, 137, 138]. Despite simplicity of this method, the ICP distribution heterogeneity problems [139, 140], properties deterioration of polymer derivatives [141, 142] and possible temperature degradation [143-145] make the synthetic approach more attractive.

The synthetic approach, including polymer grafting [146-148] and copolymerization with other monomers [149, 150], often used for composites formation by in-situ chemical polymerization on the surface of dispersed inorganic phase and results in formation of core-shell morphology [98, 151-155] or by electropolymerization in the matrix [156-158]. The latter is very convenient in the production of biosensors and supercapacitors due to a strict control of properties of obtained PANI composites, prevention of by-products formation and to convenient possibility of creation of p-n junction structure [159-161]. The main advantage of this approach is the fact that resulting product does not need to be extracted and continuously washed from the initial polymerization solution. However, the need of expensive electrochemical equipment and respective labware, problems of covering uniformity at large-size electrode surface and impossibility of PANI electrodeposition at dielectric materials make this method of little avail for large-scale production.

In contrast to the electrodeposition, the chemical polymerization is much simple and cheap method which does not require a special and expensive equipment [89]. The other advantages are possibility to form high surface-to-volume ratio core-shell structures with any type of nanoparticles, as well as good homogeneity and low percolation thresholds of obtained (nano)composites.

At the same time, it was shown that PANI structure and properties are strongly depend on synthesis conditions [1, 5, 93, 162, 163]. Additionally it was demonstrated that dopant choice significantly influences on PANI sensitivity to analytes, its structure and morphology, hydrophobicity and conductivity [90, 163-165]. The other important feature is the necessity of careful choice of the second component as it usually results in synergetic effect appearance. Authors [166-172] demonstrated substantial improvement of response time, sensitivity, detection limit, stability and durability achieved by aniline polymerization in a presence of semiconductors nanoparticles. Furthermore, Gong et al. [173] reported about formation of a p-n junction on the polymer-metal oxide interface, allowing pollutant detection at extremely low concentrations.

1.3.5 PANI doping concept and conduction mechanism

The dependence of physical, physicochemical and chemical properties on doping level is the key feature of ICPs. The doping process leads to an additional charge injection into the system of conjugated bonds, resulting in delocalization of π-electrons [174] and influences polymer conductivity, optical and magnetic properties [86, 175] (figure 1.11).

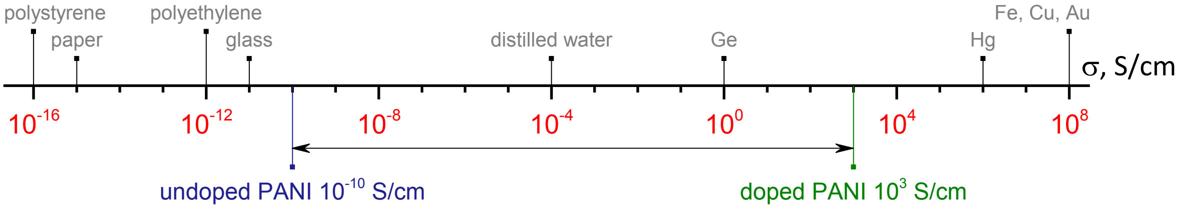

Figure 1.11 – Comparison of materials conductivity

The common way of conductivity imparting to ICPs is the change of their RedOx state which changes the total number of electrons in polyconjugated system. The only polymer can simply realize insulator-conductor transition without changes in electron number is PANI [174, 176]. It is possible due to existence of both amine and imine groups in PANI emeraldine form. It is believed [91] that imine nitrogen protonation by acid-dopant triggers the electron structure reorganization, namely in charge and electron spin delocalization along the polymer chain. As a result, all nitrogen atoms, all C–N bonds and all C_6H_6 rings become identical. Each nitrogen atom bears a +0.5 charge, all nitrogen bonds become intermediate between a single and double and all C_6H_6 rings acquire the structure intermediate between benzenoid and quinoid. Finally, the appearance of polarons which are positively charged repeated units with half-filled electron band can be observed (figure 1.12).

The polaron structure which is closer to ideal state is expectedly more stable compared to bipolaron form. The electrical conductivity appears due to the charge transfer process through intra- and inter-chain hopping mechanism [163, 177-179]. The electron shortage in cation radical nitrogen makes it a positive charge (hole) carrier, while the adjacent neutral nitrogen acts as negative charge (electron) carrier [137]. The electron jump to cation radical nitrogen eliminates the positive charge

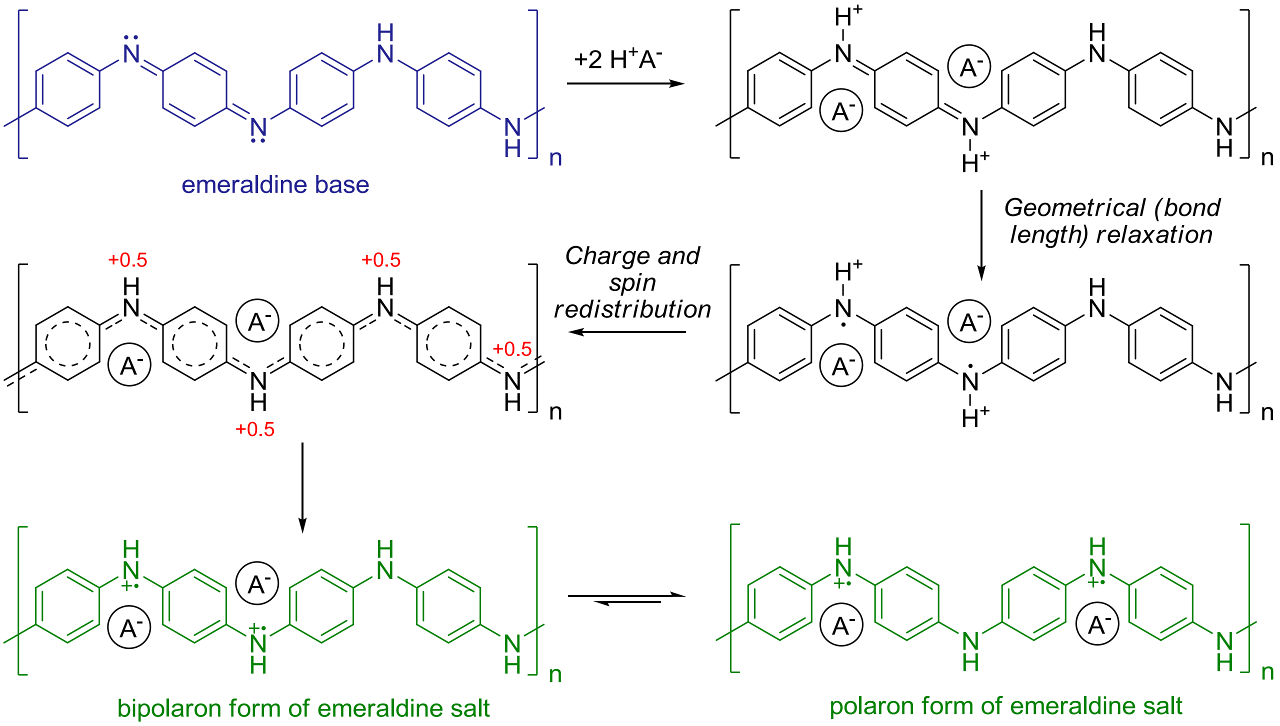

Figure 1.12 – Insulator-conductor transition by protonation induced charge and spin redistribution

excess, but creates the new hole on the previously neutral nitrogen (figure 1.13). The repetition of this process over the entire chain length creates the oppositely directed flows of holes and electrons, giving rise to electrical conduction.

However, the recent studies revealed some discrepancies with the generally accepted model and were explained by redox heterogeneity phenomenon of PANI structure [180]. It was shown that spatial distribution of oxidized and reduced units is not uniform in the polymer bulk [181, 182]. To explain this phenomenon, the coexistence of crystalline (ordered) regions with metallic-type conductivity and surrounding amorphous (disordered) non-conducting zones was suggested [183-185].

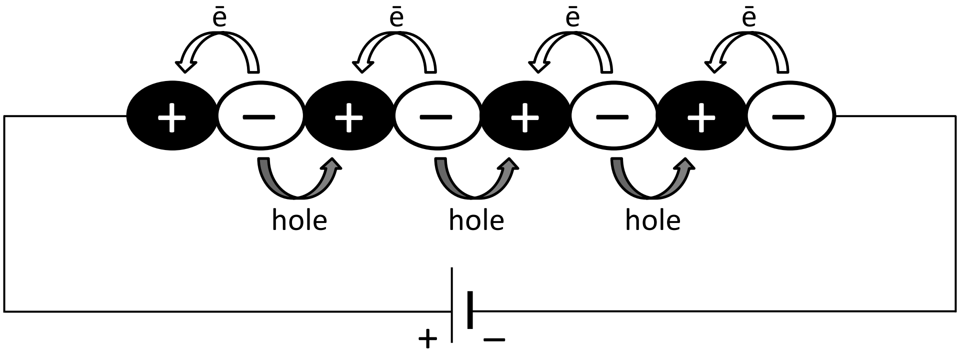

Figure 1.13 – Schematic presentation of PANI conduction pathway

The authors [186] propose to consider polymer chain as a set of defect sequences, containing separate repeating benzenoid (B) and quinoid (Q) units (figure 1.14). The total length is estimated to be no more than 16 units. The supposed main reason of their appearance is the oxidative polymerization autocatalytic character and non-linearity of mass transfer processes [181].

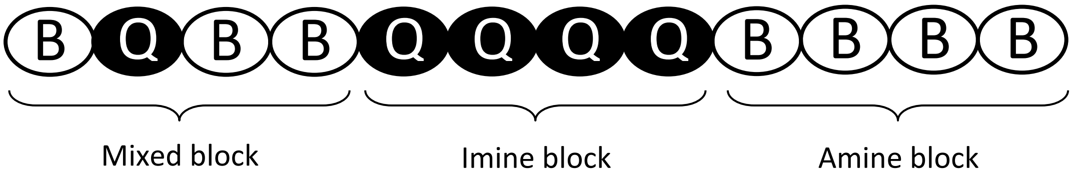

Figure 1.14 – The molecular scale redox segregation in polyaniline

The discrepancies between the theoretical and practical form can help to explain the deviations of predicted polymer behavior in some cases and to understand the occurred processes better.

1.3.6 Pollutants detection principle. P-n junction effects

The fact that significant conductivity increase can be brought about by treatment of PANI emeraldine base with acids [91], led to the beginning of polymer sensors development. The resistance in these devices is a function of doping degree and can be changed by simple acid/base or donor/acceptor interactions with analytes of interest. In particular, this PANI feature is widely used to detect such harmful for human health substances as ammonia or amines (figure 1.15).

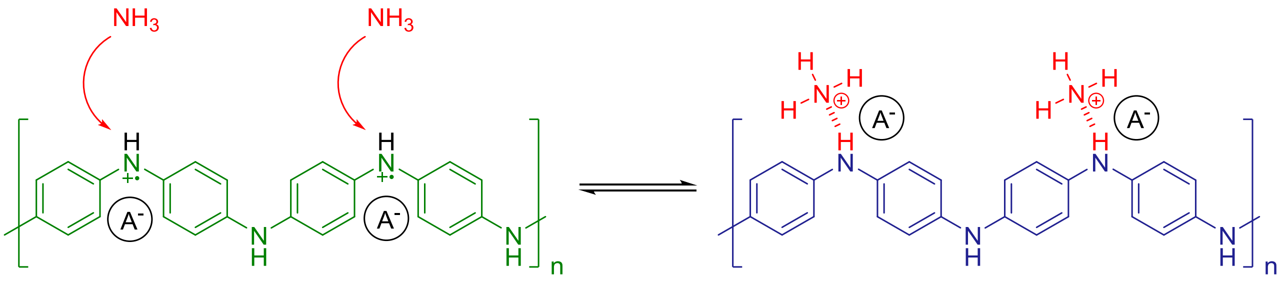

Figure 1.15 – PANI interactions with ammonia responsible for the sensor response

This process is reversible and after the ammonia atmosphere is removed the initial PANI properties restore. Thus, the quite simple conversion of chemical changes in sensing layer into electrically measurable response signal can be effectively used for pollutants concentration determination.

Obviously, the response time strongly depends on analyte diffusion rate into the polymer bulk. In this case, besides a well-known importance of physicochemical interactions of the analyte molecules and PANI, a significant impact of penetrating molecules size and shape can be also seen: small, flattened or elongated molecules diffuse considerably faster than spherical-shaped [187]. Thus, the polymer structure changes facilitating gas permeation regardless of the molecular features are of great interest.

The recent researches in the field of direct synthesis of ordered nanostructures open new prospects in polymer electronics based on highly porous polymer layers formation. However, these studies are mainly concern theoretical aspects of synthesis, whereas in practice the reliable techniques with guaranteed obtaining of desired supramolecular structures are absent not only for industrial production, but even at the laboratory scale [4, 114, 116]. In this regard, the more realistic to date is the creation of composite materials [89]. Generally, this method is proven and usually allows obtaining desirable results by simple mixing of few components. But in case of sensing materials the situation is more complicated. The direct mixing doesn't change the polymer surface area; it only leads to more or less homogeneous distribution of the components in the composite bulk and not ensures their interaction.

One of the effective solutions is inclusion of nanoparticles directly into the PANI polymer matrix. It can be simply realized by PANI synthesis in the presence of dispersed phase. The obtained core-shell structure, where the nanoparticle is core (e.g. TiO_2, ZnO, SnO_2 etc.) and conducting polymer is the shell, creates the intimate contact between composite components [98, 188]. Aside the overall improvement in properties it allows the formation of high surface-to-volume ratio nanocomposites facilitating the penetration of the analyte gas molecules inside the PANI sensing layer [84]. In comparison with molecular structure modification this technique allows avoiding complicated multistage chemical syntheses [127].

Furthermore, Gong et al. [173] reported about formation of a diode-like TiO_2/PANI nanostructure that functions as electric current nano-switch when NH_3 gas is absorbed by PANI significantly improving the sensitivity and permits ammonia concentrations detection at ppt levels. The authors explain the mechanism as follows: while applying of voltage to a highly resistive material like TiO_2, the flowing current will be very low. Obviously, after the deposition on the semiconductor surface of more conductive layer, the current would generally flow through the new layer with lower resistance, according to the Ohm law. This situation is correct, when the charge careers in both materials are of the same type – electrons or holes.

The deposition of PANI layer which is p-type semiconductor on the surface of TiO_2 (n-type semiconductor), leads to formation of the diode-like structure that passing current only in one direction. The equivalent current circuits are shown in figure 1.16, where R_1 and R_3 are the p-n junction reverse and forward bias resistances; R_2 and R_4 are the bulk resistances of PANI and TiO_2 nanoparticles respectively.

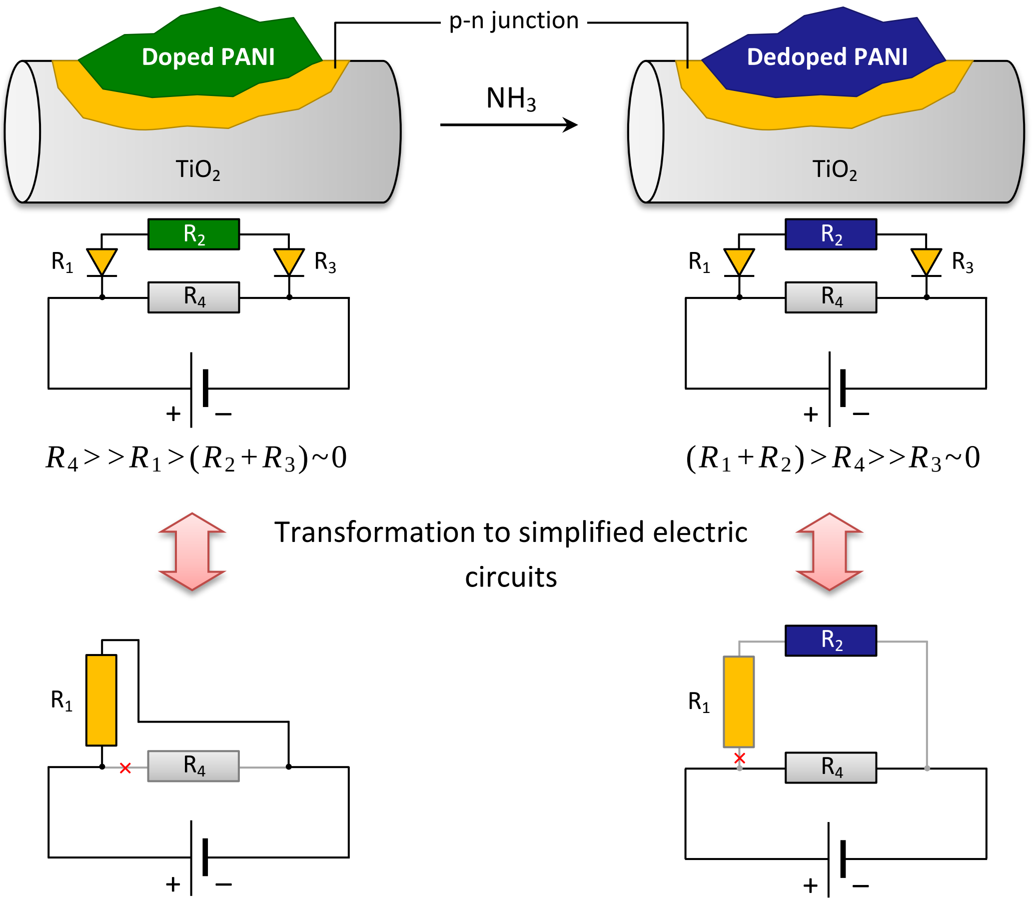

Figure 1.16 – P-n junction formation at PANI-TiO_2 grain boundaries

At a constant voltage the equation for electric field applied to the system can be written as: $U = I_1(R_1 + R_2 + R_3) = I_2 R_4$. As the PANI is more conductive the current will preferably flow through the polymer. Since the both forward-bias (R_3) and bulk PANI resistances (R_2) are considerably smaller than reverse-bias resistance (R_1), the equation can then be simplified to: $U = I_1 R_1 = I_2 R_4$.

If the applied voltage is above the diode breakdown value, the instantaneous R_1 decrease and total conductivity increase would be observed (figure 1.16 – left). The PANI deprotonation process caused by interaction with ammonia leads to substantial increase of polymer bulk resistance R_2. At a certain point, the overall resistance of (R_1+R_2) will significantly exceed the TiO_2 resistance. As a result, the PANI route will be almost completely turned off and the current will flow only through a TiO_2, leading to a large drop in the entire system current (figure 1.16 – right).

Thus, by simple variation of PANI protonation degree it is possible to construct nano-scale current switchers. Furthermore, the large number of such p-n junctions in the composite bulk can be considered as a sequence of p-n-p or n-p-n junctions offering many advantages over other materials utilized in gas sensors. The resulting sensor arrays are characterized by high discrimination, possibility to operate at high relative humidity while demonstrating linear responses for a wide range of gas analyte concentrations [188]. However, signal dependence on humidity, problems of selectivity and batch to batch reproducibility of materials properties are important challenges [72, 82, 187, 189].

1.4 Research motivation

The literature data analysis presented in first chapter indicates the importance of determination of toxic gases concentrations, connected with their significant influence on the environment. Moreover, the reported link between breath gas composition and pathologies of a human body opens the new possibilities in early diagnosis of diseases. However, the latter demands a sensitivity of a ppb level. The majority of modern measurement techniques, even with excellent performances at ppb levels, have such disadvantages as expensive, bulky and quite sophisticated equipment requiring the trained personnel and usual samples pre-collection. The good alternative is the portative devices such as gas sensors based on intrinsically conducting polymers, providing information in real time and able to answer to the targeted gases at trace levels.

The one of the most promising representatives of such polymers family is PANI. This material combines a set of unique properties, the most interesting of which from the viewpoint of using in sensors application is the PANI possibility to change electrical conductivity in a wide range by simple reaction based on acid-base interaction.

However, pure PANI has such drawbacks as poor mechanical and film-forming properties, insolubility in the majority of organic solvents, infusibility. An effective way to improve PANI properties is the creation of its composite materials with metal oxides nanoparticles. The common way of polymer materials properties improvement by mixing does not allow reaching the desirable characteristics level. In this regard the improvement of pure polymer properties by direct polymerization in the presence of dispersed nanoparticles is a promising direction in new sensing materials development. Such new materials have high specific surface area and very often demonstrate a synergetic effect, owing to emergence of specific physicochemical interactions at the polymer-nanoparticle interface.

At the same time, specificities of such nanocomposites formation and interconnection of starting synthesis parameters with resulting performances are still insufficiently studied and characterized, which hampers such materials wide use in different applications. In particular, there is no information concerning influence of dopants structure, metal oxides nanoparticles size and nature on kinetic parameters of nanocomposites formation, molecular characteristics of PANI phase, morphology, stability, electrical conductivity, sensing and other properties of hybrid materials. Thereby, this work is devoted to obtaining this information, its analysis and use in the controlled creation of hybrid nanocomposites with predetermined properties.

2 OBJECTS AND METHODS OF RESEARCH

In this chapter a brief description of used reagents and experimental procedures applied for pure polymer and its hybrid materials syntheses by chemical and electrochemical routes are provided. General details of main research methods used in characterization of materials structure and morphology, thermal and photostability, conductivity, molecular characteristics, gas sensitivity to ammonia and amines are given.

2.1 Used reagents

The lauryl sulfate (monododecyl ester of sulfuric acid) was prepared from sodium lauryl (dodecyl) sulfate (SDS) via ion exchange reaction with resin KU-2-8 (Ukraine). The 3.5 g of SDS were dissolved in 50 ml of water and passed several times through the 50 ml burette filled with 18 g of cation exchange resin. The resin regeneration was performed with HCl. The obtained lauryl sulfate concentration was determined by titration with NaOH. All other reagents were used as received. The main parameters of used reagents are presented in table 2.1.

Table 2.1 The list of used reagents

№	Reagent	Structural formula	CAS number	Notes
1.	Ammonium persulfate	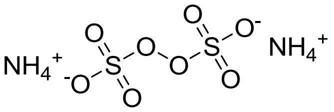	7727-54-0	Ukraine
2.	Aniline	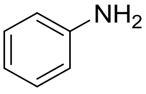	62-53-3	Merck
3.	Argon	Ar	7440-37-1	Ukraine
4.	Ascorbic acid	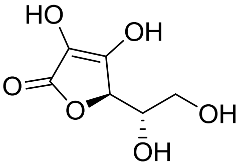	50-81-7	Ukraine
5.	Benzenesulfonic acid	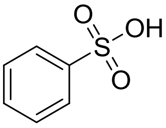	98-11-3	Aldrich, technical grade

Continuation of table 2.1

№	Reagent	Structural formula	CAS number	Notes
6.	Camphorsulfonic acid	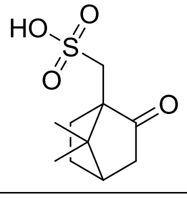	35963-20-3	Aldrich
7.	Chloroform	$CHCl_3$	67-66-3	Ukraine
8.	Dichloroacetic acid	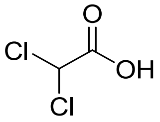	79-43-6	Aldrich
9.	Dodecylbenzene-sulphonic acid	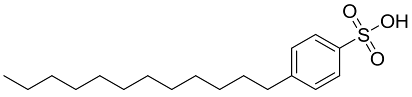	27176-87-0	Acros
10.	Ferric chloride hexahydrate	$FeCl_3{\cdot}6H_2O$	10025-77-1	Ukraine
11.	Hydrochloric acid	HCl	9004-54-0	Ukraine
12.	Lauryl sulfate	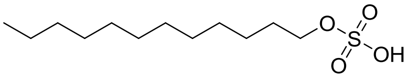	151-41-7	–
13.	N-methylpyrrolidone	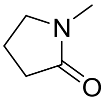	872-50-4	Ukraine
14.	Oxygen	O_2	7782-44-7	Ukraine
15.	Potassium chloride	KCl	7447-40-7	Ukraine
16.	Potassium nitrate	KNO_3	7757-79-1	Ukraine
17.	p-Toluenesulfonic acid	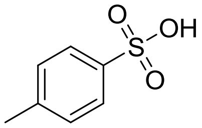	104-15-4	Aldrich
18.	Pyrrole	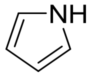	109-97-7	Aldrich
19.	Sodium lauryl sulfate	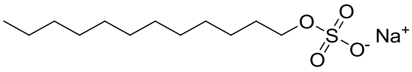	151-21-3	Ukraine
20.	Tin oxide	SnO_2	18282-10-5	MTI 50 nm
21.	Titanium oxide [anatase]	TiO_2	98084-96-9	MTI 10 nm, SSA=210 m^2/g
22.	Titanium oxide [rutile]	TiO_2	1317-80-2	MTI 20 nm
23.	Zinc	Zn	7440-66-6	Ukraine
24.	Zinc nitrate	$Zn(NO_3)_2{\cdot}6H_2O$	10196-18-6	Ukraine

The position of used semiconductors bang gaps in contact with aqueous electrolyte at pH 1 are given at a schematic energy diagram (Figure 2.1). The highest occupied molecular orbital (HOMO) and the lowest unoccupied molecular orbital

(LUMO) of PANI and band positions of used semiconductors are shown as reported in the literature [190-194]. The energy scale is indicated using either the normal hydrogen electrode (NHE) or the vacuum level as a reference and presents internal energy. The standard potentials of several redox couples against the standard hydrogen electrode (SHE) potential are given on the right side.

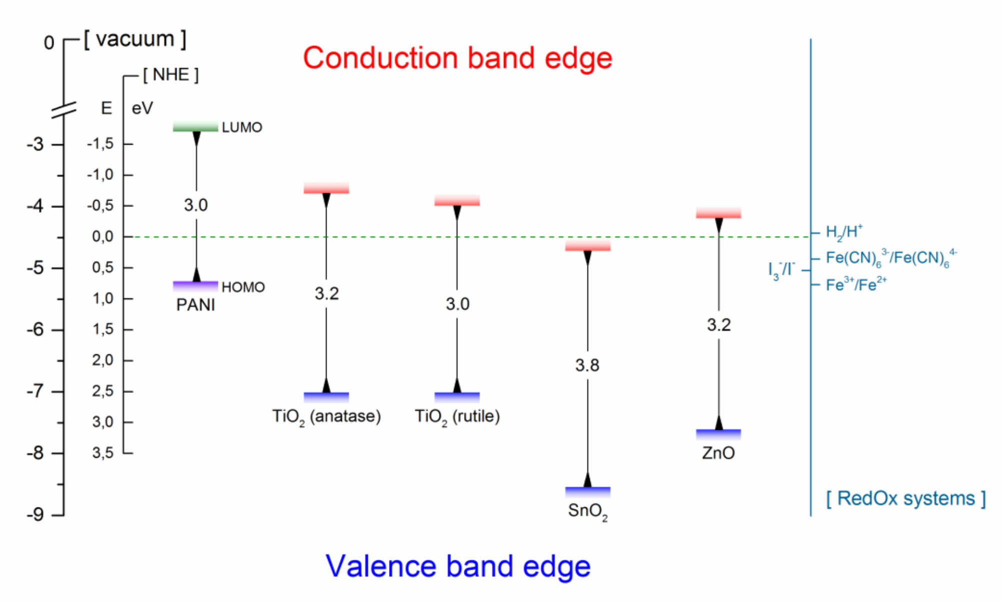

Figure 2.1 – Band positions of semiconductors used in experiments

2.2 Syntheses procedures

2.2.1 Pure polyaniline synthesis

PANI fabrication process involved the aniline oxidative polymerization under the action of ammonium persulfate (APS) in water solutions containing acids-dopants. Typically the 120 ml solution containing 0.00054 mole of aniline and 0.00081 mole of acid-dopant were prepared. The polymerization was initiated by addition of oxidant solution (0.000675 mole of APS dissolved in 40 ml of water). The process was carried during 24 hours in thermostatic mode at +10 °C with vigorous stirring. The used aniline: oxidant: acid molar ratios were 1:1.25:1.5. The formed polymer materials were purified by dialysis against distilled water during 72 hours and then dried under vacuum at 60 °C to a constant weight.

2.2.2 Polyaniline nanocomposites synthesis

The nanocomposites formation was based on typical oxidative aniline polymerization procedure with some modifications. In short, the fabrication process involved the aniline polymerization at +10 °C under action of ammonium persulfate in the presence of metal oxide nanoparticles dispersed in the solution of the anilinium salt of corresponding dopant (Figure 2.2). The necessary nanoparticles quantity was calculated to satisfy next relation:

$$\%PANI = \frac{m_{aniline}}{m_{aniline} + m_{nanopart.}} \times 100\%,$$

where $m_{aniline}$ – weight of aniline dissolved in solution;

$m_{nanopart.}$ – weight of nanoparticles dispersed in solution;

$\%PANI$ – PANI phase content (in dedoped form) in the resulted composite.

The used aniline: oxidant: acid molar ratios were also 1:1.25:1.5. The formed core-shell PANI nanocomposites were purified by dialysis against distilled water for 72 hours and dried under vacuum at 60 °C to a constant weight.

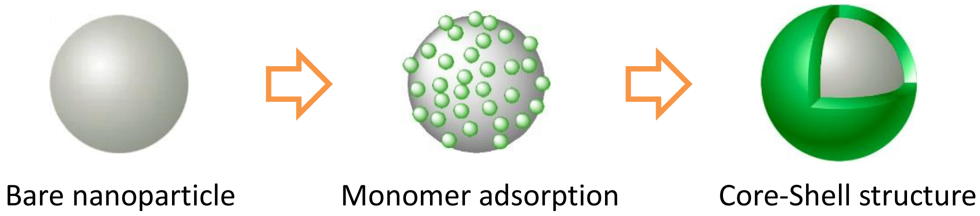

Figure 2.2 – The core-shell structure fabrication process

2.2.3 Electrochemical synthesis of pure polypyrrole and its heterostructures

The polypyrrole film was electrochemically polymerized from a solution containing 0.5 M pyrrole dissolved in 1 M KCl aqueous solution. The electrolyte was bubbled with argon for 15 min before polymerization process. The electrodeposition was performed by using potentiostat/halvanostat PI-50-1 in galvanostatic mode at room temperature and current density i=0.4mA/cm^2, with the Ag/AgCl as reference electrode. The obtained films were washed with distilled water. The formation of heterostructures included the formation of ZnO vertically oriented submicron rods layer [195, 196] on the interdigitated electrodes surface prior to polymer deposition. The ZnO structures were formed in potentiostatic mode at temperature t=70°C and potential E= –1 V (vs. Ag/AgCl) from the electrolyte containing 0.1 M KNO_3 and 0.05 M $Zn(NO_3)_2$. The Zn plate was used as a counter electrode. The electrolyte was bubbled with air for 15 min before nanostructures formation process.

2.3 Investigation methods and techniques

2.3.1 Open circuit potential (OCP) measurements

The process of aniline polymerization was monitored by continuous pH and OCP measurements [101, 102]. The reaction progress as well as the beginning of separate stages was registered by multifunctional pH/RedOx/Thermometer Greisinger GMH3530 connected to the computer. The data points were recorded with the 5 seconds interval till constant OCP value.

2.3.2 Electron spectroscopic measurements

The electronic absorption spectra were recorded using the Varian Cary 50 UV-Vis spectrophotometer. The determination of polymerization yield was performed similar to the procedure described by authors [197] with some modifications, due to the necessity of removal from PANI solution of the nanoparticles, hindering the obtaining good spectra because of light scattering. At first the powders of pure PANI and its nanocomposites were dedoped with 0.5% water ammonia solution. The dry powder of dedoped material was reduced to leucoemeraldine state by dissolution in 5 ml N-Methylpyrrolidone (NMP) containing 0.5 g of ascorbic acid. The obtained leucoemeraldine solutions were centrifuged for 15 min at 5000 rpm in order to remove the metal oxide nanoparticles. The absorption maxima of investigated leucoemeraldine solutions (after substraction of NMP spectrum) were used for the calculations of the dissolved PANI quantity and clarification of its content in the nanocomposite materials.

The polymer yield determination procedure is based on Bouguer-Lambert-Beer law and utilizes the concentration-light absorbance calibrating curve. Calibration curve is a straight line described by the equation:

$$D = 0.0073 C_{solution} + 100.9348,$$

where $C_{solution}$ – concentration of EB solution;

D – solution optical density.

The typical PANI absorbance spectrum is shown in Figure 2.3.

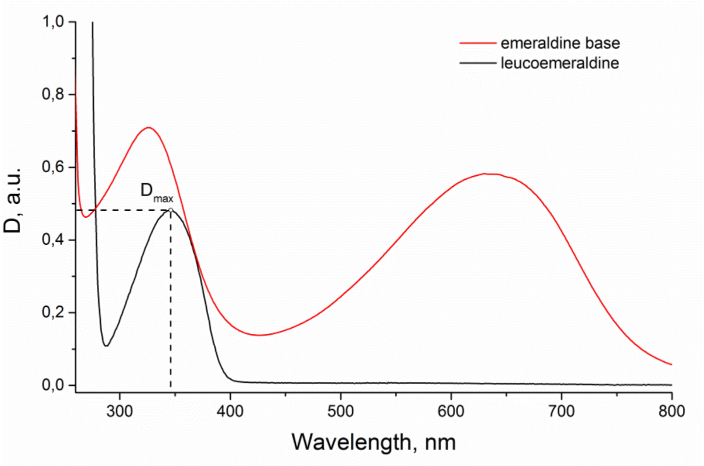

Figure 2.3 – The typical absorbance spectra of PANI nanocomposite

2.3.3 FTIR spectroscopy measurements

The Fourier Transform Infrared Spectroscopy (FTIR) spectra of PANI based materials were recorded with the Bruker Vertex 70 spectrometer at a resolution of 1 cm^{-1}. The samples mixtures with KBr were used for pellets preparation. Additionally the spectra were used for evaluation of oxidation degree of pure PANI and its phase in nanocomposites (Figure 2.4) [198-201].

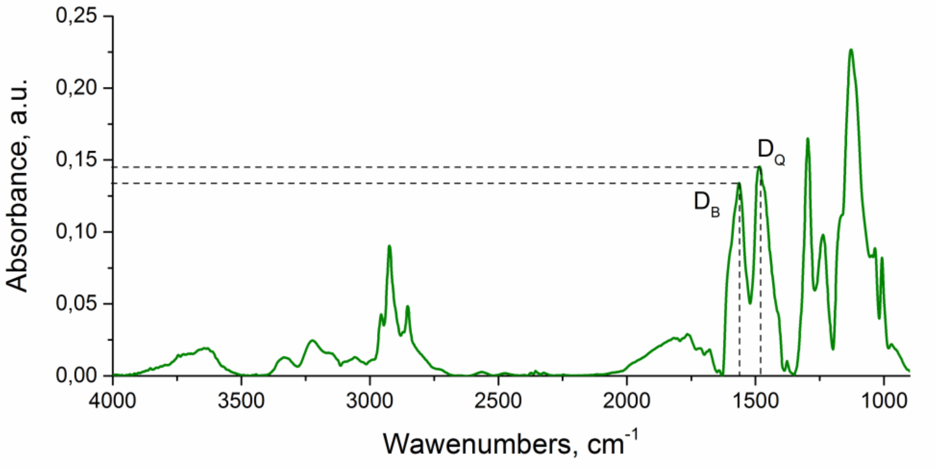

Figure 2.4 – The FTIR absorption spectrum of PANI based material

Authors [202, 203] proposed to consider the oxidation degree as a ratio of quinonoid to benzenoid units. However, the more rational is approach considering the

PANI oxidation degree (*OD*) as a ratio of quinonoid (D_Q) to total number of quinonoid and benzenoid ($D_Q + D_B$) units absorption peak heights is proposed (formula 2.1).

$$OD = \frac{D_Q}{D_Q + D_B} \tag{2.1}$$

2.3.4 Molecular mass determination

The PANI molecular weight was estimated by gel permeation chromatography method using Du Pont LC System 8800 with Azorbax bimodal exclusion columns and ultraviolet detector. Samples preparation procedures are similar to ones used for spectroscopic measurements. At first, the pure PANI and its nanocomposites were dedoped with 0.5% water ammonia solution. The dry powder of dedoped material was reduced to leucoemeraldine state by dissolution in 5 ml N-methylpyrrolidone (NMP) containing 0.5 g of ascorbic acid. The obtained leucoemeraldine solutions were centrifuged for 15 min at 5000 rpm in order to remove the metal oxide nanoparticles. The column temperature was held at 50 °C. The NMP solution containing 0.02 wt% LiCl was used as the eluent.

2.3.5 Structure and morphology characterization

The X-ray diffraction (XRD) measurements were carried on the automatic computer-controlled X-ray diffractometer DRON-3M with CuKα radiation (λ= 1.541 Å). Small-angle X-ray scattering (SAXS) data are reported in reciprocal space as intensity *vs* the scattering vector magnitude (q), where $q = (4\pi\cdot\sin\theta)/\lambda$. Transmission and scanning electron microscopy (TEM and SEM) images were obtained with a help of the JEOL JEM-1400 and HITACHI S-4300 SE/N microscopes respectively.

2.3.6 Polymer materials thermooxidation stability characterization

The data on polymer materials thermooxidation stability [204, 205] were obtained with a Paulik-Paulik-Erdey Q-derivatograph under air at a heating rate of

10°C/min. The tested range is 25 – 900 °C. The used samples weight was 50 – 100 mg.

2.3.7 PANI nanocomposites photostability examinations

The photostability of pure PANI and its nanocomposites with metal oxide nanoparticles [206] were examined under atmospheric conditions (t=18°C, RH=40%) in a closed from external lite box reactor, using the 8W ultraviolet fluorescent lamp (Delux F8W/BL) with the irradiation maximum centered at 367 nm and placed at the distance of 15 cm from the samples (Figure 2.5).

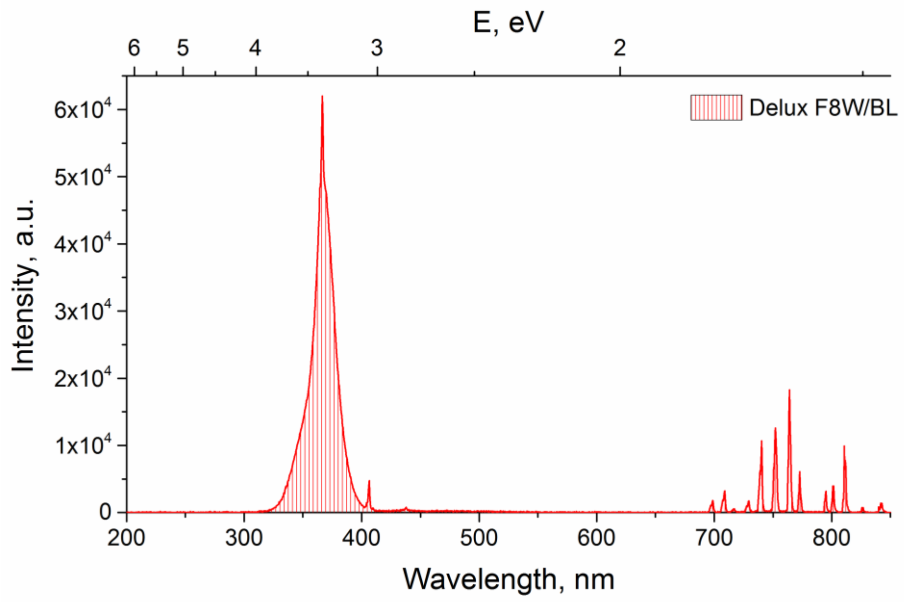

Figure 2.5 – The irradiation spectrum of Delux F8W/BL fluorescent lamp

All the samples were dispersed in chlorobenzene and casted into the Petri dish in order to form thin uniform layer with the total area ~78.5 cm^2. The irradiation was continuously carried out for 2 weeks. Then the samples were gathered, dedoped and the obtained dry powder of emeraldine base was dissolved into the NMP. The obtained solution were centrifuged in order to remove nanoparticles and investigated with the Varian Cary 50 UV-Vis spectrophotometer.

2.3.8 Conductivity measurements

The electrical conductivity measurements of powders of synthesized PANI and its nanocomposites were performed using their pellets with diameter d=2.7 mm, formed by applying a force F=600 N. The used approach utilized the two-electrode scheme, based on designed by us cell, allowing the conductivity measurements by placing the pellet between the gold covered electrodes 1 and 2, separated with the Teflon gasket (Figure 2.6). The pellet electrical resistance was measured with the UNI-T UT70D digital multimeter.

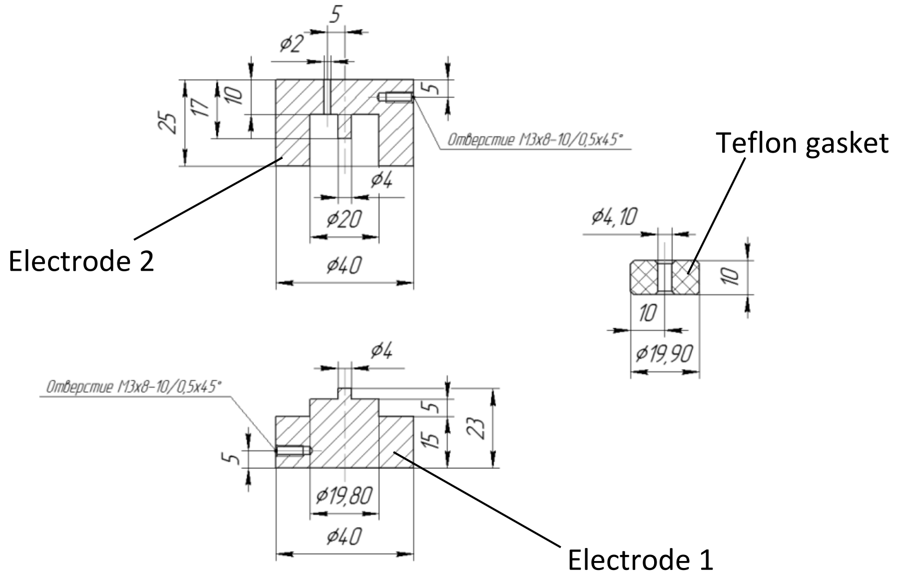

Figure 2.6 – The two electrode scheme for conductivity measurements

2.3.9 Sensing properties characterization by chemoresistive method

The metrological sensing parameters of the synthesized materials were measured using a flow-type experimental system (Figure 2.7) [84, 188].

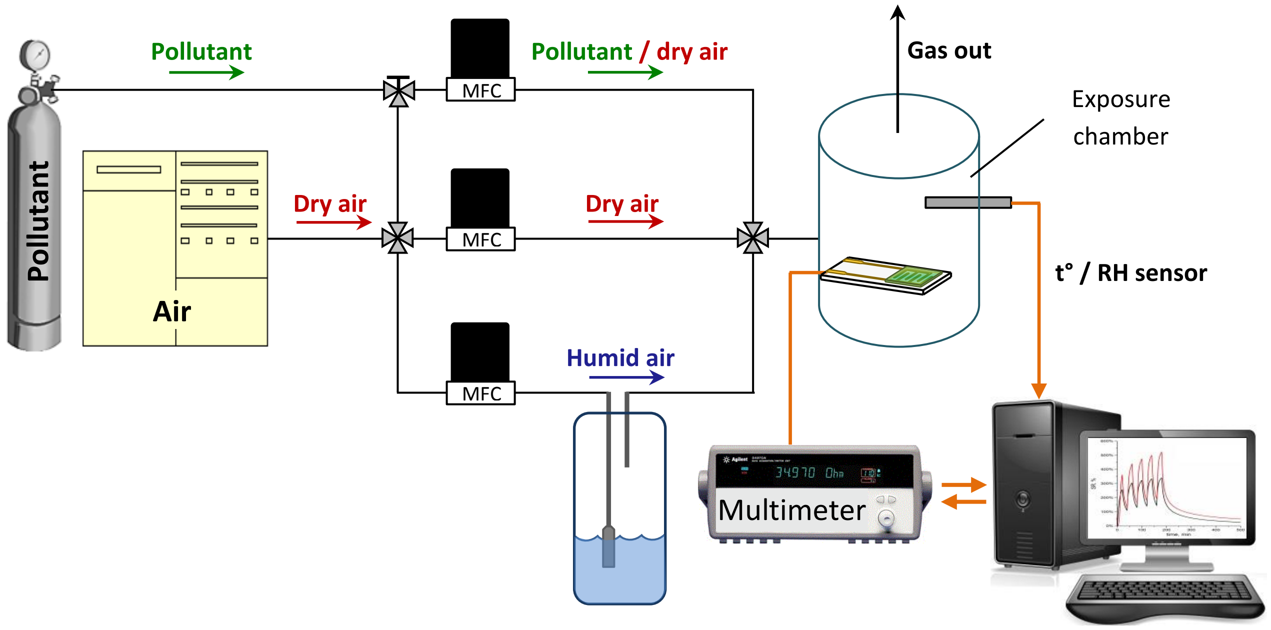

Figure 2.7 – Schematic view of sensing properties measurement system

The purified air from the zero air generator (Whatman 76-804) splits into dry and humid air flows. The humidity level inside experimental chamber was controlled by variation of their ratio. The desired analyte concentration inside chamber was generated using mass flow controllers by mixing pollutant from a standard gas cylinder (PRAXAIR Company) with purified air from zero air generator. The sensors resistance changes were continuously measured with a connected to computer digital multimeter (Agilent 34970A) as a function of pollutant concentrations and exposure time. The experimental procedure included few steps. At first, synthesized pure PANI and nanocomposites were dispersed in organic solvent (chlorobenzene, dichloroacetic acid (DCAA) and homogenized in ultrasonic bath. Then samples were deposited onto interdigitated electrodes (Au/textolite) by drop-casting and dried under vacuum at 80 °C for 72 hours (Figure 2.8). The multisensors card comprising an array of 400 electrodes (4 plates, each of 100 pcs.) with investigated materials was placed inside thermostabilized exposure chamber (Figure 2.9).

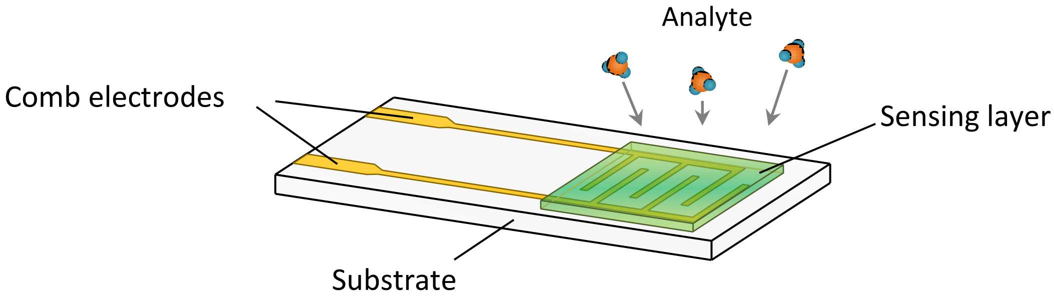

Figure 2.8 – Interdigitated electrode with deposited polymer

The measurement protocol involved three stages. At first stage (I), the initial resistance R_0 was estimated as a mean of resistance values of sensing material, measured during 5 minutes in the flow of purified air. On the next stage (II), after the exposition to analyte (ammonia or amines) sensors changed their resistance due to interaction of active layer with the analyte molecules which compete with PANI for its dopant (Figure 2.10). On the last stage (III), the sensor was flushed with air from zero air generator, resulting in desorption of adsorbed pollutant molecules and resistance decrease to its initial values level.

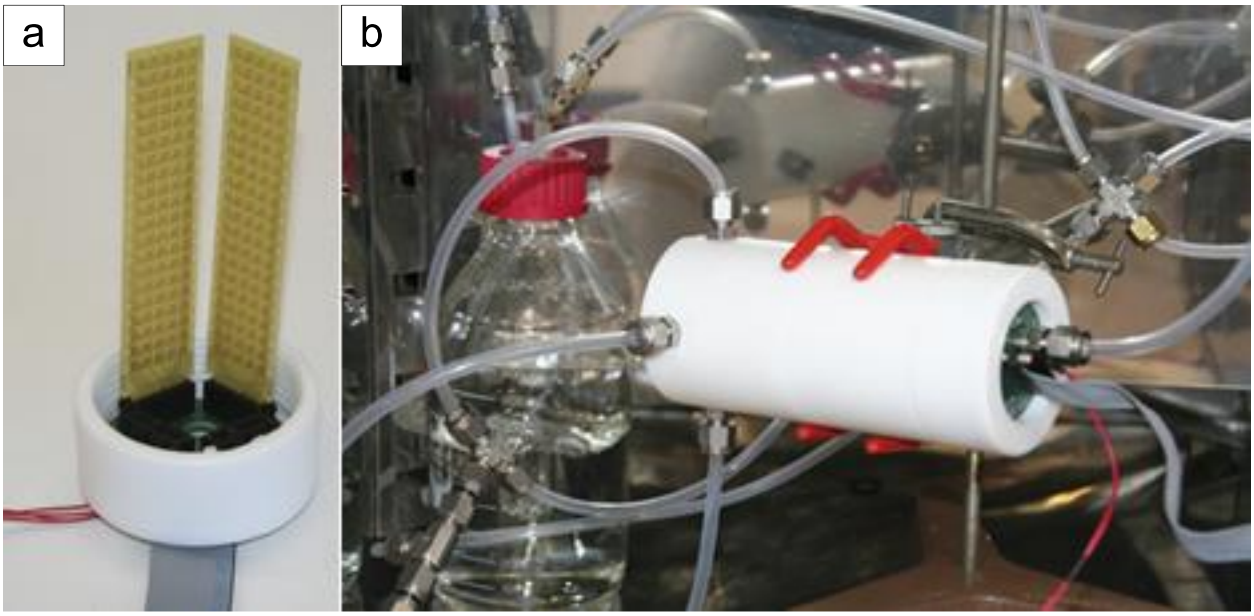

Figure 2.9 – The appearance of exposure cell built for simultaneous measurement of up to 400 sensors: **(a)** electrodes array (2 cards from 4 are shown) **(б)** exposure cell in climate control chamber

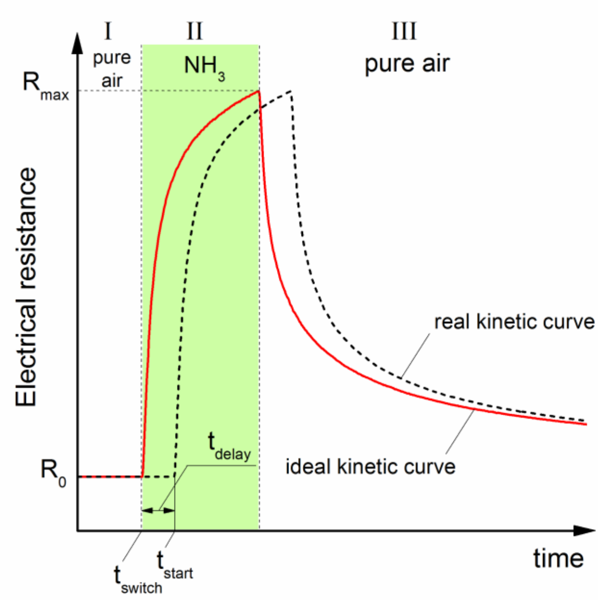

Figure2.10 – The dynamics of sensors resistance change

Normally, upon reaction with analyte, sensor reaches the saturation, corresponding to the achievement of equilibrium in adsorption-desorption processes. However, the time needed by system to reach the steady state can be quite long. That is why, in view of great adsorption potential of synthesized materials, in this work the duration of exposition to analytes was limited to 5 min, and maximum resistance value ($R_{\max}$) was used instead of $R_{90\%}$, corresponding to 90% of saturation resistance value. Thus, for the simplicity of comparison of samples with different initial resistance, the sensor responses to these analytes (SR) were calculated as relative change of the sample resistance ($R_{\max} - R_0$), compared to initial resistance value (R_0):

$$SR = \frac{\left(R_{\max} - R_0\right)}{R_0} \times 100\% \qquad (2.2)$$

It should be noted, that while in ideal case the time of switch to analyte flow (t_{switch}) coincides with the time when sensors start to react with pollutant (t_{start}), the ~2.3min time lag (t_{delay}) necessary for purging the exposure cell with an air-analyte mixture was observed for the system used in this work. In this regard, in calculations of sensors response time the t_{start} value was used as “zero time” instead of t_{switch} (figure 2.10).

3 SPECIFICITIES OF PANI NANOCOMPOSITES FORMATION

The aniline polymerization process is accompanied by synchronous spectral, color, pH, temperature and open circuit potential (OCP) changes [103, 207]. Therefore, monitoring of these kinetic parameters provides the real-time information concerning the transformations occurring in the reaction mixture. The most convenient parameter is OCP. It reflects the evolution of polyaniline oxidation state during polymerization [98, 102, 103].

The Figure 3.1 demonstrates the OCP profile typical for pure PANI polymerization. The whole process can be divided into four stages (see section 2.1): induction period (t_1) with no visible change in the reaction mixture, oligomers formation (t_2), appearance of insoluble pernigraniline phase (t_3) and final monomer oxidation by pernigraniline (t_4) [98, 103].

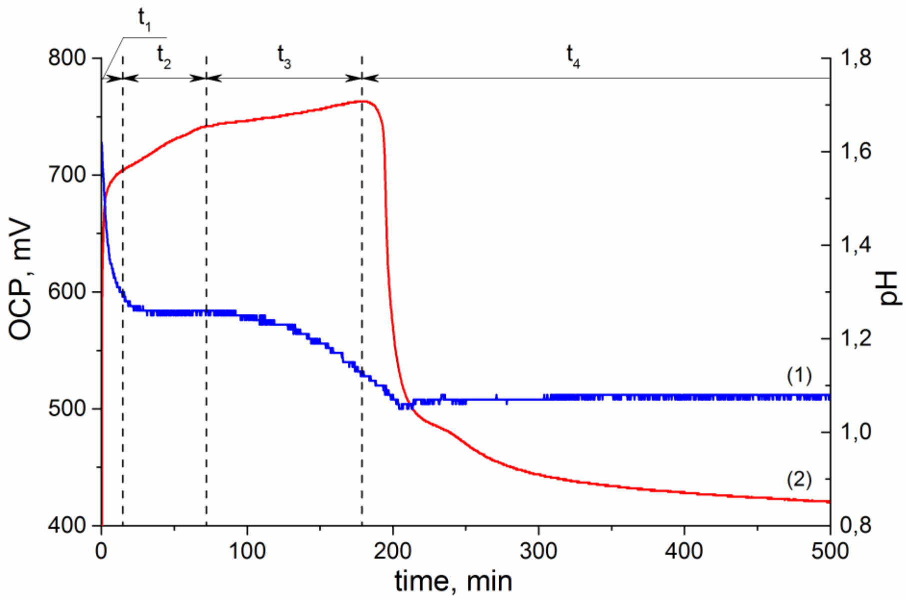

Figure 3.1 – The evolution of (1) pH and (2) OCP profiles during aniline polymerization

The presence of dispersed nanoparticles accelerates the aniline polymerization process [208]. However, the acceleration rate differs for every stage and strongly depends on synthesis conditions (e.g. reagents concentration, oxidant nature, nanoparticles type etc.). Authors [98] report about differences in OCP profile shape when the APS and weaker oxidants are used. Furthermore, the formation of pernigraniline shells on the surface of nanoparticles can shorten the t_2 and t_3 stages duration due to own catalytic activity [98]. The OCP potential is a powerful instrument that allows easy monitoring of PANI synthesis at different stages. It gives the possibility to see any abnormalities from the normal polymerization process, as well as to control the PANI layer thickness at nanoparticles surface. Altogether it affects the yield and final materials properties. Therefore, this chapter is devoted to investigation of changes occurring during the aniline polymerization and influence of synthesis parameters, in particular, metal oxides nanoparticles and used sulfonic acid-dopants structure on its kinetics.

3.1 Influence of PANI content on polymerization kinetics

The purpose of this study is to investigate the kinetics of aniline chemical oxidative polymerization both in absence and presence of different quantities of the TiO_2 nanoparticles. The used approach includes continuous monitoring of OCP and pH changes. This approach is simple and allows determining kinetic parameters of aniline polymerization process without additional procedures including linear sweep cyclic voltammetry [94], gas chromatography [208], calorimetry [209], surface pressure [210], proton NMR spectroscopy [211], visible absorption spectroscopy [212, 213], quartz crystal microbalance technique [214].

We proposed a new method based on the use of characteristic points on kinetic curves (profiles) of changes in redox and pH parameters over time, corresponding to main stages of aniline polymerization. In particular, from the known general scheme (Figure 3.2), aniline polymerization is accompanied by protons release and formation of a main intermediate product pernigraniline (PN). The latter is the most oxidized form of PANI which reduces by the remains of the monomer to the most stable final PANI form, namely emeraldine salt (ES). A typical OCP and pH curves recorded in absence and presence of TiO_2 nanoparticles are shown in Figure 3.3. From Figure 3.3a the OCP maximum value and its position changes from 680 mV and 147 min to 610 mV and 45 min when An:TiO_2 weight ratios are increased from 100:0 to 5:95 respectively. The time required by a system to reach the pH steady-state mode also decreases (Figure 3.3b), indicating the aniline polymerization process acceleration.

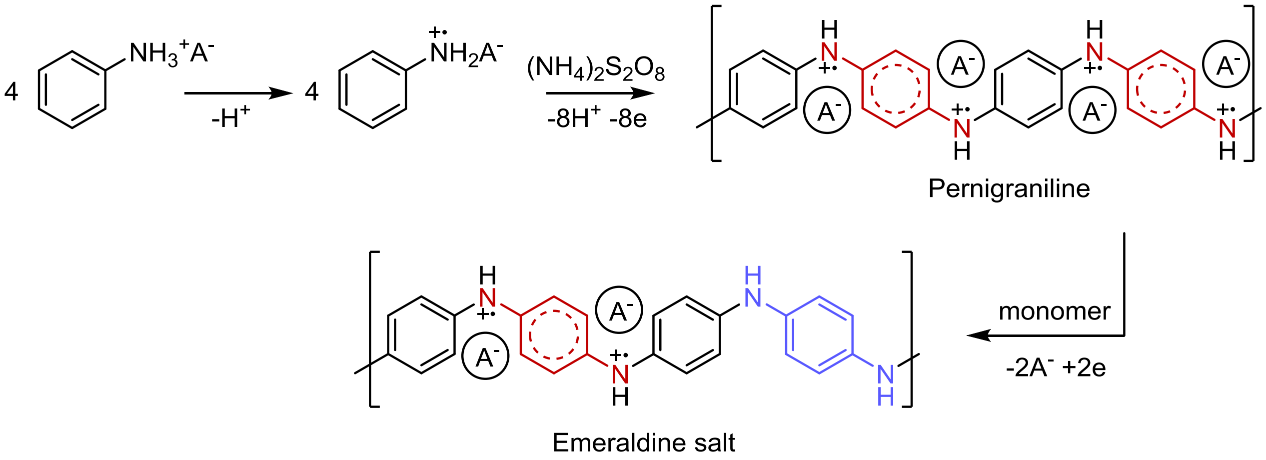

Figure 3.2 – General aniline polymerization scheme

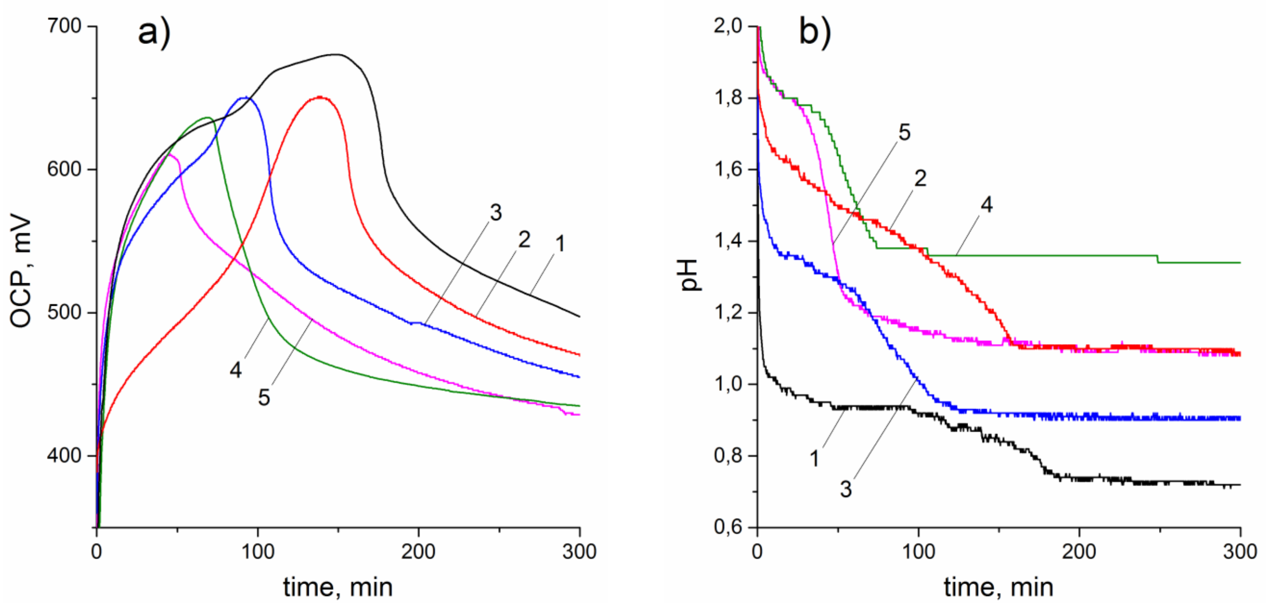

Figure 3.3 – The dependence of **(a)** OCP and **(b)** pH profiles of aniline polymerization on An:TiO_2 (anatase) weight ratio: (1) 100:0; (2) 50:50; (3) 20:80; (4) 10:90; (5) 5:95. ([An]=0.0268 M, [APS]=0.0335 M, [Acid]= 0.0402 M)

It was shown previously [215] that shape and characteristic points of the OCP profile can be used to study the effect of the dispersed phase on the kinetics of aniline chemical polymerization. These points are connected to the characteristic time corresponding to the end of induction period (t_{ip}) and OCP maximum (t_{max}). The falling part of OCP curves is described by constants (t_1 and t_2) of the approximating double exponential decay function:

$$E(t) = A_0 + A_1 e^{-t/t_1} + A_2 e^{-t/t_2} \qquad (3.1)$$

According to [215] there is a linear dependence between reciprocal values of t_{ip}, $(t_{max} - t_{ip})$, t_1, t_2 and weight fraction of the dispersed phase in the reaction medium. It allows calculation both the values of effective reaction rate constants at different polymerization stages and degree of impact of inorganic phase concentration. The presented characteristic points provide information on duration of induction period, pernigraniline accumulation and its subsequent reduction with residual aniline. The last two steps represent the two-step mechanism of aniline chemical polymerization [101, 216, 217].

In some cases the OCP profile has blurred maximum [218], significantly complicating characteristic points assessment. However, these difficulties can be eliminated if the first derivative of the OCP curve is used (Figure 3.4, curve 2).

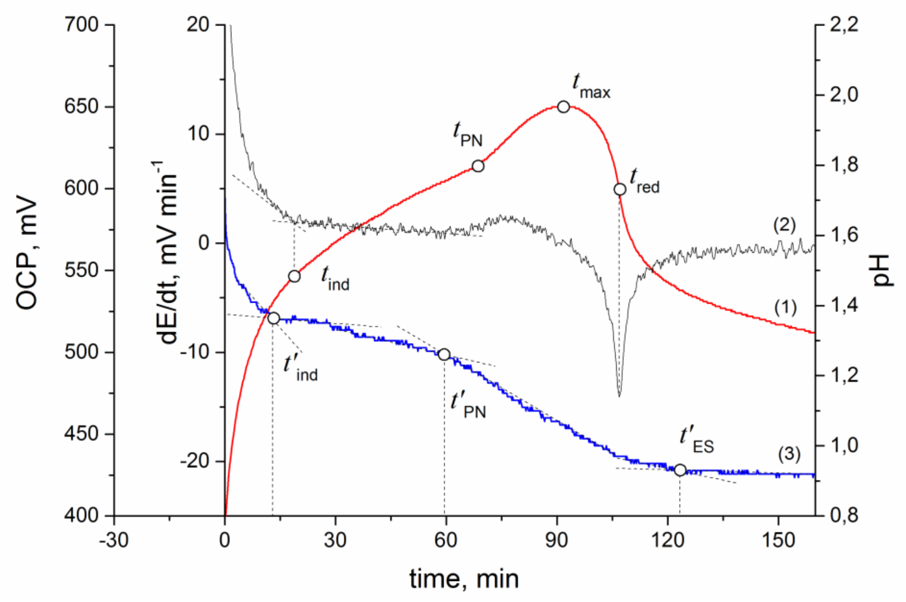

Figure 3.4 – The OCP (1), its first derivative (2) and pH (3) profiles of the aniline polymerization under anatase TiO_2/An weight ratio of 80:20. The characteristic points of curves are also shown.

One can see that position of t_{ind} characteristic point, corresponding to the induction period, correlates well with the inflection point in the graph of the first derivative. As will be shown below, the inflection point in the falling part of OCP curve (t_{red}) is easily determined by the position of the minimum on the first derivative curve and can be used instead of t_{max}. Apparently, first point more accurately defines the termination of PN formation as well as APS consumption which additionally confirms by the termination of pH value decrease and reaching the constant value.

Despite a certain difference between the values of t_{max} and t_{red} in case of blurred OCP maximum, both points almost coincide when the peak is sharp [215].

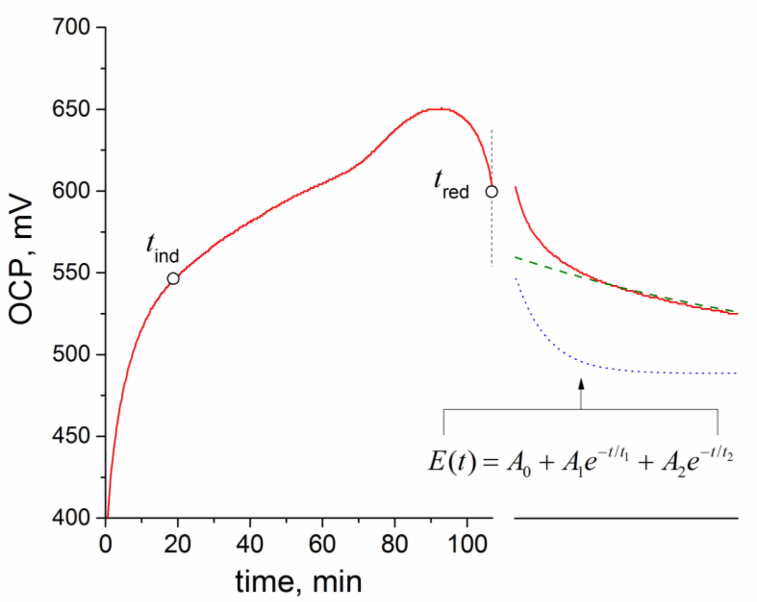

Figure 3.5 – The typical OCP profile of aniline polymerization process on the example of solution with ratio An:TiO_2 (anatase) = 20:80 wt.%

Thus, for better understanding of kinetic features of aniline polymerization in the presence of dispersed TiO_2 nanoparticles, for the first time the method of characteristic points was applied also to pH curves. From the figure 3.4 at least three additional characteristic points can be observed, namely t'_{ind}, t'_{PN} and t'_{ES}. These break points correspond to induction period and two steps of PN accumulation respectively. Since the t'_{PN} point locates close to an appearance of insoluble PN phase (t_{ind}) [98, 103] and divides pH curve into regions with strongly different slopes, it can be identified as transition from homogeneous to heterogeneous stage of PN accumulation. It should be noted, that t_{PN} point can be absent on OCP curves (Figure 3.3, curves 1, 2) and position on OCP and pH curves can diverge. Such behavior most likely stems from the different physicochemical nature of monitored parameters: pH level indicates the current proton concentration, while OCP is more complex parameter, depending on activities (effective concentrations) of all presented in the reaction mixture components. Nevertheless, the results of semiquantitative estimation of reaction kinetic parameters based on use of characteristic points give close values. In particular, the reciprocal values of separate polymerization stages duration (determined by OCP and pH profiles) linearly depend on nanoparticles weight fraction (Figure 3.6), and can be described by next equation:

$$1/t_{ch} = a + bf_{wt}^{TiO_2} \tag{3.2}$$

where t – duration of separate polymerization stages duration (t_{ind} and t'_{ind} – induction period, ($t_{\max} - t_{\text{ind}}$) – PN accumulation);

a, b – coefficients of equation;

$f_{wt}^{TiO_2}$ – weight fraction of TiO_2 nanoparticles in reaction medium.

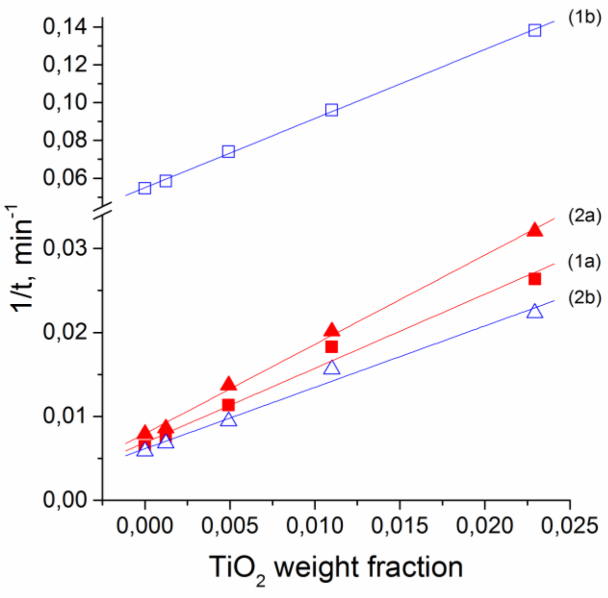

Figure 3.6 – The dependence of reciprocal values of duration of (1) induction period, (2) PN accumulation from the TiO_2 nanoparticles content in reaction medium, calculated using **(a)** OCP profiles and **(b)** pH profiles.

The results of the linear fitting are summarized in table 3.1. Almost all reciprocal values of the indicated parameters show good linear relationships (see correlation coefficients). The only exception is the value of $1/t_1$ which probably stems from the error growth in calculations with the increase of TiO_2 weight fraction in reaction medium.

Table 3.1 Parameters of linear dependences shown in figure 3.6

1/t	a	b	Correlation coefficient	Corresponding stage
$1/t_{\mathrm{ind}}$	0.046	1.02	0.976	Induction period
$1/t'_{\mathrm{ind}}$	0.055	3.66	0.998	
$1/(t_{\max} - t_{\mathrm{ind}})$	0.0078	1.06	0.997	PN accumulation
$1/t_1$	0.021	5.1	0.941	PN reduction with the residual monomer
$1/t_2$	0.0029	0.17	0.998	

The analysis of OCP profile downturn after reaching the maximum allowed us to estimate rate constants k_2 of aniline polymerization heterogeneous stage from the known general kinetic equation [208]:

$$-d[An]/dt = k_1[An][Oxidant] + k_2[An][PANI] \tag{3.3}$$

where $[An]$, $[Oxidant]$, $[PANI]$ are concentrations of aniline monomer, oxidant and PANI respectively. Constants k_1 and k_2 characterize the rate of homogeneous and heterogeneous polymerization stages.

According to the literature [102, 211, 219], the rate constant k_1 is strongly influenced by starting reagent concentrations, the presence of catalysts and temperature. As synthesis conditions and methods of measurement differ in different works, the values of the constants k_1 also vary up to several orders of magnitude. In this regard, the rate constant k_2 is considered as more reliable. We have shown for the first time, that constant k_2 can be estimated using the position of OCP profile characteristic points, in particular, k_2 is inversely proportional to the total duration of the heterogeneous stage (including PN accumulation and reduction with monomer). Typically, the beginning of the final polymerization stage coincides with OCP maximum [103, 215]. However, in presence of the dispersed phase OCP maximum is blurred, so we used the position of the inflection point (t_{ind}), which describes the PN quantity in system. In addition, since the final section of OCP curve does not have any characteristic points and is accompanied by a sharp fall with subsequent gradual decline, it can be replaced by approximation function 3.1 (figure 3.4). Taking into account that t_1 corresponds to the sharp drop in open circuit potential and the well-known logarithmic dependence between potential and concentration ratio of oxidized and reduced reaction agents (Nernst equation), the constant t_1 can be considered as a parameter characterizing the final stage of polymerization [215]. In other words, to facilitate comparison of results obtained using different kinetic approaches presented in the literature with the proposed by us method, individual stages of PN accumulation and reduction can be presented as a joint stage of emeraldine salt formation with characteristic time ($t_{\text{red}} - t_{\text{ind}} + t_1$). Therefore, reaction rate constant k_2, can be expressed as:

$$k_2 = {}^{1}\!\big/\!\left(t_{\text{red}} - t_{\text{ind}} + t_1\right)\left[An\right]^{-1} \tag{3.4}$$

It was found that increase of the dispersed phase content in reaction medium results in k_2 growth, which in turn affects the polymerization yield (table 3.2).

Table 3.2 The influence of used An:TiO_2 (anatase) weight ratio on the kinetic constant k_2

An:TiO_2, wt.%	5:95	10:90	20:80	50:50
$k_2\times10^4$, $M^{-1}\cdot min^{-1}$	3.53	1.94	1.51	0.93

Summarizing the above, comparison of approaches using redox and pH curves confirms their equivalence and possibility of their use for semiquantitative estimation of reaction kinetic parameters. An important result of this study is the finding that polymerization rate increases linearly with the growth of TiO_2 nanoparticles content. In addition, it was found that the acceleration degree of each subsequent polymerization stage is different. The reason for this acceleration is probably stems from adsorption of reaction members on the surface of dispersed phase and hence the formation of local concentration maxima of reactants, compare to the solution void volume. Furthermore, PN and PN coated nanoparticles can also accelerate the polymerization reaction due to autocatalytic effect.

3.2 The influence of dopants structure on aniline polymerization kinetics

The aniline polymerization is complex process affected by many factors (see section 1.3) one of which is used acid-dopant. This factor is in close dependence with resulting polymer structure can be crucial for PANI sensing properties [93, 137, 164]. However, despite the extensive use of sulfonic acids as dopants, there is still no consistent study on the influence of their alkyl moieties length on polymerization kinetics, as well as resulting PANI properties. Thus, in order to shed more light on this aspect of aniline formation peculiarities, the current study was made.

Naturally, the investigation of dopants effect on the polyaniline formation presupposes the maximum isolation from other factors interference. Thus, the study was performed in the absence of nanoparticles in order to exclude their possible influence on polymerization process. The used acid-dopants were represented by the raw of sulfonic acids with different length of alkyl chain, namely dodecylbenzene-, benzene-, toluene- and camphorsulfonic acids. The additional experiment with hydrogen lauryl sulfate was also performed. The kinetic curves of the aniline polymerization in the presence of different dopants are presented in figure 3.5.

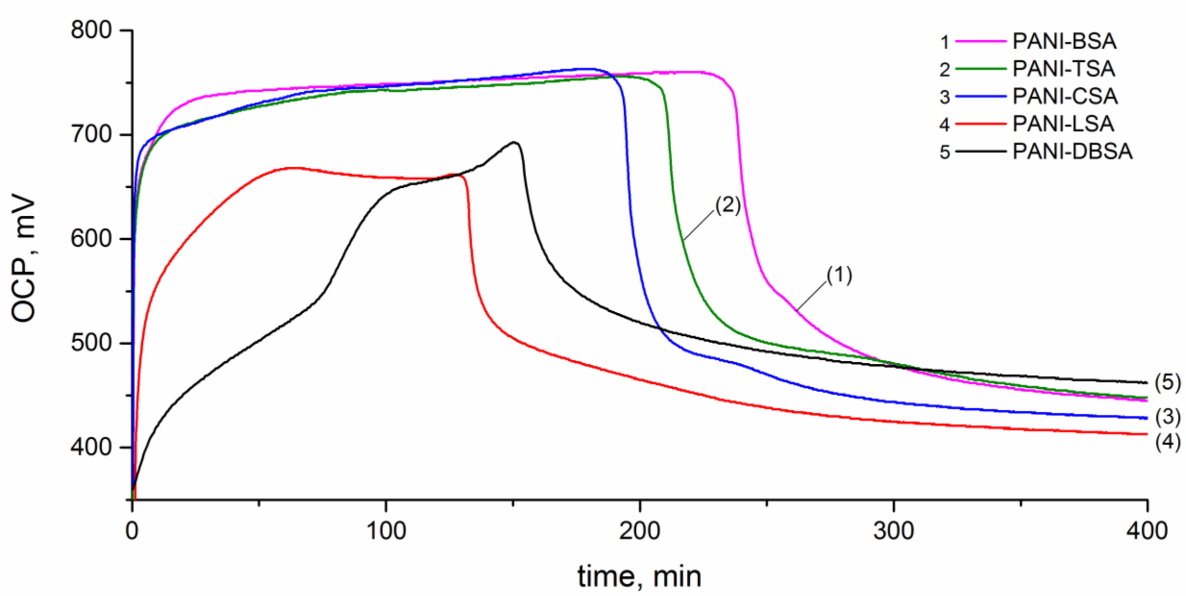

Figure 3.5 – The dopants influence on aniline polymerization speed ([An]=0.0268 M, [APS]=0.0335 M, [Acid]= 0.0402 M)

The kinetic constants of aniline polymerization in the presence of different dopants were calculated using the equation 3.4 and presented in table 3.3.

Table 3.3 Dopant effect on the aniline polymerization process

Dopant	t_{ind}, min	t_{max}, min	t_1	$k_2 \times 10^4$, $M^{-1} \cdot min^{-1}$
BSA	20.1	223.4	5.0	1.29
TSA	20.2	198.0	7.2	1.45
CSA	24.3	181.9	5.1	1.65
LSA	60.2	130.5	3.1	3.65
DBSA	72.1	151.6	13.9	2.52

Presented data indicate the significant effect of used acid-dopant anion size and surface activity on aniline polymerization process. In particular, from the OCP profiles one can see that aniline polymerization in the presence of relatively “small” anions (BSA, TSA, CSA) occurs slower compare to “large” surface active LSA and DBSA. In particular, constants k_2 in case of LSA and DBSA 1.5 – 2 times higher compare to BSA, TSA and CSA (table 3.3). At the same time, acids are not directly involved into the polymerization process and their influence is limited to dissociation into proton and organic anion. The latter, depending on a size and surface activity, can affect not only the oxidant access to monomer, limiting the polymerization rate, but also determines the PANI final morphology and properties [220].

The existence of such anion effect matches well with the radical-cation character of the aniline polymerization in the micellar solution. Thus, the positive charge of aniline intermediates (monomer cation-radicals / growing PANI chains) is significantly compensated by acid-dopant anions. Taking into account the constancy of used in experiments acid-dopants concentration and the fact that sulfonic acids are relatively strong acids (pKa < –1) [221-224], the differences in polymerization media pH values can be neglected (Figure 3.8).

Therefore, under the synthesis conditions the practically complete aniline/PANI protonation is expected, allowing assigning the aniline polymerization peculiarities to acid-dopant anions effect. In particular, the bulky hydrophobic groups of the DBSA and LSA anions possess the surface-active properties and hence are able to solution structuring. They can form a hydration shell through hydrophilic-hydrophobic interactions with water. As a result, at concentrations above critical

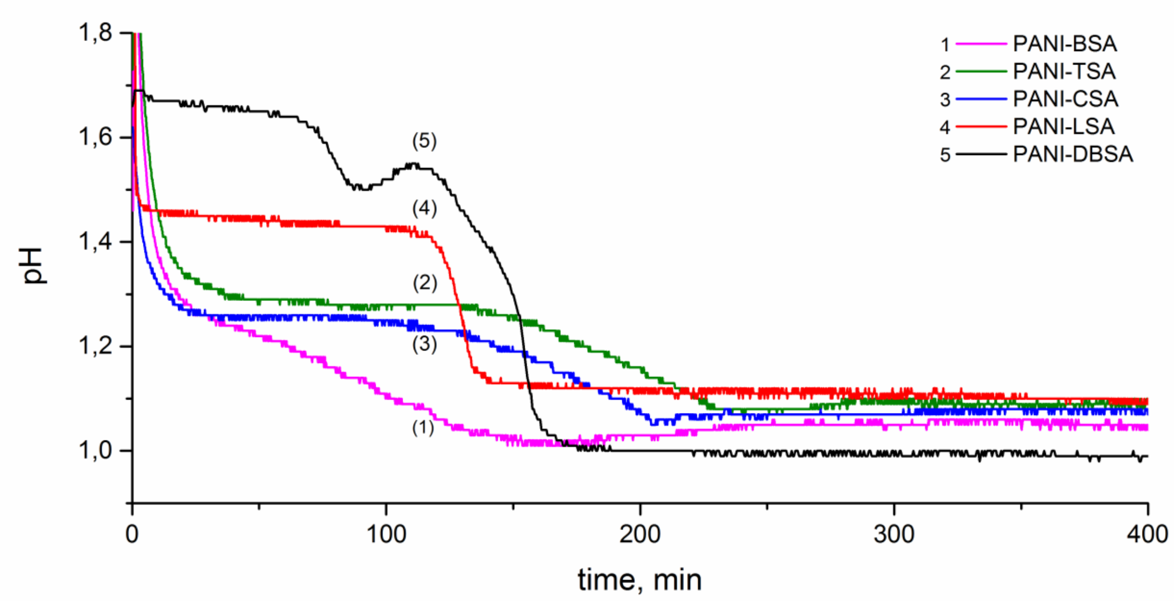

Figure 3.6 – The dopants influence on pH value during aniline polymerization ([An]=0.0268 M, [APS]=0.0335 M, [Acid]= 0.0402 M)

micelle concentration (CMC) these acids can form micelles, hindering interactions between reaction medium components (protonated aniline, growing charged PANI chains, water, oxidant and acid anions). Taking into account, that DBSA and LSA CMC values (~ $8.4 \cdot 10^{-3}$ M and ~ $6.9 \cdot 10^{-3}$ M respectively [225, 226]) are significantly lower than used in this work acid-dopants concentration (0.0402 M), and the excess (0.0134 M) of free acid is present even after interaction with aniline (0.0268 M). In other words, the coexistence of two types of micelles formed of only acids anions and acids anion-anilinium cations complex is assumed (Figure 3.7).

It is known [226], that at lower concentrations micelles have the form of short prolate spheroids or cylinders, with a possibility of transformation to the long cylindrical or worm-like micelles. Furthermore, the high surfactant concentrations lead to the formation of complex lamellar and hexagonal structures. Taking into account the presence of acid-dopant excess and the fact that organic counterions strongly decrease CMC [227], the formation of “shielding” micelles close around the anilinium salt micelles can be suggested. Such micellar “shell” hinders the access of oxidant anions ($S_2O_8^{2-}$) to monomer and prolongs the duration of induction period (see table 3.3). However, the surfactant micelle self-organization effect is observed. It leads to concentration of the low molecular weight aniline species and accelerates the

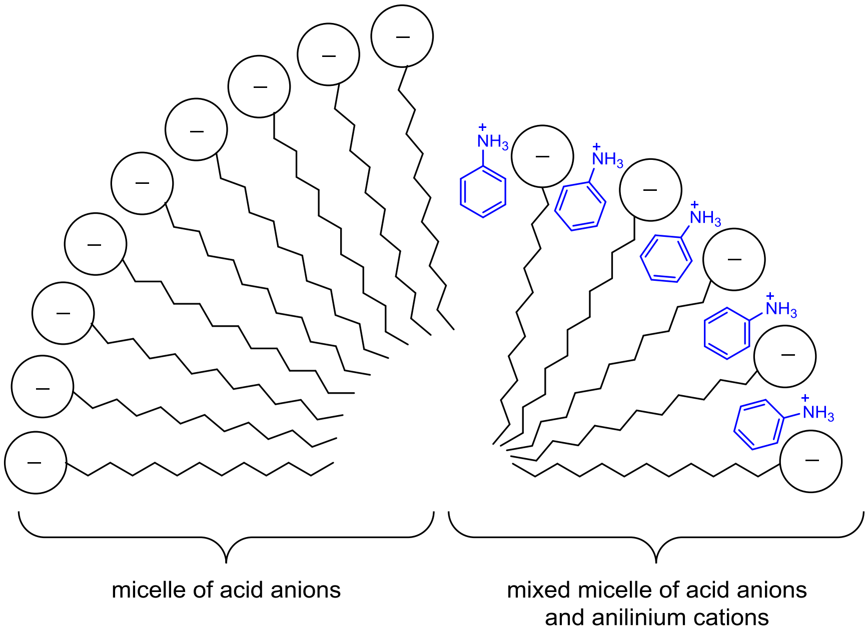

Figure 3.7 – The scheme of micelles presented in reaction medium

last polymerization stage. The aniline chain growth in the presence of micelles, acting also as a kind of matrix, is possible both by the polymerization of bound to matrix aniline and accession of the formed in solution bulk short PANI chains. Naturally, the difference in micelles shape influences morphology and final properties of PANI structure.

At the same time, non-surfactant acids with small anions (BSA, TSA, CSA) demonstrate opposite behavior: the initial polymerization stage occurs fast, while the rate of oligomers/pernigraniline accumulation occurs slower. Such phenomenon is most likely due to their decreased formation rate in the solution void volume.

Summarizing the above, the rate of polymerization process in the presence of small dopants (BSA, TSA, CSA) occurs fast at the initial polymerization stage and slows down at final, while character of the process in presence of surfactants with long alkyl moieties (LSA, DBSA), demonstrates the opposite behavior, namely slow initial and fast final stage.

3.3 Nanoparticles influence on polymerization kinetics

Among different methods of PANI composites preparation the common ones are mechanical mixing and chemical polymerization in the presence of dispersed phase. The advantage of first method is its simplicity. However, due to poor PANI solubility in majority of solvents, it is impossible to form strong interactions between the used components.

At the same time, chemical PANI synthesis in the presence of TiO_2 nanoparticles leading to polymer chains nucleation directly on the organic/inorganic interface, allows formation of strong interaction between the source components and often results in synergetic effect [228-230], manifested in advanced mechanical, electrical, optical and sensing properties. The nature of this phenomenon is probably relates to specific physicochemical interactions between aniline molecules, growing PANI chains and acid-dopant with the TiO_2 nanoparticles, possessing large surface area containing numerous hydroxyl groups [231]. The well-known PANI ability to precipitate in a form of thin layer onto any surface being in contact with the reaction medium [98, 103, 232] results in formation of core-shell. Naturally, the shell thickness and morphology depend on polymerization conditions (temperature, pH, reagents loading, etc.) and predetermine final properties of the synthesized hybrid materials.

Under the conditions of the colloidal system formed in the presence of TiO_2 nanoparticles, the use of spectroscopic methods for monitoring of transformations occurring in the system significantly complicates [103]. Nevertheless, the characteristic feature of aniline polymerization, manifested in synchronous changes of the reaction medium redox-potential, pH and temperature [103, 207], allows polymerization monitoring. The typical changes of the reaction medium pH and OCP parameters corresponding to different stages of PANI formation in the presence of dispersed phase are presented in figure 3.10.

The shown changes in pH and OCP profiles at different stages of polymerization demonstrate synchronous changes similar to reported earlier in literature [103, 207]. The period (I) corresponds to the DBSA dissolution in water. It accompanied by gradual pH and, in full accordance to Nernst equation, OCP decrease due to the solution homogenization and establishing of the same acid-dopant concentration in every point of solution.

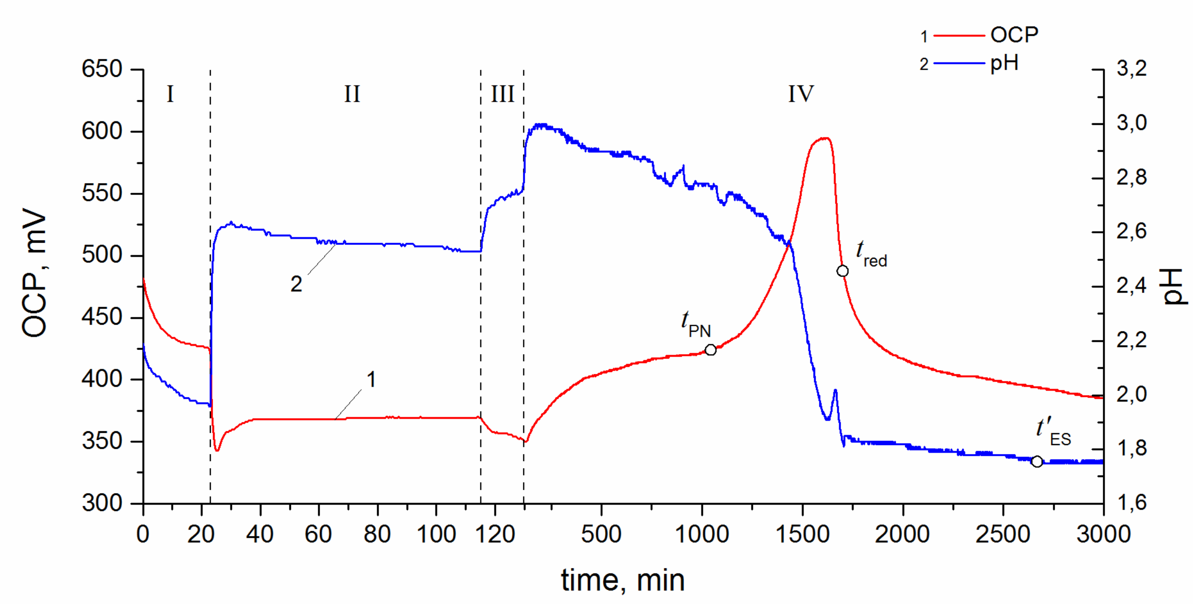

Figure 3.10 – The changes of pH and OCP parameters at different stages of PANI formation in the presence of TiO_2 (anatase) nanoparticles ([An]=0.0034 M, [APS]=0.00419 M, [Acid]= 0.00503 M)

The period (II) starts after the addition of aniline monomer and accompanied by the sharp increase in pH values, corresponding to anilinium cations formation through aniline protonation. The further reaction medium structural transformations occur due to salt-forming interaction between anilinium cation and acid anion, and in case of large dopants are manifested in the solution transparency and viscosity changes owing to micellar system formation. The completion of this process corresponds to the stabilization of OCP and pH values.

The period (III) begins after the addition of TiO_2 nanoparticles. The introduction of dispersed phase leads to solution alkalization on account of hydroxyl groups inevitably present on TiO_2 surface [233]. At the same time, the amphoteric properties inherent to TiO_2 [234-236] promote to adsorption of all solution components on the nanoparticles surface. Thus, the possibility of amines adsorption at Lewis-acid sites, via hydrogen-bonds or electrostatic interaction was shown by authors [236, 237]. The latter is more inherent to anatase (compare to rutile), due to a higher proton acidity of the surface hydroxyl groups [231]. The authors [238] also suggested the possibility of acid-base interaction with amines at Brønsted acid sites, generated upon surface sulfation by SO_4^{2-} ions which concentration under conditions of use of ammonium persulfate as oxidant is quite high. The proposed mechanisms of interaction between ionic surfactants and metal oxide nanoparticles presented in solution include covalent bonding, electrostatic interaction, formation of bilayers and micelles at high concentrations [239-241]. However, the latter is possible only in case of DBSA and LSA, while the small dopants do not form micelles. The latter studies on the interaction of sulphate species with the TiO_2 surface indicate the presence of only electrostatic interaction [242]. The authors [231] used sodium dodecylsulfate (laurylsulfate) and also did not observe direct sulphate bonding to the TiO_2 surface and suggest its adsorption rather due to electrostatic interactions.

The period (IV) starts from the OCP growth with simultaneous gradual pH decrease, corresponding to the oligomers formation and protons release. The OCP curve inflection at about 1000 min (Figure 3.10) indicates the appearance of insoluble PN phase through the macromolecules formation from low molecular mass oligomers. The OCP maximum corresponds to the PN concentration maximum [103]. The subsequent sharp OCP decrease indicates the exhaustion of oxidant, which triggers the PN reduction by monomer incorporation into polymer chain. The constancy of OCP and pH values signifies the polymerization completion. Figures 3.11 and 3.12 demonstrate nanoparticles influence on aniline polymerization process in the presence of different dopants.

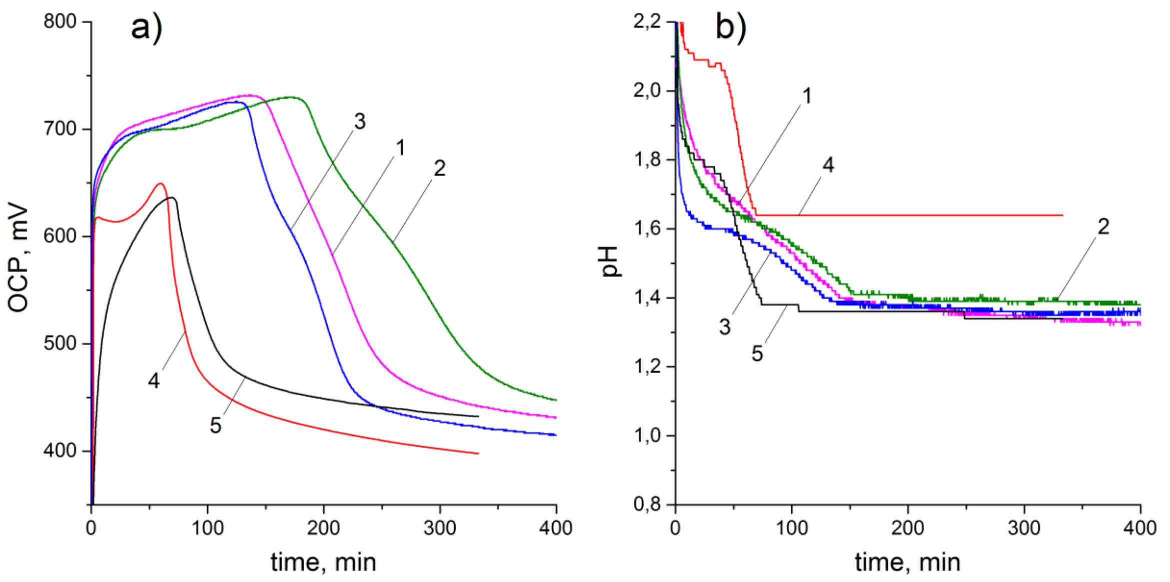

Figure 3.9 – The influence of TiO_2 (anatase) nanoparticles on the **(a)** OCP and **(b)** pH profiles of the PANI polymerization process in the presence of different dopants: (1) – BSA, (2) – TSA, (3) – CSA, (4) – LSA, (5) – DBSA. ([An]=0.0134 M, [APS]=0.01678 M, [Acid]= 0.02013 M)

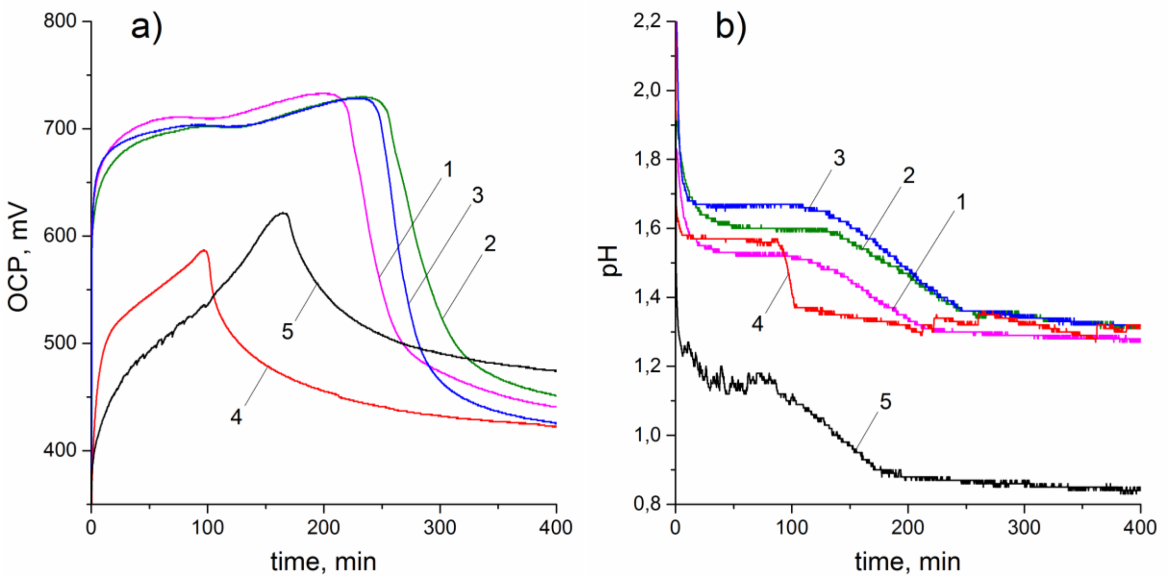

Figure 3.10 – The influence of SnO_2 nanoparticles on the **(a)** OCP and **(b)** pH profiles of the PANI polymerization process in the presence of different dopants: (1) – BSA, (2) – TSA, (3) – CSA, (4) – LSA, (5) – DBSA. ([An]=0.0134 M, [APS]=0.01678 M, [Acid]= 0.02013 M)

The results of OCP profiles kinetic analysis recorded in the presence of TiO_2 and SnO_2 nanoparticles are summarized in table 3.4.

Table 3.4 The effect of nanoparticles on parameters of aniline polymerization

Dopant	**TiO_2 (anatase)**			**SnO_2**		
	t_{ind}, min	**t_{max}, min**	**$k_2\times10^4$, $M^{-1}\cdot min^{-1}$**	**t_{ind}, min**	**t_{max}, min**	**$k_2\times10^4$, $M^{-1}\cdot min^{-1}$**
BSA	33.8	158.5	0.69	65.7	222.3	0.50
TSA	56.8	176.3	0.65	61.4	255.2	0.60
CSA	44.4	134.3	0.90	40.2	247.3	0.56
LSA	21.7	66.0	2.37	18.4	98.9	1.49
DBSA	15.4	68.3	1.77	40.2	168.1	0.91

From the table 3.4 the aniline polymerization rate constants k_2 are higher in case of TiO_2 then in the presence of SnO_2 nanoparticles. Comparing figures 3.9a and 3.10a one can see that time at which the maximum OCP is reached (corresponding to pernigraniline concentration maximum) noticeably differs for two systems. Additionally, the process of PN reduction also proceeds with different speed, manifested in different slopes of the OCP profiles final section. The nature of this phenomenon probably explained by less alkalization of reaction solution after introduction of SnO_2 nanoparticles compare to TiO_2 ones. Therefore, while the starting pH in TiO_2 containing solutions gradually decreases during the syntheses, the pH at SnO_2 containing solutions is practically constant during about first 100 minutes. Taking into account, that first period corresponds to formation of low molecular mass oligomers and comparing the positions of the OCP profiles inflection points (figures 3.11a and 3.12a), the more complete monomer to oligomers conversion in case of dispersion of SnO_2 nanoparticles can be assumed. Thus, the time necessary to reach maximum pernigraniline concentration is greater, resulting in lower k_2 values.

At the same time, in case of solution containing TiO_2 nanoparticles, aniline monomer converts to oligomers not completely which results in gradual OCP decline after reaching maximum. It should be noted, that OCP profiles obtained in solutions containing surfactants (LSA and DBSA) differ from the ones obtained with “small” dopants, which is probably connected to micellar system formation. The obtained data are in good agreement with the results on polymerization reaction yield determination (see section 3.4), namely the nanocomposites obtained in the dispersions with SnO_2 have higher yields.

3.4 The dopant and dispersed phase influence on PANI yield

The result of dopant and dispersed phase influence on aniline polymerization kinetics also manifests in different PANI yield. Indeed, from the figure 3.13a the polymerization yield in dispersion systems both for SnO_2 and TiO_2 anatase nanoparticles reaches maximum values with the surface active dopants LSA and DBSA (see section 3.2). At the same time, yields of PANI obtained in the presence of “small” dopants (BSA, TSA, CSA) are noticeably lower. This difference probably originates from micelles formation in case of use of surface-active ions LSA and DBSA, leading to monomer concentration in these micelles and, therefore, increases polymerization effectiveness. This suggestion is in good agreement with the fact that

CMC values for LSA and DBSA are 0.0069 and 0.0084 M respectively, while the concentrations of these acids during syntheses were ~0.02 M. At the same time, using these dopants in the presence of SnO_2 nanoparticles (S90, An:SnO_2 = 10:90 wt.%) results in higher yields compare to anatase TiO_2 (A90, An:TiO_2 = 10:90 wt.%), which probably connected with more complete conversion of monomer (see section 3.3).

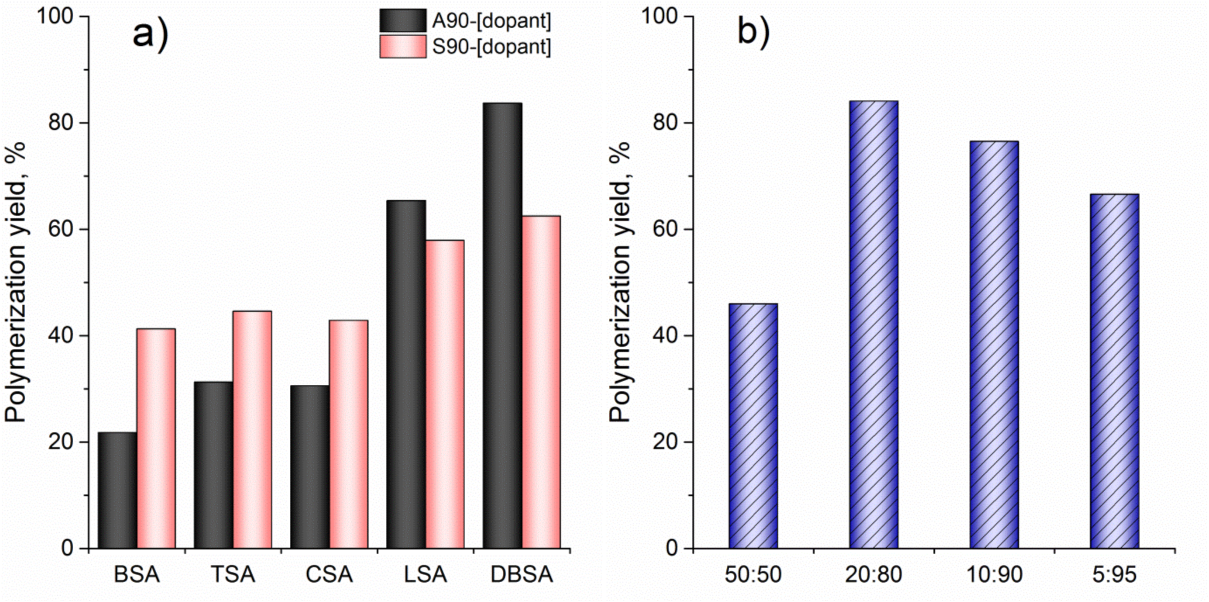

Figure 3.13 – The nanoparticles effect on PANI yield **(a)** depending on used dopant and **(b)** An:TiO_2 (anatase) weight ratio in the presence of DBSA. ([An]=0.0134 M, [APS]=0.01678 M, [Acid]= 0.02013 M)

Figure 3.13b demonstrates the influence of An:TiO_2 weight ratio into reaction mixture on polymer yield in the presence of DBSA. The increase of TiO_2 nanoparticles ratio from 50 to 80% leads significant growth (~2 times) in PANI yield, which correlates with growth of k_2 values (see section 3.3). However, further nanoparticles content increase from 80 to 90% practically do not influence on PANI yield. Moreover, further addition of TiO_2 nanoparticles results in noticeable decrease of polymerization yield. Such behavior, in general, can be explained by passing through the optimum of the polymerization An:TiO_2 ratio, which is probably connected to the degree of surface coverage by monomer and, therefore, to the ratio of aniline polymerization rates in the adsorption layer on the surface of nanoparticles and in the solution void volume.

The impact of surface coverage factor also confirms by the estimations of dimensional parameters of used chemical species. Since the molar weight (*M*) of An is 93.13 g/mole and its density (*d*) is 1.02 g/cm^3, taking the amount of substance (*n*) equal to one mole, we get:

$$V_{1\ \mathrm{mole}}^{\mathrm{An}} = \frac{M}{d} \times n = \frac{93.13}{1.02} \times 1 = 91.30\ \mathrm{cm}^3$$

As is known, the one mole of substance contains the constant number of constituent particles (Avogadro constant, N_A) namely $6.022\cdot 10^{23}$, hence the volume of one An molecule can be estimated by dividing the volume of one mole An by Avogadro constant:

$$V_{1\ \mathrm{molecule}}^{\mathrm{An}} = \frac{91.30}{6.022\cdot 10^{23}} = 1.516\cdot 10^{-22}\,\mathrm{cm}^3$$

Thus, taking the simplification that aniline molecules are spherical and during adsorption on the nanoparticles surface cover the area equal to its sphere sectional area, the minimum monomer quantity to cover all the nanoparticles with monomolecular layer at An:TiO_2 weight ratio 5:95, can be estimated as follows:

$$V_{An} = \frac{4}{3}\pi r_{An}^3 \Rightarrow r_{An} = \sqrt[3]{\frac{3V_{An}}{4\pi}}$$

$$S_{An} = \pi r_{An}^2 = \pi\left(\sqrt[3]{\frac{3V_{An}}{4\pi}}\right)^2 = 3{,}14\left(\sqrt[3]{\frac{3\cdot 1{,}516\cdot 10^{-28}}{4\cdot 3{,}14}}\right)^2 = 3{,}44\cdot 10^{-19}\ \mathrm{m}^2$$

Therefore, taking 1 g of mixture aniline with TiO_2 anatase nanoparticles (SSA=210 m^2/g), the necessary amount of An substance will be:

$$m_{An} = n_{An}\cdot M_{An} = \frac{N_{An}}{N_A}\cdot M_{An} = \frac{S_{TiO_2}\cdot M_{An}}{S_{An}\cdot N_A}$$

$$m_{An} = \frac{(210 \cdot 0.95) \cdot 93{,}12}{3.44 \cdot 10^{-19} \cdot 6.022 \cdot 10^{23}} = 0.09 \text{ g}$$

where V_{An} – volume of one aniline molecule;

r_{An} – radius of aniline molecule;

S_{An} – surface covering by one aniline molecule;

n_{An} – amount of aniline substance;

M_{An} – molar mass of aniline;

N_{An} – number of aniline molecules;

N_A – Avogadro constant;

S_{TiO2} – total surface area of dispersed TiO_2 nanoparticles.

Therefore, taken monomer quantity ($1 - 0.95 = 0.05 < 0.09$ g) is not enough to cover all the surface of nanoparticles. However, the presented calculations for simplicity do not take into account the fact that aniline in reaction solution is presented in a salt form. The latter has greater dimensions, and in case of DBSA dopant, considering the total volume taken by An-DBSA molecular complex as a sum of separate volumes of An and DBSA molecules, the necessary quantity of substance decreases to 0.03 g. Obviously, the increase of aniline fraction in An:TiO_2 weight ratio would result both in decrease of surface required to cover and increase of available in solution bulk An-DBSA molecules (table 3.5).

Table 3.5 The dependence of An:TiO_2 (anatase) weight ratio on nanoparticles covering surface

Used An:TiO_2 weight ratio	**5:95**	**10:90**	**20:80**	**50:50**
Taken An, per 1 g of composite / resulting An-DBSA weight, g	0.050/0.313	0.100/0.626	0.200/1.252	0.500/3.130
Minimum monomer / An-DBSA weight to cover all nanoparticles, g	0.090/0.034	0.085/0.032	0.076/0.028	0.047/0.018

The introduction of nanoparticles leads to the formation of core-shell structure, where the TiO_2 is a core covered with PANI shell. However, nanoparticles high surface energy leads to their agglomeration and to decrease of total specific surface area. In turn, it leads to the appearance in reaction medium of two types of particles existing in dynamic equilibrium: free polyaniline and polyaniline-encapsulated TiO_2 nanoparticles or agglomerates is assumed [117]. This suggestion is in good agreement with provided calculations on dispersed phase adsorption capacity.

The additional factor stimulating oligomers formation in the bulk of reaction solution is the use of DBSA as dopant. Anions of this acid have large size stipulating imposition of steric limitations and, therefore, hindered oxidant delivery to aniline molecules adsorbed on the surface of nanoparticles in form of An-DBSA salt [6]. The increase of nanoparticles content leads to the decrease of concentration of not-adsorbed part of An-DBSA, and therefore increases both PANI yield and molecular weight. However, the too high content of disperse phase reduces the reaction yield and significantly decreases polymer molecular weight (see section 4.1). Such phenomenon probably explained by the peculiarities of the used nanoparticles. In particular, introduction of relatively large quantity of nanoparticles with surface hydroxyl groups results in partial solution alkalization and shifts the starting pH, which leads to incomplete conversion of monomer into oligomers (see section 3.2). Additionally, the highly developed surface of TiO_2 nanoparticles stipulates the growth of macromolecules in thin layer or, even, to appearance of discontinuity in reagents adsorption layer and formation of separate polymerization “islands”.

* * *

Summarizing the above, the main factors influencing the kinetic features of the aniline polymerization of PANI yield under used experimental conditions are the presence of dispersed phase in the reaction solution and nature of used acid-dopant. The formation of insoluble PANI phase on the surface of nanoparticles allows obtaining nanocomposite materials, which differ from conventional mechanical mixtures by greater uniformity of polymer distribution and significantly stronger interaction between source components. The latter is achieved through the growth of polymer chains directly on the surface of the nanoparticles resulting in core-shell structure.

Obviously, characteristics of the polymer membrane covering nanoparticles depend on used polymerization conditions (reagents ratio, nature of nanoparticles, dopant type, etc.). In turn, it could affect performance properties of PANI nanocomposites.

4 PROPERTIES OF PURE PANI AND ITS HYBRYD MATERIALS

The characterization of synthesized materials is an important stage, giving possibility to evaluate the influence of different parameters on resulting properties. Naturally, the understanding of impact of used in hybrid materials synthesis nanoparticles, their content, as well as nature of used acid-dopants plays crucial role in creation of the composites with good processability, improved chemical and physical parameters.

Thus, in this chapter, we present the results of obtained materials comprehensive characterization by different methods and techniques. In turn it allows us to understand better the impact of aforementioned kinetic aspects on nanocomposites formation, influence of nature of used dopant, inorganic phase, conducting polymer content in the nanocomposite, as well as influence of dispersing solvent onto important from the practical point of view nanocomposite properties.

4.1 Molecular mass measurements of pure PANI and its nanocomposites

The results on molecular weight determination of pure PANI and its phase in nanocomposites are presented in figure 4.1. The molecular weight distribution has typical for PANI character [243, 244]. In all cases the low molecular weight fraction dominates, similar to that of conventional polyaniline [245].

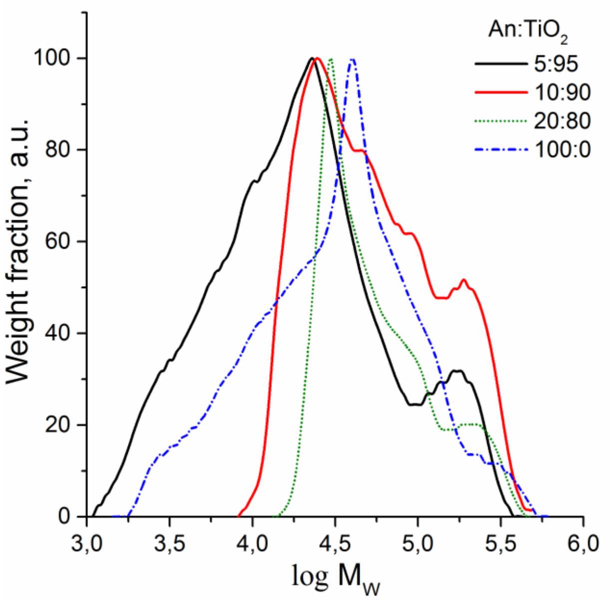

Figure 4.1 – PANI phase molecular weight distribution depending on used An:TiO$_2$ weight ratio.

Despite the mass-average molecular weight (M_w) of pure PANI synthesized in presence of DBSA is 56 000, which is practically the same as for one typically obtained in HCl solution (M_w=53 000) [122] the polydispersity (M_w/M_n) is almost two times higher (3.93 vs. 2.08). Such growth of polydispersity suggests the presence of macromolecules with relatively low molecular weight, which probably stems from their more facile formation in the presence in polymerization medium of micelles formed by surface-active DBSA (see section 3.2). This suggestion allows considering the polymerization of aniline adsorbed on micelles as an interfacial process. It is known [246], that common homogeneous system allows the three-dimensional access of oxidant to monomer, while contacts in aqueous/micelle system are limited to the two dimensions of the formed interface. This can be the reason for appearance of well pronounced peak in pure PANI molecular weight distribution curve, corresponding to a fraction with higher molecular weight [246]. However, the large number of oligomeric components typical for aniline oxidative polymerization [247] is still observed.

The dispersion polymerization with the aniline:TiO_2 ratio 20:80 results in practically bimodal molecular weight distribution. The obtained PANI phase has high average molecular weight (75 800) together with significantly lower polydispersity (M_w/M_n=1.71). This phenomenon can be explained as follows: the introduction of nanoparticles causes the aniline salt adsorption on their surface, thus creating the local concentrational maxima. Therefore, the nucleation of new chains is preferably occurs on such TiO_2 core sites, which also has the orientational effect on growing macromolecules [248, 249].

The further increase of nanoparticles content (aniline:TiO_2 ratio 10:90) leads to further grow of average molecular weight up to 79 000, as well as to increase of polydispersity (M_w/M_n=2.09). Furthermore, the molecular weight distribution acquires the weakly pronounced polymodal character, observed for heterogeneous polymerization systems [244, 250].

The composite with lowest aniline:TiO_2 ratio (5:95) demonstrates both significant drop of average molecular weight (38 000) and increased polydispersity

(M_w/M_n=3.26). Such phenomenon can be explained by presence of TiO_2 nanoparticles excess in the reaction solution. The growth of specific surface area with the increase of dispersed phase content leads to discontinuity of the adsorbed monomer layer and appearance of individual “islands” on which polymerization occurs (see section 3.4). This assumption partially confirms by left shift of the molecular weight distribution main peak with the growth of nanoparticles content in the reaction solution and by SEM images (see section 4.2.2). The influence of used acid-dopant on PANI phase molecular characteristics is presented in table 4.1.

Table 4.1 Acid-dopant effect on molecular characteristics of PANI synthesized at ratio An:TiO_2 = 10:90 wt.%

Acid-dopant	BSA	TSA	CSA	LSA	DBSA
M_w	40 800	48 600	42 000	99 800	79 000
M_w/M_n	2.19	2.92	3.33	2.16	2.09

As can be seen from the table, the type of used in the synthesis acid-dopant influences PANI molecular weight and polydispersity. Thus, it was found that PANI obtained in the presence of acids with surface activity (LSA, DBSA) is characterized by 1.6 – 2 times higher M_w values and narrower molecular weight distribution, compared to PANI synthesized in the presence of dopants without surface activity (BSA TSA, CSA). As aniline presents in reaction solution in the form of salt, the partial concentration of monomer in the micelles of LSA and DBSA can appear. Probably, along with nanoparticles orientational effect it promotes the formation of polymer with better molecular characteristics.

Summarizing the above, introduction of nanoparticles into reaction medium increases PANI molecular weight and decreases its polydispersity. The highest molecular weight was obtained when 10:90 An:TiO_2 weight ratio and surface-active dopants were used.

4.2 Structure and morphology characterization of pure PANI and its nanocomposites

4.2.1 X-Ray diffraction measurements

The patterns of the wide-angle X-ray scattering (WAXS) of PANI anatase based nanocomposites demonstrate only weak changes of pure TiO_2 pattern with the increase of PANI-DBSA content (Figure 4.2).

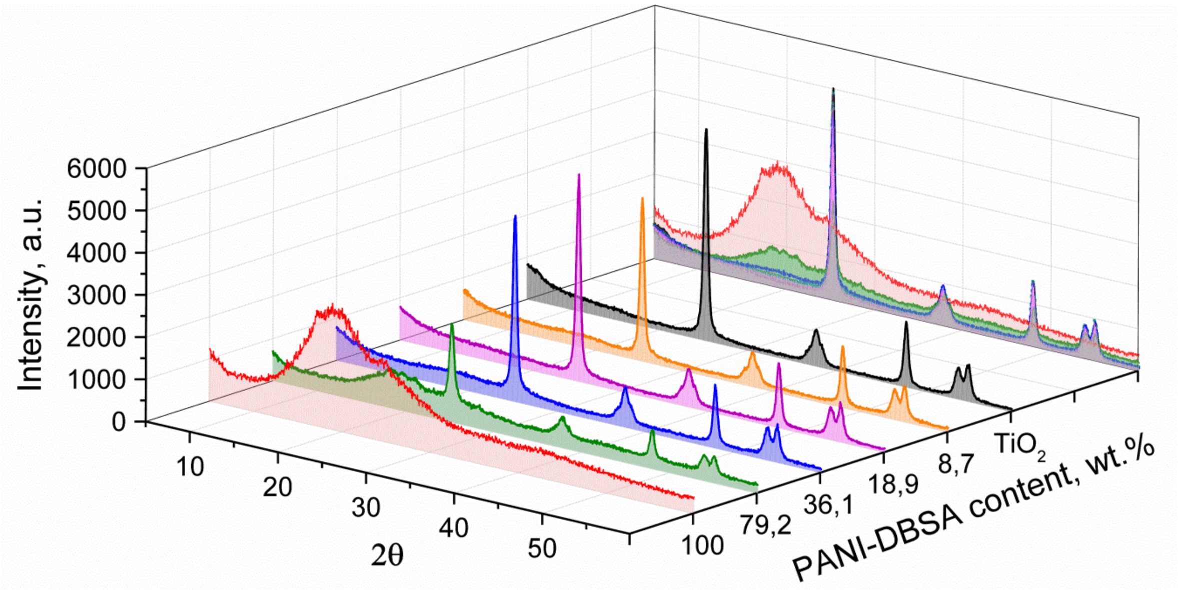

Figure 4.2 – XRD patterns of the anatase based nanocomposites with different PANI-DBSA content, determined by thermogravimetric measurements

At the same time the absence of any PANI crystalline peaks at low polymer content is observed. The authors of [117] and [118] attribute this phenomenon to aniline adsorption on the surface of nanoparticles leading to molecular chains tethering and thus hampering polyaniline crystallization. In case of pure PANI or at its high content in the nanocomposites, main peaks are localized in the range 12° – 35°. Thus, the pure PANI-DBSA pattern contains both the visible peak near 25° and shoulders at ca. 17.4°, 29.1° assigned to the crystalline phase, as well as a broad asymmetric scattering corresponding to the amorphous phase [197, 251]. The diffraction peaks pure TiO_2 and nanocomposites practically coincide and are located at $2\theta = 25.3$, 37.9, 48, 54 and 55.1° corresponding to the (101), (004), (200), (105) and (211) crystallographic planes respectively.

The patterns of the small-angle X-ray scattering (SAXS) reveal only small difference in structure of the synthesized nanocomposite and pure PANI (Figure 4.3).

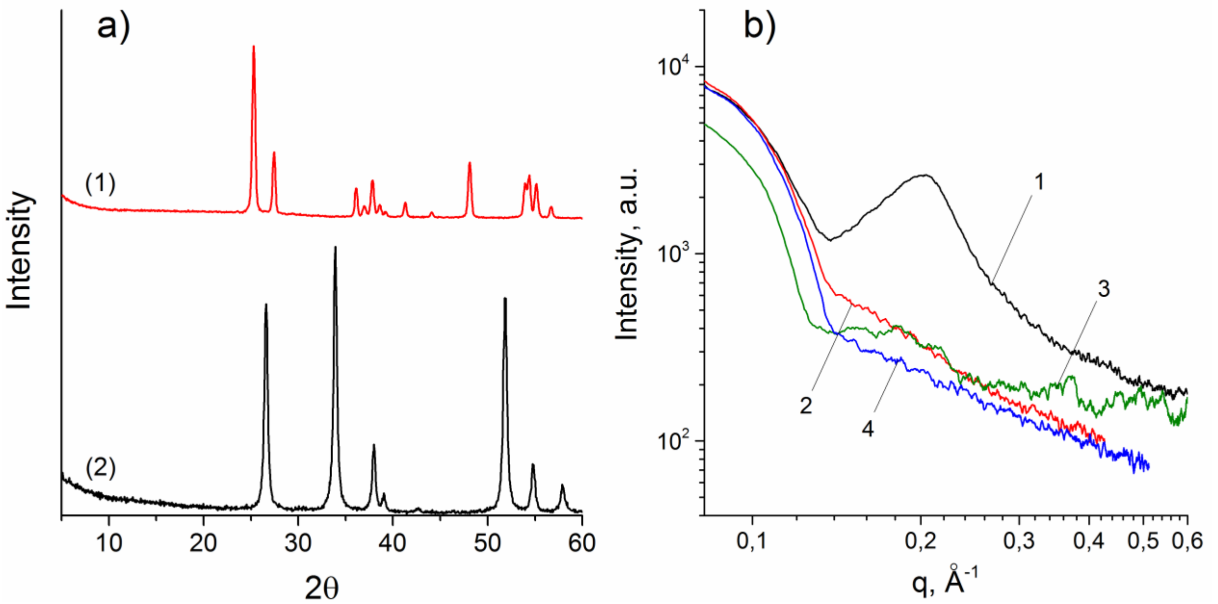

Figure 4.3 – The XRD patterns of pure PANI and its nanocomposites: **(a)** WAXC patterns of (1) R90-DBSA, (2) S90-DBSA; **(b)** SAXC pattern of (1) PANI-DBSA, (2) A90-DBSA, (3) R90-DBSA, (4) S90-DBSA.

The similarity of observed intensity decays at $q < 0.14$ $Å^{-1}$ suggests the absence of both large-scale and lower-scale structural heterogeneities in PANI nanocomposites [252]. At the same time, the well-resolved SAXS reflection near $q = 0.204$ $Å^{-1}$ of PANI-DBSA pattern, corresponding to mean interchain distance $d = 2\pi/q \approx 3.1$ nm can be observed. In other words, a specific non-structured polymer condition due to small thickness of the layers covering nanoparticles in the nanocomposites with small PANI content can be suggested.

Summarizing the above, the presence of polymer has no effect on nanoparticles crystallinity. At the same time, the polymer in the nanocomposites with small PANI content appears in non-structured condition. At higher PANI contents the evidence of own polymer crystallinity is observed.

4.2.2 Solvent influence on pure PANI and its nanocomposites morphology

TEM images of TiO_2 nanoparticles showed that used nanoparticles have asymmetric rice-like form with the average length of about 20 – 30 nm and a diameter of 10 - 15 nm (Fig. 4.4a). During the aniline polymerization in the presence of different dopants and these nanoparticles the latter do not change their shape, and PANI precipitates on their surface in a form of shell (figures 4.4b and 4.4c). However, as seen in figures 4.4b and 4.4c in case of DBSA the nanocomposite structure is more agglomerated compared to formed in the presence of LSA.

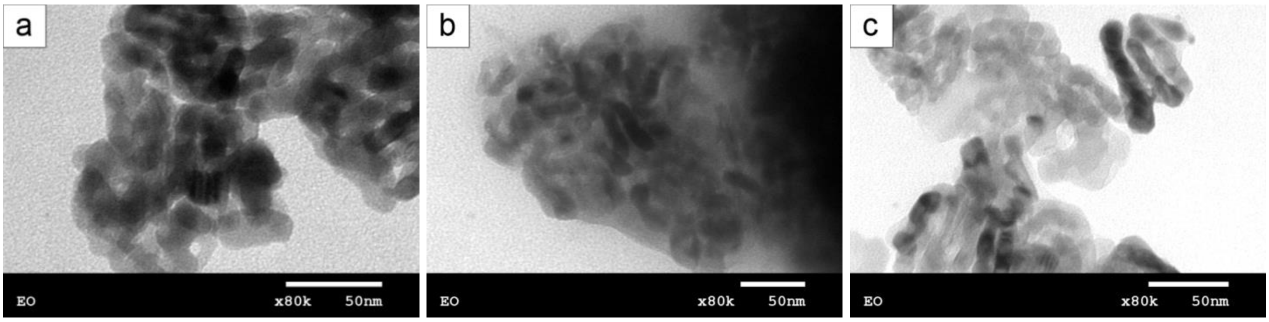

Figure 4.4 – TEM images of **(a)** bare TiO_2 nanoparticles and nanocomposites **(b)** TiO_2/PANI-DBSA, **(c)** TiO_2/PANI-LSA synthesized at polymerization ratio An:TiO_2= 10:90 wt.%

Detailed analysis of enlarged TEM images showed that PANI shell thickness in the nanocomposites taken after synthesis in the aqueous medium (before the action of dispersing solvent) is quite close in both cases and varies in the range of 6 – 12 nm. However, it was found that nanocomposites morphology significantly changes at the stage of dispersing in the organic solvents, required for the sensing layers deposition onto interdigitated electrodes. We found that these changes depend on nature of dispersing solvent, used dopant (dopants can facilitate solubility [89]) and content of polymer phase in the nanocomposite.

In particular, we compared the influence of common solvents used for sensing layers deposition, namely dichloroacetic acid (DCAA) and chlorobenzene (CB) on PANI polymer phase in the nanocomposites. Taking into account the positive impact of DBSA on PANI solubility and processability [89], our study was conducted using nanocomposite TiO_2/PANI-DBSA and pure PANI-DBSA.

It was found that careful addition of DCCA into the bottle containing the powder of pure PANI or its nanocomposite is accompanied by practically instantaneous appearance of the green color in the solution bulk. At the same time, the change of solvent to chlorobenzene allows to obtain two separate phases. The color change occurs slowly and with gradient, characteristic for diffusion limited processes. In order to confirm the difference in DCAA and chlorobenzene PANI dissolving ability, the UV-Vis spectra of both pure PANI and its TiO_2 based nanocomposite were recorded after the 60 min action of corresponding solvents.

The prepared dispersions were of the same concentration and centrifuged for 45 min at 5000 rpm prior to measurements in order to remove dispersed nanoparticles. To exclude the interference of solvents, their spectra were subtracted from PANI solutions spectra. Results on influence of used solvent on the PANI dissolution speed both in pure and nanocomposite form are presented in figure 4.5.

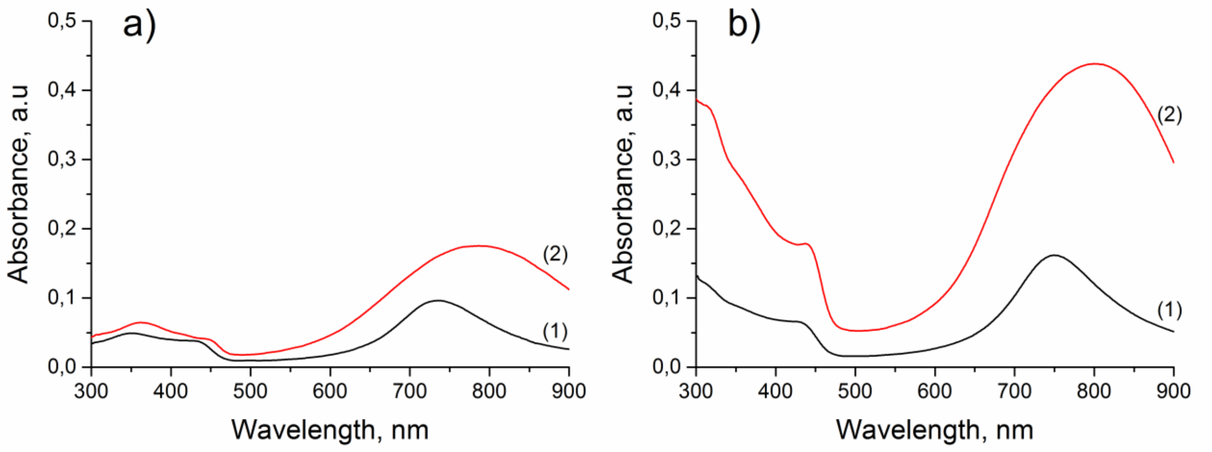

Figure 4.5 – The optical absorbance of **(a)** pure PANI and **(b)** A90-DBSA nanocomposite solutions after the 60 min of solvent action

From the figure 4.5 the higher intensity of the typical for doped PANI bands [123] in both pure PANI and its TiO_2 based nanocomposite dissolved in DCAA can be observed. The direct consequence of such dissolution is changes in synthesized materials morphology.

The differences in influence of used dispersing solvents on pure PANI and its nanocomposites morphology was visualized by SEM. We found that chlorobenzene is milder solvent that practically do not dissolve PANI-DBSA (figure 4.5), while allows satisfactory polymer dispersion with simultaneous saving of the original structure. Figure 4.6 shows the quite porous nature of pure PANI-DBSA dispersed in CB and cast on the glass substrate.

Such difference can be connected to different boiling points (t_{bp}) of both solvents. Thus, DCAA forms viscous true solutions with PANI DBSA, suitable for casting of sensing layers onto electrodes. However, due to the high boiling point (t_{bp} = 194 °C) it forms dense non-porous layers with low specific area. The PANI-DBSA solubility in CB (t_{bp} = 131°C) is very low, additionally CB quickly evaporates from the cast layer and promotes the formation of a large number of micro- and macropores. At the same time, the continuous influence of DCAA totally changes the original structure: the cast films have the form of flat dense multilayer assemblies.

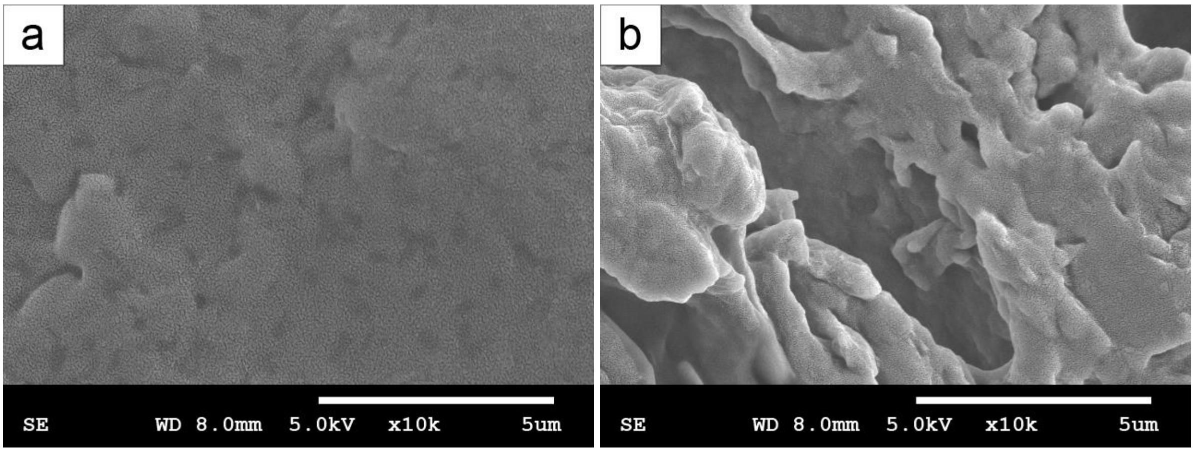

Figure 4.16 – The SEM images of pure PANI-DBSA cast from **(a)** DCAA and **(b)** CB

We found that at high PANI-DBSA phase content (79.2 wt.%) the synthesized materials exist in fully occluded structures with understated surface form (figure 4.7 e–h). Nevertheless, the average agglomerates size is practically the same in all nanocomposites (600 – 620 nm). Moreover, the high polymer content (see section 3.4) stimulates the self-assembly processes manifesting in growth of PANI fibres. The effect is more apparent in the nanocomposite containing 79.2 wt.% of doped polymer. The length of formed PANI-DBSA fibres is 5 – 14 μm (main fraction ~8 μm) and thickness 280 – 480 nm (main fraction ~440 nm) (figure 4.7). It should be noted, that fibres also have the tendency to coalesce while growing.

The use of DCAA washes the upper PANI layer and denudes nanoparticles surface. Therefore, planar-type pure PANI formations observed on SEM images are most likely rests of fibres agglomerates at different stages of dissolution (figure 4.7a), while the shapeless inclusions are PANI particles formed in the solution void volume (see section 3.4). Probably, these particles were included at the polymerization stage and hidden by overall polymer layer. These shapes can also be seen at lower contents

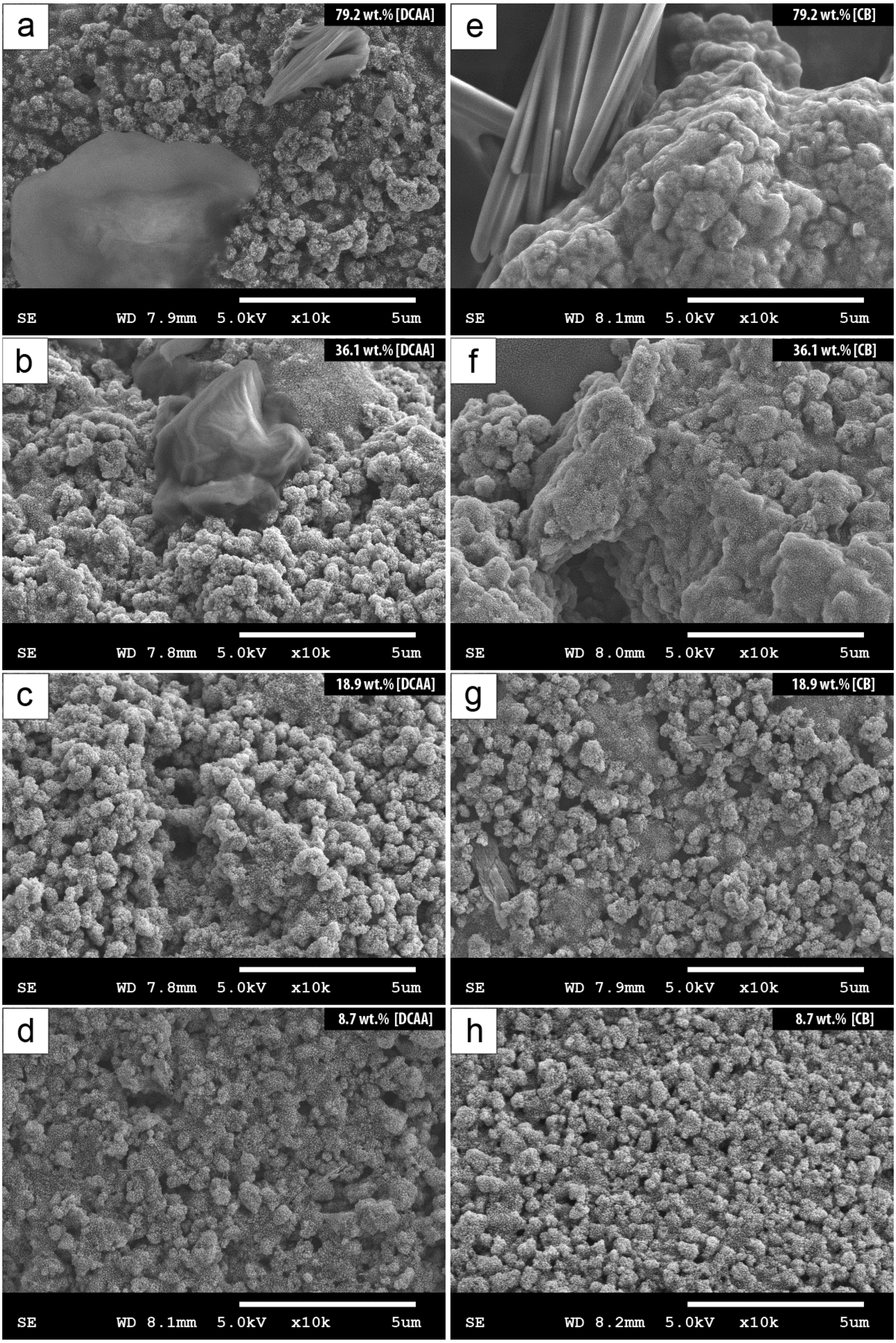

Figure 4.7 – The SEM images of TiO_2/PANI-DBSA nanocomposites with different polymer content treated in different solvents

of PANI-DBSA (36.1 wt.%) in the nanocomposite dispersed in DCAA (figure 4.7b) and expectedly hidden when the chlorobenzene is used as solvent (Figure 4.7f).

Further decrease of PANI-DBSA content in the nanocomposites (18.9 wt.%) (figure 4.7c and g) allows optimal polymer distribution on the nanoparticles surface without pure PANI inclusions. As a result the more porous layer with enhanced sensing properties can be obtained. Therefore, treatment in DCAA disturbs already optimized structure and results in sensitivity drop (see section 5.2).

The PANI-DBSA content of 8.7 wt.% is too low and is insufficient for covering the surface of all nanoparticles. Thus, PANI rather works as glue connecting TiO_2 agglomerates. The indirect evidence of this fact is the noticeable decrease in agglomerates average size down to 450 nm (figure 4.7h). Obviously, the small polymer content easily washes out by DCAA from the composite. As a result, after sensing layer deposition process the two-layer structure comprising individual TiO_2 phase covered with dense polymer layer with small specific surface can form (figure 4.7d).

The presence of differences in PANI nanocomposites morphology after use of different solvents is also confirmed by TEM. In particular, after dispersing of nanocomposite containing 36.1 wt.% PANI-DBSA in DCAA, the separate polymer phase (stroked with black lines, figure 4.8a) can be observed. At the same time, the low dissolving ability of CB practically does not change the initial structure.

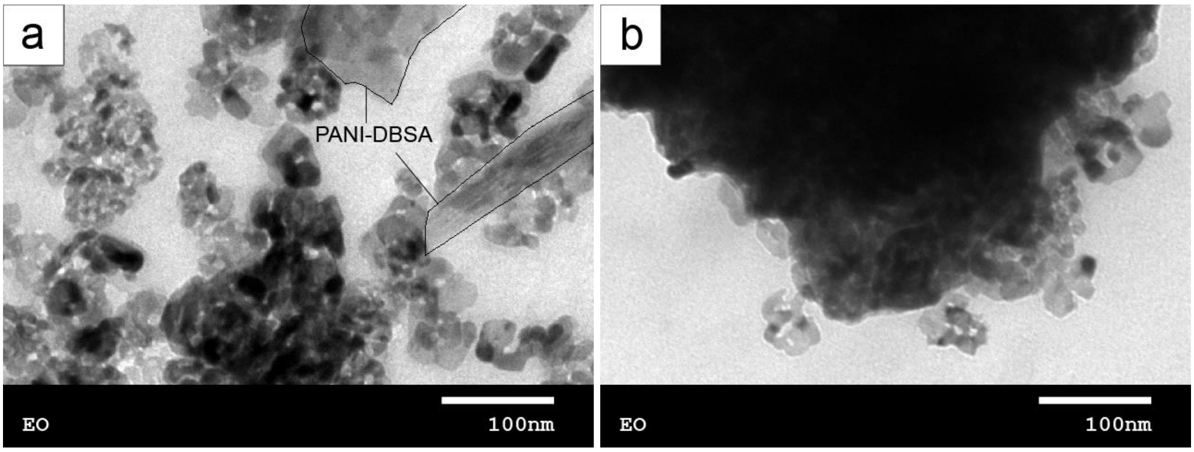

Figure 4.8 – The TEM images of TiO_2/PANI-DBSA nanocomposite (36.1 wt.% PANI-DBSA) dispersed in **(a)** DCAA and **(b)** CB

Summarizing the above, the use of DCAA as a dispersing solvent significantly changes target morphology of synthesized nanocomposites and decreases their sensing properties. In this regard the use of chlorobenzene as solvent is more rational, as it does not affect the PANI nanocomposites structure. Additionally, it helps to avoid the superposition of DCAA secondary doping effect [253] and allows more precise evaluation of the synthesized materials sensing properties.

4.2.3 Dopants influence on morphology of synthesized materials

The influence of dopants on synthesized materials morphology is shown in figure 4.9. It can be seen, that morphology of pure PANIs synthesized in the presence of small dopants (BSA, TSA, CSA) has very similar structure (Figure 4.9a-c), conformable with the one obtained by authors [254] under vigorous stirring.

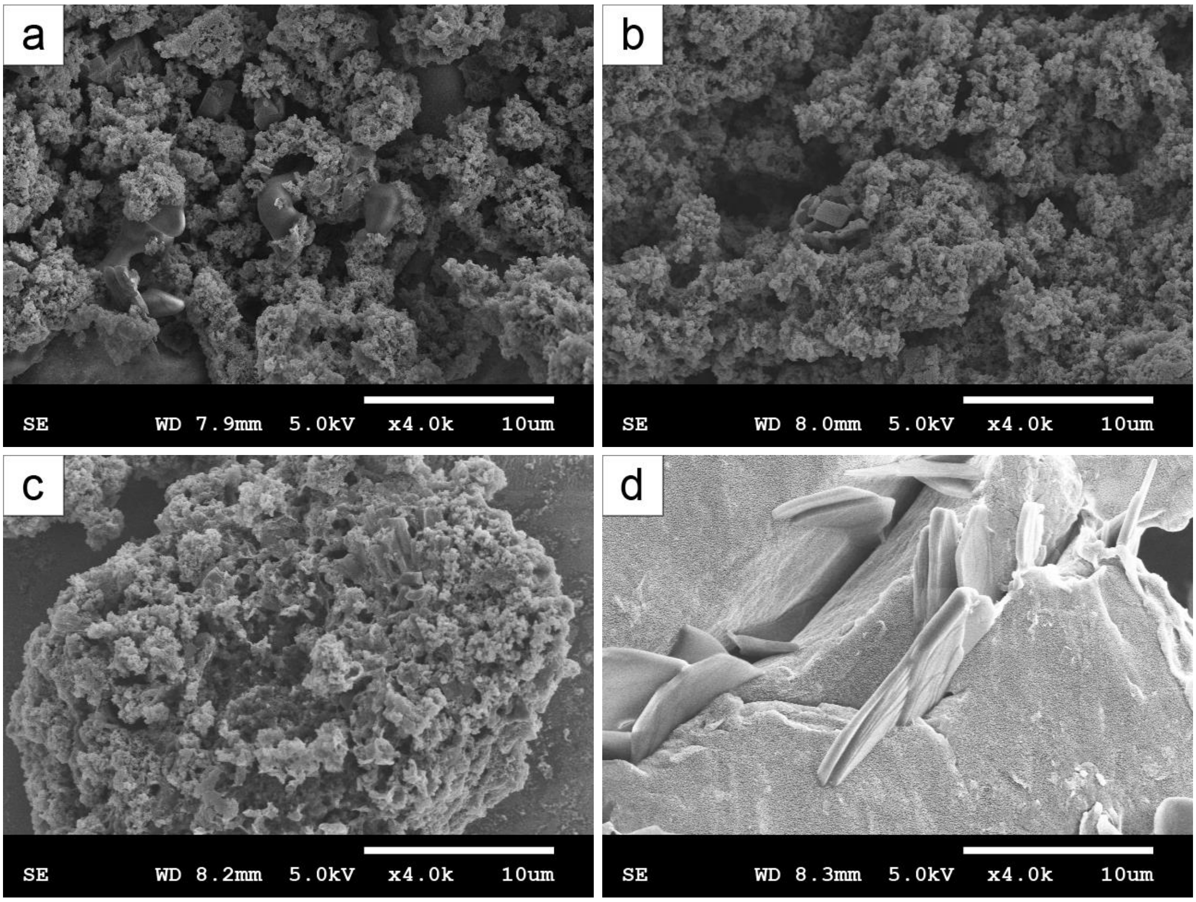

Figure 4.9 – SEM images of pure PANI doped with **(a)** BSA, **(b)** TSA, **(c)** CSA, **(d)** LSA.

At the same time, the pure PANI obtained in presence of LSA (Figure 4.9d) demonstrates relatively dense structure compared to sponge-like ones obtained in case of BSA, TSA and CSA dopants. This phenomenon probably stems from the fact that among used acids only LSA similarly to DBSA has surface activity. The formation of micelles increases viscosity of the reaction medium, and decreases the real speed of solution agitation. Therefore, the PANI growth tends to homogeneous nucleation [254] manifesting in appearance of planar structures.

The more porous structure of pure PANIs (without nanoparticles) synthesized in presence of small dopants suggests the higher sensors responses to ammonia. However, despite the close OD values (see section 4.3), the sensors responses are of comparable level with LSA and DBSA doped samples in case of use of chlorobenzene as solvent (see chapter 5). This phenomenon apparently originates from lower protonation degree in case of PANIs synthesized in presence of small dopants. This suggestion is in good agreement both with thermogravimetric measurements, demonstrating comparatively small weight changes corresponding to dopants loss (see section 4.5), as well as lower materials conductivity (see section 4.4). Furthermore, the use of DCAA as a solvent which is also induces PANI partial protonation [253], significantly increases their sensing responses (see section 5.2), compared to already highly protonated PANIs doped with LSA and DBSA.

Summarizing the above, pure PANIs synthesized in presence of small dopants (BSA, TSA, CSA) have highly porous structure. However, the responses to ammonia of sensing layers cast from chlorobenzene are low. The use of DCAA leads to partial protonation and increase of sensing responses.

4.2.4 Influence of nanoparticles on resulting morphology of hybrid materials

The influence of nanoparticles on resulting nanocomposites morphology is shown in figure 4.10. For convenience, nanocomposites synthesized in the presence of different nanoparticles were labeled with: R – for rutile, A – for anatase, S – for SnO_2; the number after the letter shows nanoparticles weight content used for synthesis.

The rutile based nanocomposites R90-DBSA and R90-CSA have a structure similar to A90-DBSA (Figures 410a, c and 4.7g). It is worth to note, that R90-CSA has higher porosity than both R90-DBSA and A90-DBSA, as well as close to ideal oxidation degree of 0.48 vs. 0.46 and 0.49 respectively. The combination of these two factors probably results in sensors responses enhancement (see section 5.2).

The S90-DBSA and S90-CSA nanocomposite materials also demonstrate the morphology similarity (Figures 4.10b, d), while the S90-DBSA is less porous. The latter is apparently stems from higher polymerization yield in case of DBSA dopant (see section 3.4), and therefore higher polymer content in the nanocomposite. Also, taking into account higher conductivity of S90-DBSA (see section 4.4), the higher doping degree can be suggested. Therefore, considering the close OD values of S90-DBSA and S90-CSA, the nanocomposite porosity is suggested as a main factor influencing sensors response magnitudes.

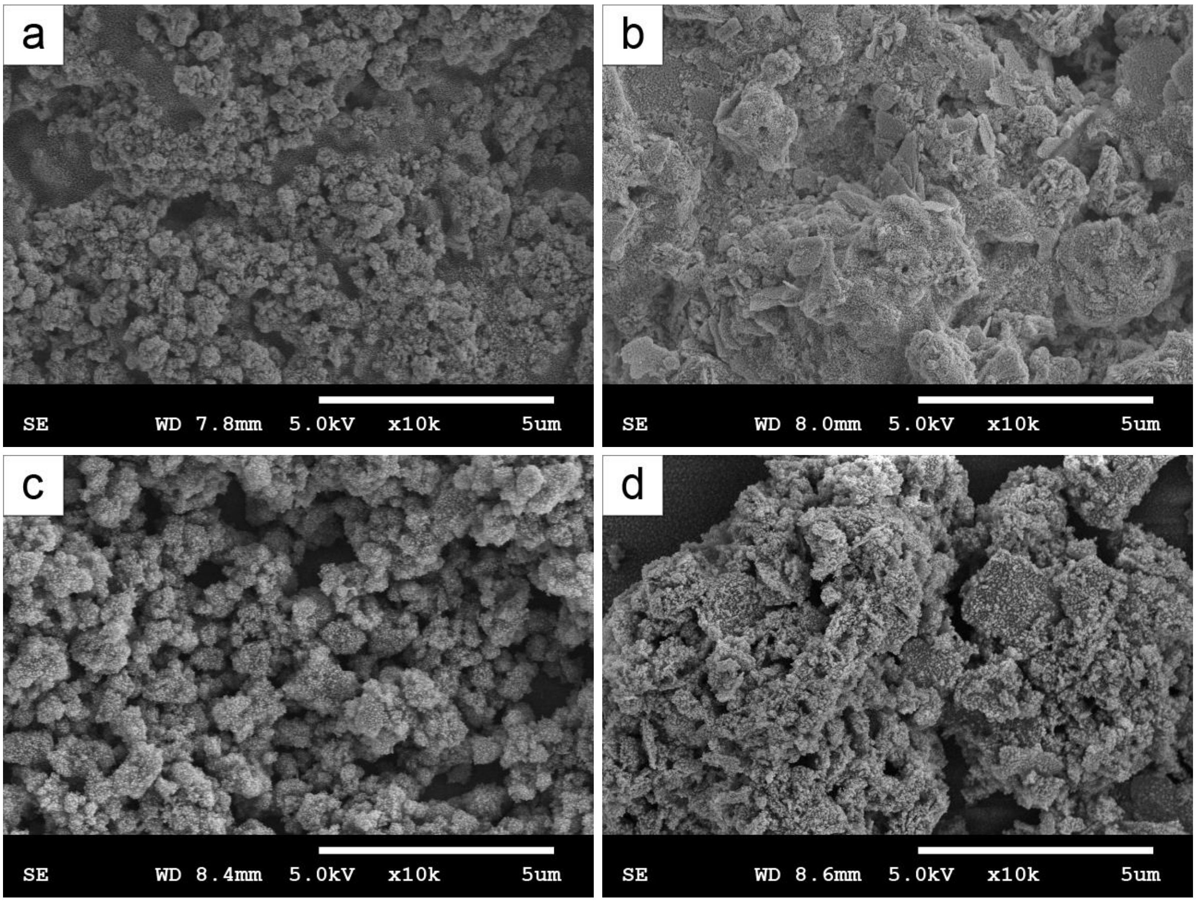

Figure 4.16 – SEM images of PANI nanocomposites **(a)** R90-DBSA, **(b)** S90-DBSA, **(c)** R90-CSA, **(d)** S90-CSA.

Summarizing the above, the nanocomposites have similar structure regardless of used dopant. At the same time, the hybrid materials synthesized in the presence of small dopants demonstrate higher porosity. The latter is the more significant and determines sensors response magnitudes, while doping degree factor takes second place if samples have the same polymer phase oxidation degree in the nanocomposite.

4.2.5 Morphology of electrodeposited PPy and ZnO/PPy heterostructure

The differences in morphology of electrochemically deposited pure polypyrrole (PPy) and ZnO/PPy heterostructures are shown in figure 4.11.

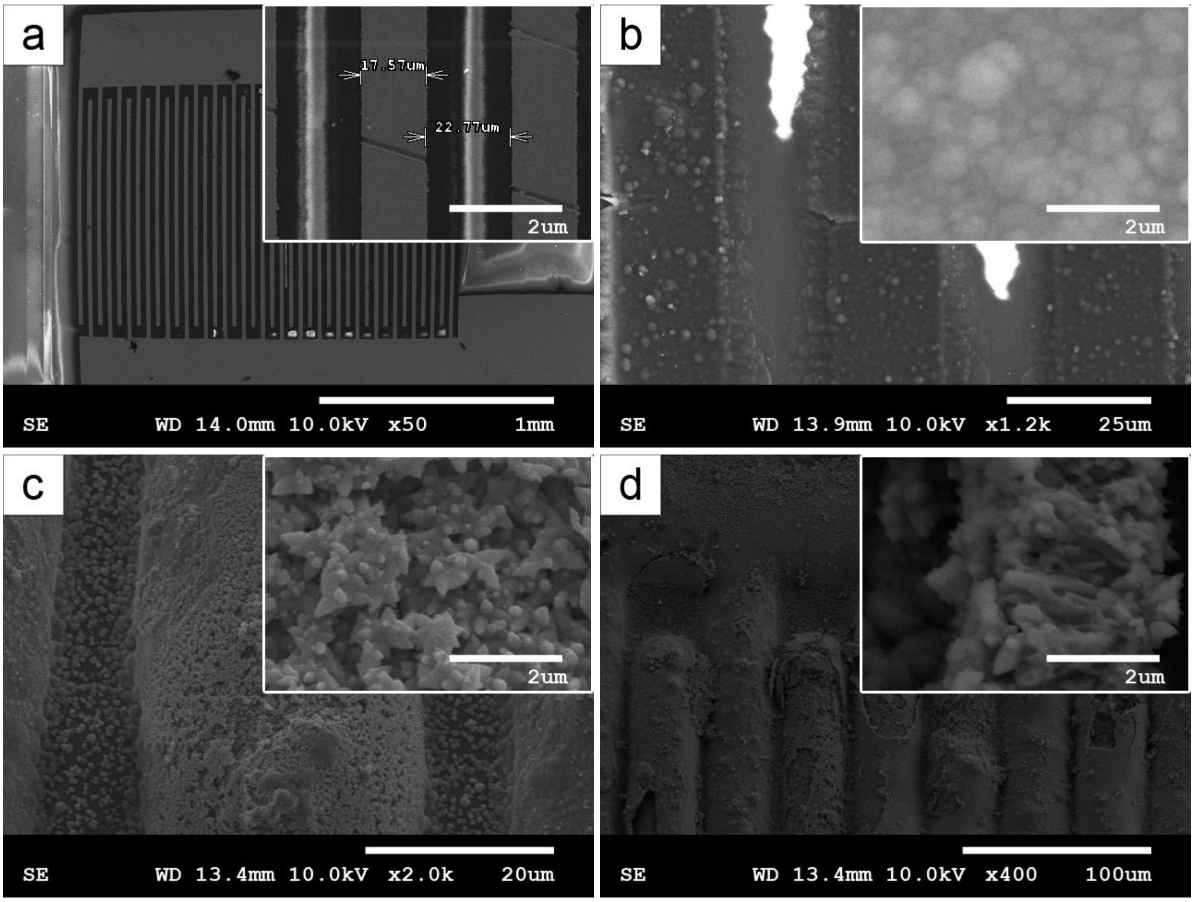

Figure 4.11 – SEM images of electrochemically deposited polypyrrole and ZnO/PPy heterostructure: **(a)** clean interdigitated electrode, **(b)** electrodeposited pure polypyrrole layer, **(c)** electrodeposited ZnO layer, **(d)** resulting ZnO/PPy heterostructure.

As one can see the pure PPy has very dense structure comparable with the one obtained in case of pure PANI cast from DCAA (Figures 4.11b and 4.6a). While the electrodeposited ZnO layer (Figure 4.11c) has more porous structure than pure polypyrrole, the presence of a large number of nucleation centers leads to structure densification and lower specific surface compared to chemically synthesized nanocomposites. The resulting ZnO/PPy heterostructure has higher porosity then pure PPy layer and therefore shows higher sensitivity to pollutants. At the same time, both electrochemically deposited polypyrrole and ZnO/PPy heterostructure have lower porosity compared to chemically synthesized PANI nanocomposites and, therefore lower sensitivity to pollutants.

4.3 FTIR spectroscopic investigations of pure PANI and its hybrid composite materials

The difference in infrared spectra of chemically synthesized pure PANI and its nanocomposites on the example of large (LSA, DBSA) and small dopants without surface activity (BSA) are shown in the figure 4.12.

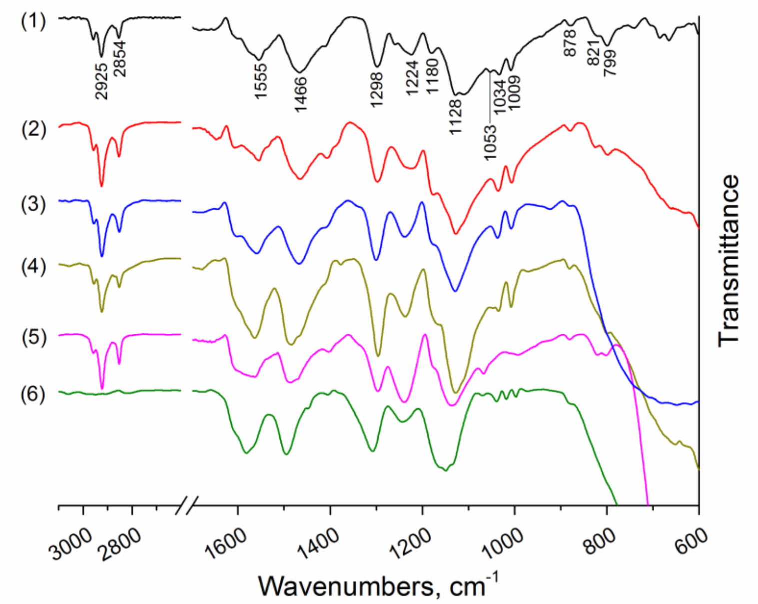

Figure 4.12 – The FTIR spectra of (1) PANI-DBSA, (2) A80-DBSA, (3) R90-DBSA, (4) A90-DBSA, (5) S90-DBSA and (6) A90-BSA.

The FTIR spectra of the both pure PANI and its nanocomposites contain typical for doped polyaniline bands [109, 110, 255, 256]. The peaks at 2924 and 2854 cm^{-1} are assigned to the –CH_3 and symmetric −CH_2 stretching of alkyl chains. Naturally, these peaks are present only in DBSA doped materials and absent in case of BSA dopant. The characteristic for PANI peaks are situated at 1555 and 1466 cm^{-1} and correspond to the quinoid and benzenoid rings stretching vibrations respectively.

However, the PANI nanocomposites demonstrate small blue shift with the change of dopant or nanoparticles type. This effect is most clearly seen after comparison band positions of pure PANI-DBSA and nanocomposites (R90-DBSA, A90-DBSA, S90-DBSA and A90-BSA). According to Ping [255] such shifts suggest a higher protonation degree of the PANI-DBSA, and therefore higher material conductivity [257]. The peaks at 1298 and 1224 cm^{-1} are assigned to primary and secondary amines respectively. The observed variation of their height is most likely due to different doping degree as well as dopants chemical structure differences. The additional factor influencing the peaks shape and shift is the formation of additional hydrogen bonds between doped polymer and (–OH) groups, inevitably existing on the both SnO_2 and TiO_2 surface. The absorption band located at 1128 cm^{-1} corresponds to $B–N^+H=Q$ or $B–N^+H–B$ structures [110, 203]. The band at 1111 cm^{-1} is assigned to in-plane –CH= bending. The weak bands observed at 1034 and 1009 cm^{-1} correspond to the S=O stretching vibrations of the sulphonic acid-dopants. The band at 799 cm^{-1} is assigned to –CH= out-of-plane bending in 1,4-substituted benzene ring. However in case of rutile and anatase based nanocomposites it is overlapped by strong absorption band of TiO_2 nanoparticles. The main PANI and its hybrid materials bands and their assignments are summarized in table 4.2.

It is known [259, 260] that protonation do not change the electrons number in the chain backbone, while the changes in oxidation degree affect the density of electrons. The estimation of synthesized pure PANI and its nanocomposite materials oxidation degree (OD), based on quinonoid (D_Q) and benzenoid (D_B) absorption peak heights ratios (see formula 2.1), confirms different electronic states of the PANI backbones in the pure PANIs and its nanocomposites [201]. According to Wei [261], the bands ratio around 80% is typical for emeraldine form and decreases to about 20% for leucoemeraldine. All the materials demonstrate a weak correlation of OD with the dopant nature. However, in case of nanocomposites the OD values are significantly closer to ideal value of 0.5 (table 4.3) and suggests greater quinodiimine sites quantity in the polymer phase of PANI nanocomposites.

Table 4.2 Summary of major PANI infrared bands and their assignment [109, 110, 203, 256, 258]

PANI-DBSA	A80-DBSA	R90-DBSA	A90-DBSA	S90-DBSA	A90-BSA	Band assignement
2925	2925	2923	2925	2925	–	–CH_3 vibrations of alkyl chains
2854	2853	2853	2853	2853	–	Symmetric −CH_2 stretching of alkyl chains (LSA, DBSA)
1555	1555	1559	1564	1564	1581	Quinonoid ring stretching vibrations
1466	1465	1467	1483	1486	1495	Benzenoid ring stretching vibrations
1298	1297	1300	1296	1297	1308	C–N stretching vibrations, out-of-plane –NH– bending
1224	1223	1238	1237	1239	1245	C–N^{+}* stretching vibrations
1180	1176	~1178	~1174	~1176	~1166	C–H in-plane bending vibrations
1128	1127	1129	1130	1136	1149	Q=N^{+}H–B or B–NH^{+}–B vibrations/d(C–H)
1053	–	–	1048	1067	–	N=Q=N vibrations, SO_3^-
1034	1036	1037	1036	–	1038	S=O stretching (BSA, LSA, DBSA)
1009	1007	1008	1008	–	1018	S=O stretching (BSA, LSA, DBSA), −CH_3 bending
878	878	880	880	881	~880	Quinonoid ring breathing
821	825	–	–	821	–	Out-of-plane –CH= bending of 1,2,4-trisubstituted ring
799	798	–	798	802	–	−CH= out-of-plane bending in 1,4-substituted benzene ring

Table 4.3 Oxidation degree of pure PANI and its nanocomposites

Material / Dopant	Pure PANI	R90	A90	S90
	OD = $D_Q/(D_Q+D_B)$			
BSA	0.443	0.484	0.495	0.469
TSA	0.438	0.479	0.479	0.465
CSA	0.435	0.481	0.490	0.465
LSA	0.440	0.472	0.463	0.469
DBSA	0.441	0.456	0.480	0.468

This phenomenon gives the direct evidence of the coordination effect of nanoparticles in aniline polymerization [248, 249], allowing formation of more regular structure with fewer defects. Practically, this fact implies stronger nanocomposites responses to analytes of base nature (see section 5.2). Therefore, FTIR spectra of both pure PANI and its nanocomposites confirmed the presence of typical for doped polyaniline bands. At the same time, acid-dopant nature has very weak influence on synthesized materials oxidation degree, when the SnO_2 nanoparticles are used. Such phenomenon can be explained by different degree of physicochemical interactions between NH groups of PANI and oxygen on the surface of TiO_2 and SnO_2 nanoparticles.

4.4 Conductivity measurements of pure PANI and its nanocomposites

The influence of PAN-DBSA content on the electrical conductivity of synthesized TiO_2 (anatase) based nanocomposites is shown on the figure 4.13. The polymer phase content in the nanocomposites (PANI-DBSA volume fraction) was calculated using data on polymerization yield, assuming full PANI doping and taking densities of 3.83 and 1.14 g/cm^3 for TiO_2 and PANI-DBSA respectively [262, 263]. We found that this dependence has non-linear character.

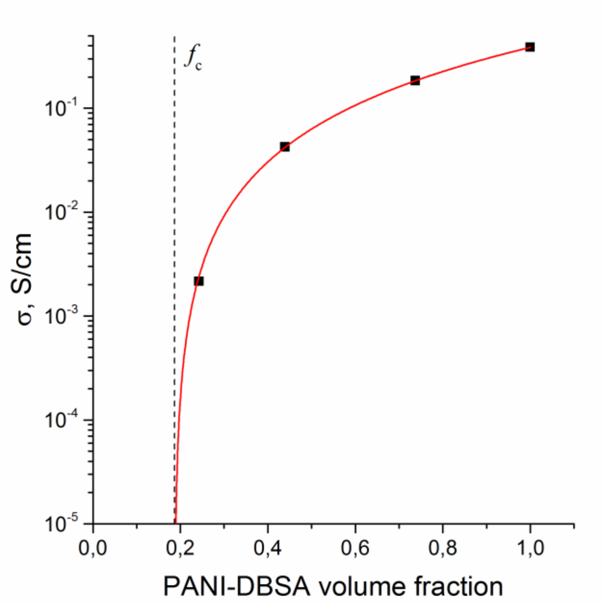

Figure 4.18 – The dependence of synthesized materials conductivity on polymer phase volume fraction

As nanocomposites have core-shell structure and the measurements were conducted for the pressed pellets, in the first approximation, they can be considered as an analog of percolation-like system, where the conducting polymer phase is distributed in non-conductive inorganic matrix. Based on this assumption and using the statistical percolation theory, following a scaling law of the form [264, 265], we obtained next dependence of nanocomposites electrical conductivity on PANI-DBSA phase content:

$$\sigma = \sigma_0 \left(f - f_C \right)^t = 0.57 \left(f - 0.19 \right)^{1.9} \tag{4.1}$$

where σ –nanocomposite conductivity;

σ_0 – calculated conductivity of PANI-DBSA phase in the nanocomposite;

f – PANI-DBSA volume fraction in the nanocomposite;

f_C – percolation threshold;

t – critical exponent.

From equation 4.1, calculated percolation threshold corresponds to the volume fraction of 0.19. Obtained results are in good agreement with reported earlier systems [117, 266-268], as well as with theoretically predicted value $f \cong 0.16$ [269] for a random lattice of spheres. Moreover, calculated PANI-DBSA phase conductivity in the nanocomposite σ_0^{calc}= 0.57 S/cm is higher than measured σ_0^{measur}= 0.386 S/cm (table 4.4). This fact evidence the higher quality of polymer obtained in the presence of nanoparticles and in good agreement with the molecular weight measurements (see section 4.2). At the same time, the measurements of conductivity of pure PANI and its nanocomposites with different nanoparticles obtained at fixed An:nanoparticles ratio 10:90 wt.% (R90 – rutile, A90 – anatase, S90 – SnO_2), demonstrate low correlation with type of used dopant (table 4.4).

Table 4.4 Dopant influence on pure PANI and its nanocomposites conductivity

Material / Dopant	Pure PANI	R90	A90	S90
	Conductivity [σ ×10³], s/cm			
BSA	2.89	13.92	0.008	0.85
TSA	58.4	4.36	0.033	1.26
CSA	24.5	2.30	0.039	0.11
LSA	55.0	17.1	0.552	4.48
DBSA	386.0	30.77	24.3	76.9

However, the materials doped with LSA and DBSA generally have better conductivity compared to the ones synthesized in the presence of BSA, TSA and

CSA. This phenomenon probably can be explained by the complex impact of different factors, namely better plasticization ability of large dopants, which promote better polymer distribution in pressed pellet, higher molecular weight of the nanocomposite polymer phase, stipulating the higher conjugation degree in polymer chains and, probably, different polymer content in nanocomposites due to differences in polymerization yield (see section 3.4). The significant influence of used nanoparticles most likely connected with their size, causing different thickness of polymer shell and therefore different levels of overall conductivity.

Summarizing the above, polymer obtained in the presence of dispersed nanoparticles is of better quality compared to the one synthesized without nanoparticles, which confirms by results of molecular weight measurements. Additionally we found that materials doped with large surface active dopants LSA and DBSA have higher conductivity, compared to doped with small dopants (BSA, TSA, CSA).

4.5 Thermal behavior of pure PANI and its hybrid composite materials

4.5.1 Pure PANI thermooxidation stability

The results on pure PANI-DBSA thermooxidation stability measurements are presented in figure 4.14.

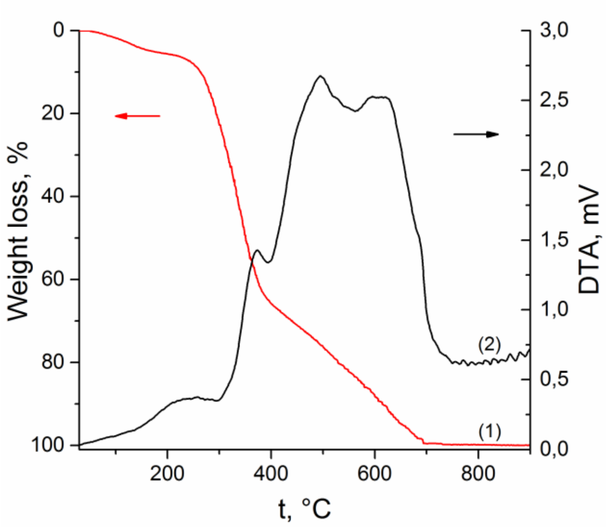

Figure 4.14 – (1) TG and (2) DTA curves of PANI-DBSA thermal decomposition

The presented thermogram is characterized by three-step weight loss. The first small weight loss (~5%) occurring at temperature less than 150°C is usually attributed to the loss of water and small molecules such as solvents and impurities [204]. The both peaks on the DTA curve in the interval 150 – 394°C correspond to evaporation of the DBSA. The first small peak belongs to the evaporation of the dopant excess (compared to stoichiometric PANI:DBSA = 1:0.5 ratio) [270] and masks the beginning of the PANI-DBSA salt decomposition. Both of processes are responsible for ~60% of total weight loss.

The direct PANI degradation starts after the end of volatilization of major part of dopant at c.a. 400°C and accompanied with the TG curve slope change. The strong exothermic peak at 400 – 560°C probably corresponds to the PANI chains crosslinking (Figure 4.15) [271]. The crosslinking at imine sites does not require external oxidant and occurs by the transition of quinoid structure to benzenoid. The same result can be obtained with aminogroups, however it requires the external oxidant [271].

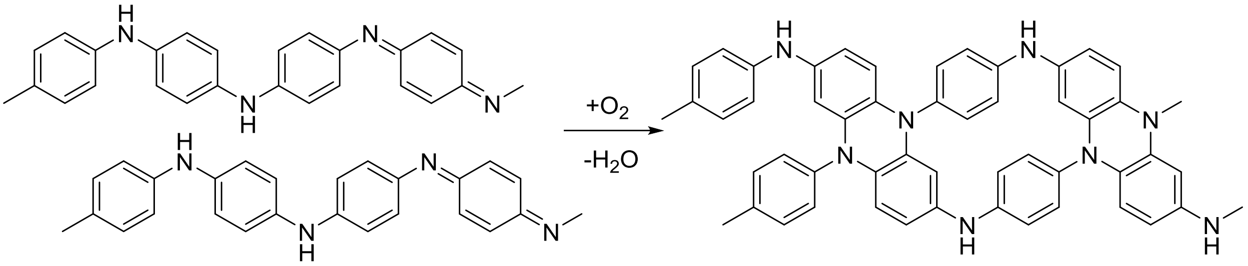

Figure 4.15 – The scheme of possible PANI chains crosslinking

The further heating (560 – 700°C) leads to the PANI decomposition with the formation of polymer chain fragments oxidation products (Figure 4.16) [272].

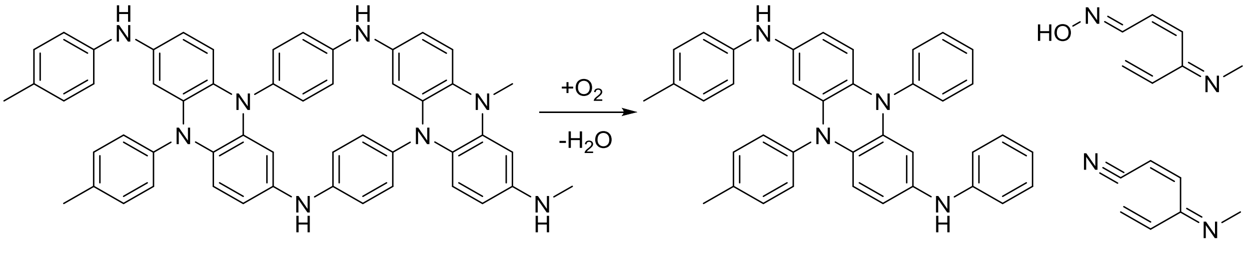

Figure 4.16 – The possible PANI chains decomposition products

At temperatures above 700°C the almost no weight loss together with the sawtooth-like signal on DTA curve can be observed. Such behavior is typical for combustion processes and corresponds to deeper PANI decomposition [272], probably with the formation of typical for products such as CO_2, H_2O and N_2. The results on thermooxidation stability of pure PANIs depending on used acid-dopant are presented in figure 4.17.

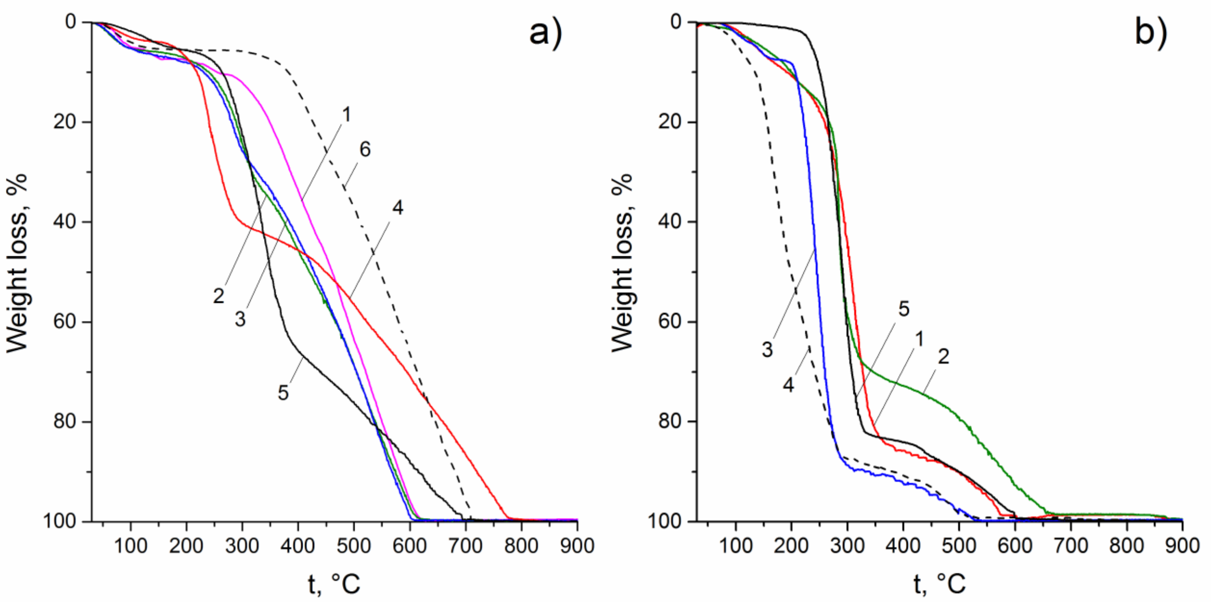

Figure 4.17 – TG curves of **(a)** pure PANIs doped with sulfonic acids (1) – BSA, (2) – TSA, (3) – CSA, (4) – LSA, (5) – DBSA, (6) – dedoped PANI; **(b)** used acids -dopants (1) – BSA, (2) – TSA, (3) – CSA, (4) – LSA, (5) – DBSA.

The character of TG curves demonstrates the closeness of characteristics of two PANI groups, namely doped with small (BSA, TSA, CSA) and large surface active dopants (LSA, DBSA). The same tendency can be observed both at synthesis stage and in sensors responses of synthesized materials (see section 3.3 and 5.1).

Summarizing the above, PANI doped with small dopants demonstrates lower thermal stability compared to large dopants. Such behavior probably originates from lower molecular mass of PANI obtained in case of small dopants (see section 4.2).

4.5.2 PANI nanocomposites thermooxidation stability

The results of PANI chemically synthesized nanocomposites thermooxidation stability measurements in the air environment are presented in figure 4.18.

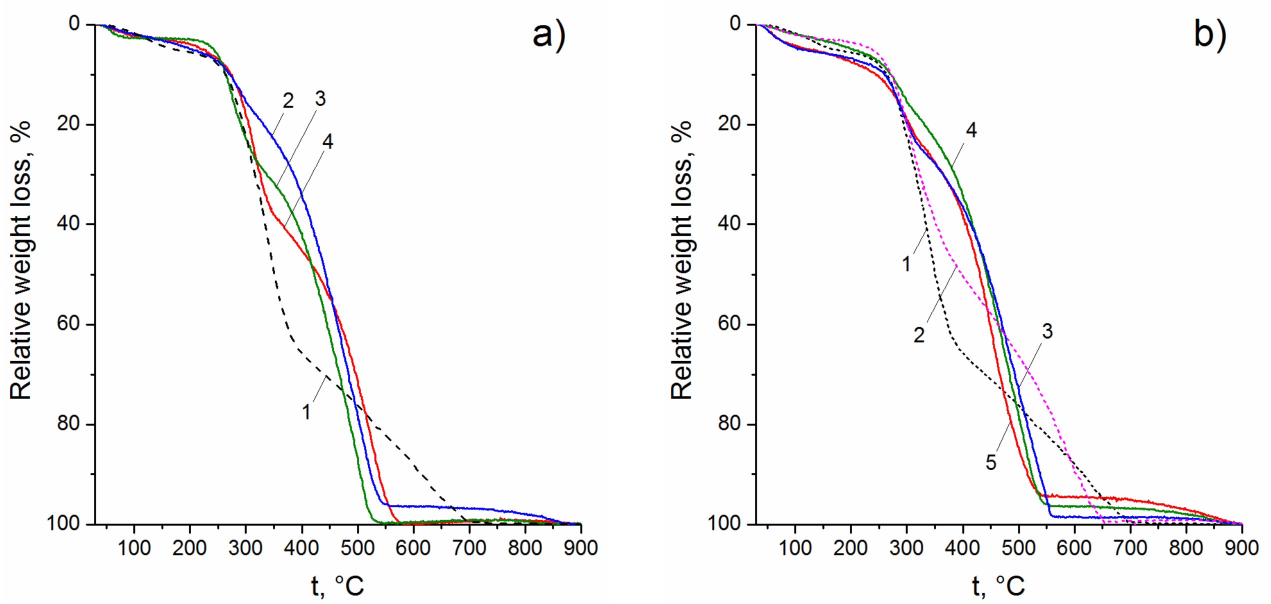

Figure 4.18 – Thermostability of synthesized material depending on **(a)** nanoparticles type: (1) pure PANI-DBSA, nanocomposites with (2) TiO_2 anatase (10 nm, 18.9 wt.% PANI-DBSA), (3) TiO_2 rutile (20 nm, 12.3 wt.% PANI-DBSA), (2) SnO_2 (50 nm, 15.7 wt.% PANI-DBSA); **(b)** PANI-DBSA content in TiO_2 (anatase) nanocomposite, wt.%: (1) 100, (2) 79.2, (3) 36.1, (4) 18.9, (5) 8.7.

Taking into account the different content of polymer phase in synthesized nanocomposites due to different PANI yield (see section 3.4) and presence of remaining incombustible nanoparticles, in order to facilitate comparison of synthesized materials thermal stability, thermograms are represent relative weight loss of samples. All synthesized nanocomposites demonstrate high stability in the air up to temperatures of ~280°C, regardless of the used oxide nature and dopant structure. In particular, their thermograms (figure 4.18) indicate slight losses of moisture (20 – 120°C) and unbound dopant.

In the range of 280 – 450°C all nanocomposites exhibit moderate weight losses that can be attributed to thermal dissociation of PANI salt, accompanied by dopant evaporation and destruction (on the example of DBSA). However, these losses significantly depend on the oxide nature and increase in a raw SnO_2> TiO_2 (rutile)> TiO_2 (anatase) (figure 4.18a). Greater stability of the polymer phase in latter case, probably associated with higher oxidation degree of PANI and therefore emergence of specific interactions between dopant and hydroxyl groups on the oxides surface, which appears to be stronger in case of anatase nanoparticles compared to rutile and tin oxide nanoparticles. At temperatures t> 450°C, after the practically complete dopant loss by samples, materials thermal stability mainly depends on the initial content of PANI phase, and significantly less depends on used oxides and acid-dopants nature. In particular, if the content of doped polymer phase (PANI-DBSA) exceeds 79.2 wt.%, the behavior of nanocomposite materials is closer to pure PANI-DBSA (figure 4.18b, curves 1 and 2). At lower content of polymer phase (<79.2 wt.%) TG curves of synthesized nanocomposites almost coincide.

4.6 Influence of UV light exposure on stability of pure PANI and its nanocomposites

Polyaniline is very promising material due to high absorption coefficients in the visible part of spectrum, high mobility of charge carriers and good stability [86]. In this regard, the electrons/holes transportation ability of PANI upon visible light excitation [273], can be effectively used for the creation of hybrid materials with inorganic semiconductors, where PANI acts as stable photo-sensitizer [274]. However, the photoactivity inherent to metal oxide nanoparticles used in this work [191, 193, 194, 275-278], raises the question about possible photodegradation of polymer phase into nanocomposites under visible and near ultraviolet radiation. Therefore, considering the well-known dependence of PANI properties on its redox state [86, 207, 279], the investigation of UV-light irradiation effect on synthesized materials properties, including sensing ones, is of big interest.

In order to evaluate the influence of UV-light irradiation on polymer backbone, the samples of pure PANI and its hybrid materials with TiO_2 (rutile and anatase) and SnO_2 nanoparticles were separated into two groups. Group (1) was not exposed to UV irradiation, while the group (2) was dispersed and cast from chlorobenzene (to form the thin uniform layer) and continuously exposed (14 days) for the light with maximum at wavelength λ=367 nm. After the experiment all samples were dedoped and changes in their spectra were investigated by UV spectroscopy. Spectral changes between group (1) and group (2) samples are shown in figure 4.19.

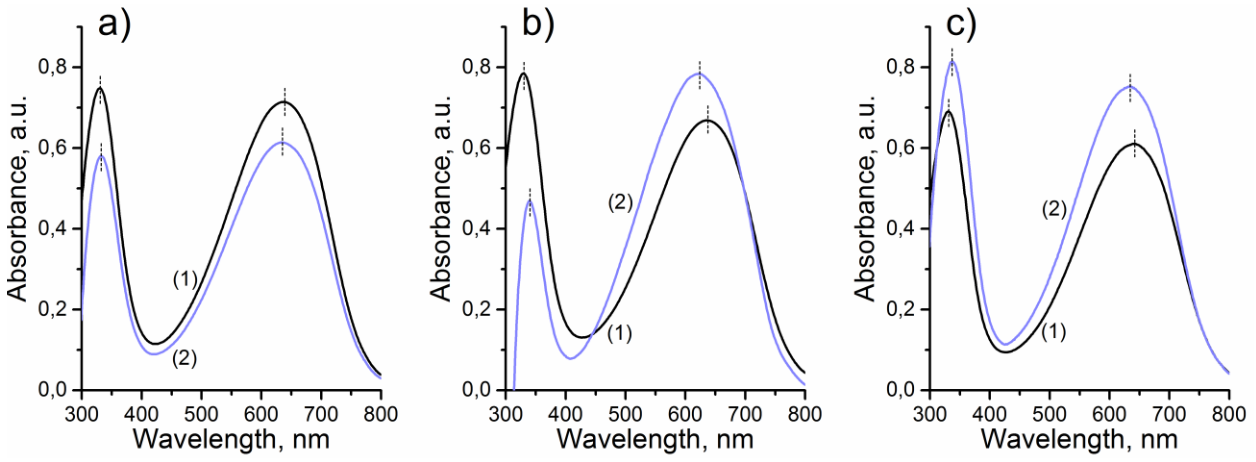

Figure 4.19 – Electronic spectra of dedoped PANI solutions after dispersing in NMP nanocomposites base on **(a)** TiO_2 anatase, **(b)** TiO_2 rutile, **(c)** SnO_2 nanoparticles, obtained (1) before and (2) after UV exposure.

The typical UV-Vis absorption spectra of PANI in dedoped state have two absorption bands at c.a. 330 and 638 nm. The first one (B) corresponds to the π–π* transition of the benzenoid rings, while the second (Q) is attributed to π–π* transitions from benzenoid HOMO to quinoid LUMO in PANI backbone [110, 280].

Based on the known fact that exciton peak position and height ratio of both bands (Q/B) characterizes PANI oxidation degree (OD), we evaluated changes occurred under UV irradiation (λ= 367 nm) in nanocomposite materials based on different semiconductor oxide nanoparticles (table 4.5).

Table 4.5 Influence of UV irradiation on peaks position and PANI oxidation degree depending on used nanoparticles, on the example of DBSA dopant

Nanocomposite / Conditions of investigation	anatase TiO_2/PANI (ΔE= 3.2 eV)			rutile TiO_2/PANI (ΔE= 3.0 eV)			SnO_2/PANI (ΔE= 3.8 eV)		
	λ_{maxB}	λ_{maxQ}	OD	λ_{maxB}	λ_{maxQ}	OD	λ_{maxB}	λ_{maxQ}	OD
Initial state	330	638	0.49	330	636	0.46	332	639	0.47
After UV exposure	333	634	0.52	340	623	0.63	338	634	0.48

*OD is the oxidation degree calculated by formula 2.1, using the absorbance maxima at λ_{maxB} and λ_{maxQ}.

It should be noted that although the effect of UV irradiation was investigated for doped forms of nanocomposites, the qualitative changes were evaluated by their dedoped forms, because dedoped PANI is more soluble in NMP, which is convenient solvent for spectrophotometric studies. Peak positions and ODs of PANI phase in synthesized materials (table 4.5) before exposure indicate their very close state in all cases. After UV exposure the different by value bathochromic shifts of B bands and hypsochromic shifts of Q bands together with changes in PANI OD are observed. Thus, unlike nanocomposites with anatase and SnO_2, where only minor changes occur, nanocomposites with of TiO2 (rutile) nanoparticles demonstrate a noticeable shift of both bands for 10 – 13 nm and an OD increase for ~17%, indicating a significant changes in the polymer phase electronic state. Considering the range of used for irradiation lamp (figure 2.5) and the band gap of used oxides, apparently, excitation of valence band electrons with their subsequent transfer to the conduction band, followed by reduction to superoxide anion $*O_2^-$, which oxidizes PANI, is probable only in case of TiO_2. However, much larger band gap of SnO_2 (3.8 vs. 3.2 eV) and relatively lower lamp radiation intensity in this spectral region, causes minimal changes in the polymer phase. However, it remains unclear the difference in activity of rutile and anatase nanocomposites, as in both cases the radiation energy of used light source completely covers TiO_2 band gaps. Possible explanation for the higher stability of nanocomposites based on anatase is the emergence of specific interactions at the polymer-nanoparticle interface. Obtained results are in good agreement with the experimental data on pure PANI and its nanocomposites sensitivity to ammonia (see section 5.2).

* * *

Thus, it was found that molecular characteristics of PANI and its phase in nanocomposites, structure and morphology, electrical properties, thermal and photostability substantially depend on the nature and content of dispersed metal oxides nanoparticles in hybrid materials and type of used in the synthesis acid-dopant. In turn, this may also influence the sensing properties of PANI nanocomposites.

5 SENSING PROPERTIES OF SYNTHESIZED MATERIALS

Polyaniline and its derivatives have been used as the active layers of gas sensors since early 1980s [75] owing to high sensitivity, synthesis simplicity and ability to detect gases even at room temperature [84]. However, pure polymer has number of shortcomings suppressing its wide commercialization, such as inferior mechanical properties, moderate stability and low specific surface area, hindering analytes penetration deep into the sensing layer and, therefore, affecting response magnitudes and sensors regeneration speed. The use of sulfonic acids as dopants improves PANI processability and solubility. Obviously, in case of dopant-induced PANI solubility [125, 281] polymer content in the nanocomposite has substantial influence on technological aspects of sensing layers formation. The common deposition methods include drop-casting and spin coating, demanding the additional separate stage of PANI dispersing in proper solvent. The latter is an important issue, which can significantly influence materials sensitivity through changes of target morphology by the polymer phase partial dissolution [282].

Therefore, in this chapter the dependence of synthesized materials sensing properties to ammonia and amines on nature of used acid-dopants, metal oxides nanoparticles, polymer content and active layers morphology is presented.

5.1 Pure PANI sensing properties

5.1.1 Solvent effect on pure PANI sensing responses

The authors [123] demonstrated the positive effect of pure PANI dissolution in m-cresol on electrical, optical and structural properties of polymer, and was explained by transition of polymer chains packing structure from compact to expanded coil through the so called “secondary doping”. According to this concept the used solvents are “inert” substances and their influence is limited only to PANI conformational changes. However, in later works the formation of strong hydrogen bonds between polymer and solvent (m-cresol) leading to competition of solvent and primary dopant was shown [283, 284]. The authors [253] proposed the DCAA as a good alternative to m-cresol, allowing achievement of high crystallinity and conductivity of formed PANI layers. Moreover, the authors [84] used DCAA as a medium for solution blending of CSA-doped PANI with polyurethane, allowing fabrication of thin sensitive layers in for ammonia detection. However, such approach implies full polymer dissolving and partial protonation with DCAA in addition to primary dopant [253]. Therefore, the question concerning influence of such PANI component dissolution on sensing and other properties still remains open.

The mechanism of changes in sensing layer is quite well known [87] and in case of ammonia, for simplicity of understanding, can be reduced to the next scheme [285]: $PANI–H^+ + NH_3 \leftrightarrow PANI + NH_4^+$.

In particular, ammonia (or other basic substances e.g. amines) molecules adsorbing on the polymer surface partially withdraw protons from previously protonated imine groups of the emeraldine salt, thereby changing its electronic properties (conductivity, optical density etc.). Therefore, the formation of labile complexes in PANI sensing clusters, namely “ammonia – PANI – proton – charge compensating dopant anion” can occur. During the interaction between gas phase and doped PANI the sensing material resistance proportionally increases depending on analyte concentration. When the sensing layer is exposed to pure air, formed complexes decompose into constituents, analyte molecules desorb from the sensing material surface and the process of restoring of initial doping degree and PANI sensing layer resistance is observed. It should be noted that dispersing solvent and dopant choice plays an important role in regeneration processes (figure 5.1).

From the figure 5.1 response magnitudes to ammonia of pure PANI doped with the same dopants are strongly depend on used solvent. The use of DCAA positively influences on the pure PANI doped with small dopants, while in case of big dopants the only continuous signal growth with no decrease after blowing with pure air can be observed (figure 5.1a). Possible explanation of this phenomenon is polymer chains transition from compact to expanded coil form (see section 1.3). The latter improves charge transport processes as well as changes in doped PANI crystallinity during the process of dissolving or films casting from the DCAA. However, the PANI doped

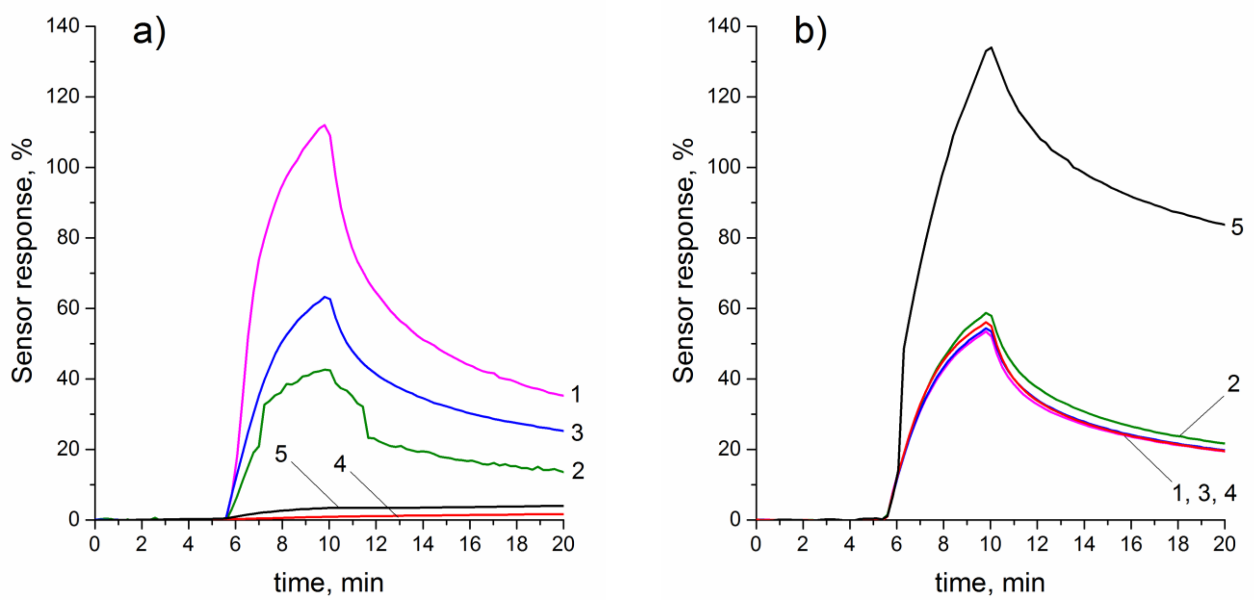

Figure 5.1 – Kinetic curves of PANI sensing responses depending on used dopant: (1) BSA; (2) TSA; (3) CSA; (4) LSA; (5) DBSA cast from **(a)** DCAA and **(b)** CB to 50 ppm of ammonia.

with big dopants such as LSA and DBSA already has optimized expanded coil structure formed at polymerization stage. The use of the bulky dopants as counter-ions increases inter-chain distance between adjacent PANI chains, allowing formation of porous structure with decreased number of inter-chain interactions and facilitating analyte penetration [286]. Therefore, the treatment with DCAA leads to an increase in chains packing density resulting in improved crystallinity and polymer chains stiffness [287]. The new formed dense structure hinders penetration of analyte molecules deep into as well as slows down regeneration processes. The use of mild solvent as chlorobenzene does not induce changes in polymers structure and, thus, allows evaluation of the real response level, which is in good agreement with SEM TEM data (see section 4.3).

Results on PANI responses measurement to ammonia at the concentration range of 1 – 100 ppm allow estimation of PANI materials sensitivity. The latter is defined as a slope of the fitting linear function drawn through signal maxima in “sensor response- analyte concentration” coordinates (figure 5.2).

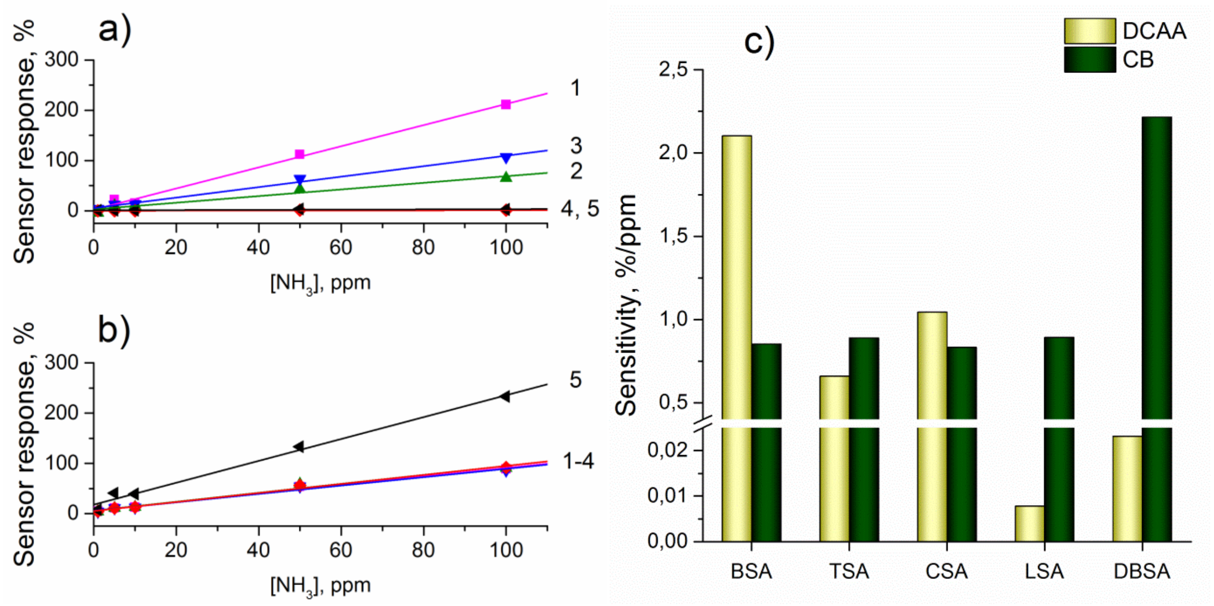

Figure 5.2 – Influence of dopants: (1) BSA; (2) TSA; (3) CSA; (4) LSA; (5) DBSA to ammonia (1 – 100 ppm) cast from **(a)** DCAA and **(b)** CB; **(c)** comparison of pure PANIs sensitivity.

From the figure 5.2 the best sensing properties were demonstrated by PANI-BSA cast from DCAA and PANI-DBSA cast from chlorobenzene. Considering the fact that these dopants are typical representatives of “small” dopants without surface activity and “large” dopants, hereinafter more attention in discussion of sensing properties will be paid to these materials. The comparison of pure PANI-DBSA sensing properties with literature data is presented in table 5.1.

Table 5.1 The comparison of pure PANI materials sensing properties given in literature

Material / [dopant]	Sensitivity to ammonia, %/ppm for 5 min exposure	Detection limit	Ref.
PANI [DBSA]	2.22	< 1 ppm	This work
PANI [H_2SO_4]	0.625*	7 ppb	[88]
PANI [HCl]	1.94*	< 1 ppm	[288]
PANI [HCl]	0.872*	10 ppm**	[289]
PANI [DBSA]	1.86*	5 ppm**	[290]
PANI [DBSA]	0.51*	2 ppm	[291]

*Published data after “sensitivity” parameter conversion to units used in present work, using formula 2.2. Response values were taken from given in literature kinetic curves at time 5 min.

**The lowest tested concentration in study.

5.1.2 Humidity effect on pure PANI sensing responses

The known advantages of polymers, such as light weight, flexibility, low cost and simple fabrication process [292] makes PANI an ideal candidate for sensors applications. Specifically, it can be effectively used as an active material in humidity sensors [293-295]. However, the application of PANI for ammonia and amines detection makes humidity sensing unwanted, as the interference of signals from pollutant and moisture can misrepresent real situation. Therefore, it is important to isolate signals, in particular, by observing sensors response changes to analyte of interest at different humidity level. Synthesized materials response dependences on humidity are presented in figure 5.3.

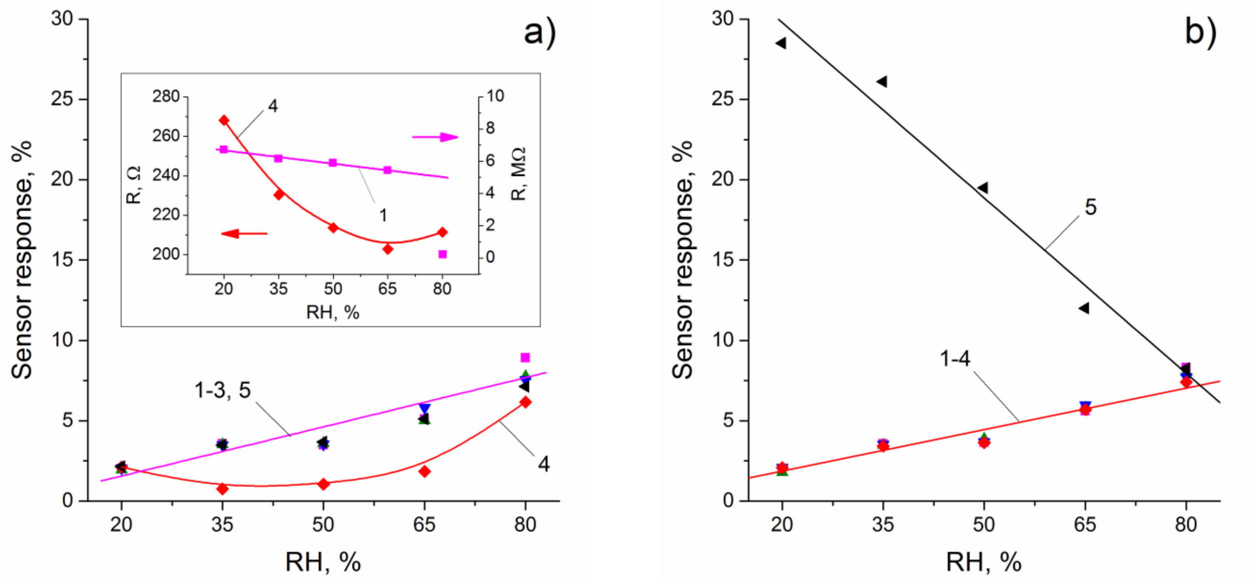

Figure 5.3 – Response magnitudes comparison of pure PANIs doped with: (1) BSA; (2) TSA; (3) CSA; (4) LSA; (5) DBSA cast from **(a)** DCAA and **(b)** CB to 10 ppm of ammonia at different humidity. Inset is the dependence of sensing layer resistance on relative humidity level.

Responses of pure PANI materials treated in DCAA generally demonstrate the linear growth of signal magnitude with increase of humidity level. Such behavior is usually assigned to PANI physicochemical state and conformation changes, affecting proton hopping and ionic transport along charged polymer chains [291, 295-297]. However, the different from other materials behavior of the PANI-LSA sensor treated in DCAA was observed with humidity level changes. Figure 5.3a demonstrates the bimodal variation of sensor response as well as non-linear resistance dependence on humidity (figure 5.3a inset). At first electrical resistance of the film decreases with RH grow, corresponding to increased efficiency of charge transportation. Nevertheless, at RH= 65% the inflexion point of resistance-humidity dependence is observed. After this point the increase in film resistance can be observed (figure 5.3a inset).

Authors [298] suggest water dissociation as the main reason for PANI layers conductivity increase in the presence of water vapors. As PANI in emeraldine salt form has numerous H-bond accepting/donating and charged bearing sites (i.e. –NH–, –N– , $–NH^{+}–$, $–NH_2^{+}–$ etc.), the reaction equilibrium shifts to protons formation [295]. Therefore, the absorbed water can act as a source of protons, increasing polymer doping level and/or to create alternative charge-transfer path through the network of absorbed water molecules and thus increasing overall conductivity.

Authors [295] additionally propose to take into account the accompanying process of polymer swelling caused by water molecules absorption and leading to conductivity decrease. The overall process can be characterized by partition coefficient (K) which is a ratio between concentrations of water vapors absorbed into the polymer (C_S) and in gas phase (C_G):

$$K = \frac{C_S}{C_G}$$

Coefficient K is constant at given temperature and depends only on polyaniline chains structural arrangements. The PANI swelling process leads to polymer chains distortion and hence increases packing disorder resulting in decrease of π-conjugation and restricts movements of charge carriers [299, 300]. Additionally, sensors responses are modulated by acid-base reactions between polyaniline dopants and ammonia, which is most evident in case of LSA (figure 5.3a). At low humidity level the sensor response is mainly determined by ammonia interaction with dopant, leading to partial deprotonation and resistance decrease. However, with RH level increase the contribution of water caused protonation increases and can compensate this resistance decrease. Therefore, the only slight increase of sensors responses in the humidity range from 35 to 65% is observed. At higher RH, when the polymer surface saturates with water molecules, partial PANI swelling causes resistance decrease and sensor responses increase. In other words, the contribution ammonia and water interaction with PANI layer into the sensors response magnitude varies with the relative humidity level.

In case of sensing layers cast from chlorobenzene (figure 5.3b), the original polymer structure remains intact and thus, DBSA doped PANI has significantly higher porosity compared to other materials and respectively higher surface to volume ratio (see section 4.2). Therefore, the protonation effect caused by water adsorption is more pronounced, while the resistance decrease caused by polymer swelling has no substantial effect on the overall electrical conductivity changes. In this case conductivity depends only on surface coverage and linearly grows with the relative humidity increase. Parvatikar et al. [301] explain the effect of conductivity growth by increase of holes concentration, which makes the polymer more p-type in nature. Tai et al. [302] also suggest the formation of improved links between PANI grains.

In case of PANI materials synthesized with small dopants (BSA, TSA, CSA) and cast from DCAA the linear increase of response magnitude with RH growth is observed. Initially lower porosity of these materials practically do not change under the influence of DCAA, thus response magnitudes are close regardless of used dispersing solvent. The only exception is PANI-DBSA, where the changes of structure are noticeable and the slope of response-humidity dependence changes to opposite.

Summarizing above, PANI samples electrical conductivity is a result of simultaneous action of two opposite effects, namely protonation with water molecules and partial polymer swelling. The degree of their influence on resulting sample resistance value determines by PANI materials surface to volume ratio. Samples with high surface are characterized by linear conductivity increase with humidity growth.

5.1.3 Temperature effect on pure PANI sensing responses

The response-temperature dependences of the synthesized materials to ammonia are presented in figure 5.4. Responses of pure PANI materials cast from DCAA generally demonstrate linear growth of signal magnitude with temperature increase. This is in good accordance with data on sensors response-relative humidity dependences. In should be noted, that same relative humidity value at different temperature implies different absolute humidity, i.e. water content in air at higher temperature exceeds the one at lower temperature. Therefore, despite sensors responses were measured at same humidity conditions (RH= 50%), the shift of equilibrium vapor pressure with the variation of temperature leads to results similar to humidity variation at a given temperature.

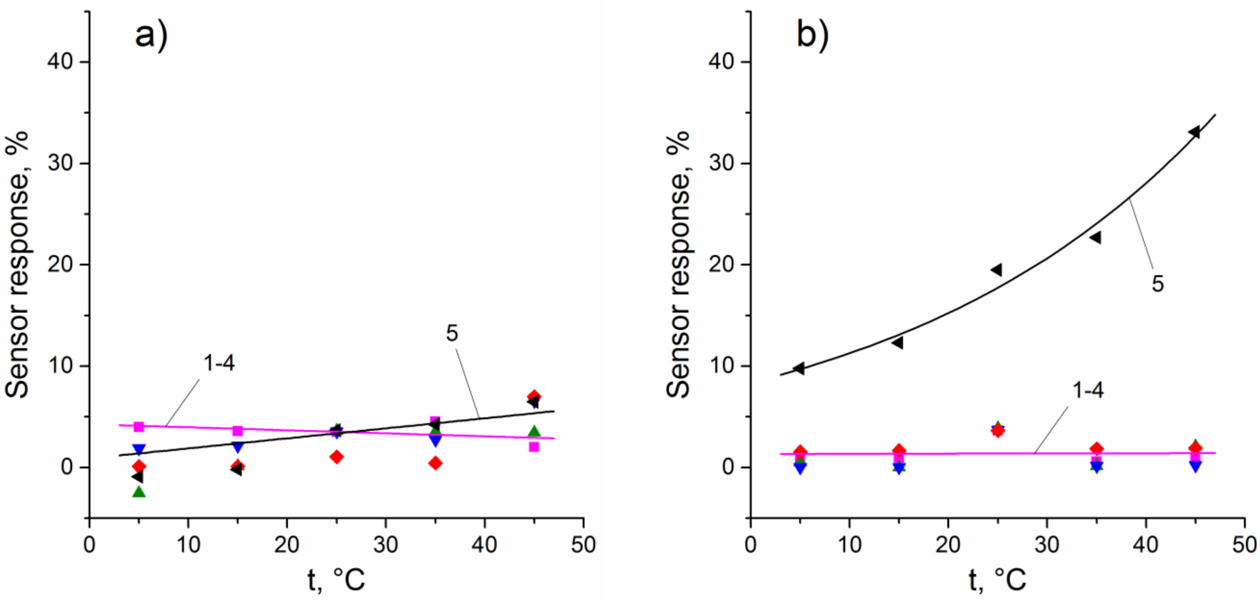

Figure 5.4 – Response magnitudes comparison of pure PANIs doped with: (1) BSA; (2) TSA; (3) CSA; (4) LSA; (5) DBSA cast from **(a)** DCAA and **(b)** CB to 10 ppm of ammonia at different temperature.

PANI-BSA demonstrates a behavior opposite to other samples cast from DCAA. The sensor response decreases with temperature growth, while in other cases the slight improvement is observed. This phenomenon apparently stems from starting resistance decrease with temperature growth (figure 5.5a). However, in contrast to DBSA doped sample, the conductivity decrease caused by sensors interaction with ammonia practically completely compensates by PANI protonation with water.

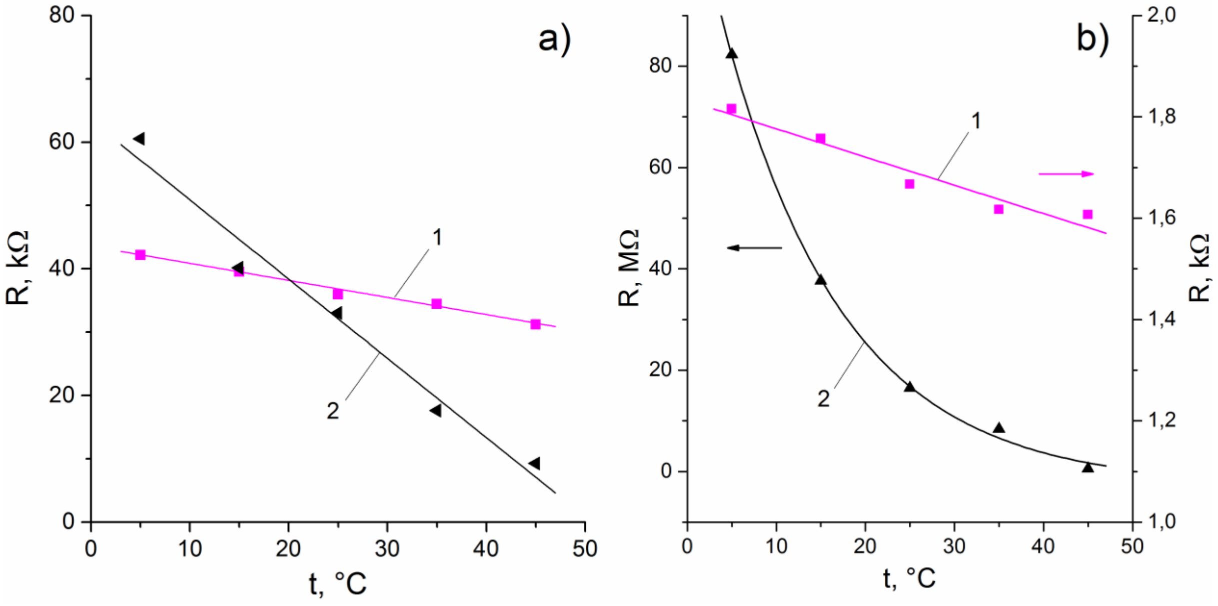

Figure 5.5 – Resistance variation of pure PANIs cast from **(a)** DCAA and **(b)** chlorobenzene to 10 ppm of ammonia at different temperature

Most of samples cast from chlorobenzene do not show the noticeable increase in sensors response with temperature change. At the same time, the DBSA doped sample demonstrates significant improvement of sensors response with temperature increase (figure 5.5b). The best fitting curve has next parameters: $SR = 0.051 + 0.079e^{0.031t}$. The resistance-temperature dependence of PANI-DBSA has the inverse exponential character (figure 5.5b) with the next fitting curve parameters: $R = \frac{122.61}{e^{0.073t}} - 2.81$. In other words, the increase of response magnitude with simultaneous resistance decrease is observed. Such behavior is opposite to observable in case of PANI-BSA sample cast from DCAA, where due to high sensing layer conductivity and lower sponginess the interaction with ammonia practically do not change sample resistance. In case of PANI-DBSA the extremely high initial resistance of the fabricated layer also does not allow seeing changes caused by interaction with ammonia. In this way, the facilitation of the charge transport through the interaction with water vapors has a positive effect on sensors responses.

Additionally, sensing layers resistance is influenced by semiconducting character of polyaniline, which electrical conductivity increases with temperature growth [303, 304]. Taking into account the complex character of interaction of a variety of different factors, in particular joint influence of water-doping effect, ammonia caused dedoping and water-ammonia interactions, we can assume that occurring of competitive processes of protonation/deprotonation can lead to the reprotonation of different nitrogen atoms and thus, to redistribution of protonated sites in polymer chain. Moreover, the increase of average protonated sequence length by partial conversion of previously non-conducting phase is possible.

Summarizing the above, the highest responses were obtained with the DBSA doped PANI cast from the chlorobenzene. This sample demonstrates exponential growth of response with the temperature increase.

5.2 Chemically synthesized PANI-metal oxide nanocomposites sensing properties

5.2.1 The PANI content effect on the nanocomposite sensing properties

The common drawbacks inherent to pure conducting polymers such as bad mechanical properties, moderate processability, low specific surface area etc. hinder their commercialization. One of the effective solutions to overcome these drawbacks is the formation of hybrid nanocomposite materials, in particular through incorporating of a second component (e.g. metal oxide nanoparticles) into reaction medium at the polymerization stage. The polymer grows directly on nanoparticles surface leading to a formation of core-shell structure nanocomposites.

Naturally, the majority of nanocomposites properties, including sensing ones, depend on doped PANI content in the nanocomposite, its morphology and interactions between the constituting components [84, 155, 167, 302]. In particular, when the polymer phase prevails, nanocomposites characteristics are closer to pure polymer. At low PANI contents the input of specific chemical and physical interactions between polyaniline and second component becomes stronger and leads to changes in doped PANI structure and morphology [197].

In case of core-shell morphology the low PANI content allows to form a thin polymer shell. It enhances the reactivity/responsivity to different analytes due to ease of access to PANI sensing clusters by forming high surface to volume ratio nanocomposites [84, 173]. However, taking into account the results on dispersing solvent effect on pure PANIs, this raises the question about possible changes in nanocomposites original structure and, therefore, in sensing properties.

One of the important characteristics of sensing materials is the response magnitude to analyte, allowing estimation of sensitivity. The latter is defined as a slope of the linear section of fitting curve drawn through the signal maxima in the “sensor response – analyte concentration” coordinates [305] (figure 5.6).

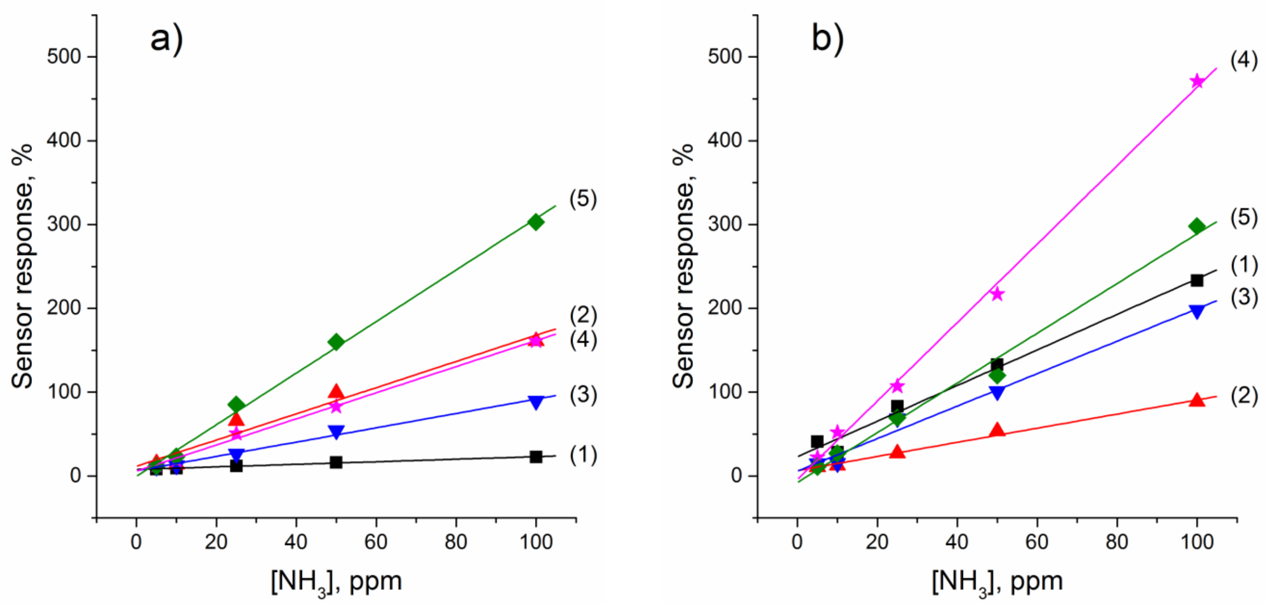

Figure 5.6 – Sensors responses of anatase TiO_2/PANI-DBSA nanocomposites depending on doped polymer content, wt.%: (1) 100, (2) 79.2, (3) 36.1, (4) 18.9, (5) 8.7 cast from **(a)** DCAA **(b)** CB to 5 – 100 ppm of ammonia.

From the figure 5.6 all the nanocomposite materials regardless of used dispersing solvent demonstrate linear growth of sensor responses to ammonia in the range 5 – 100 ppm. This fact suggests their applicability as sensing materials regardless of their preparation conditions. However, sensing layers formed from chlorobenzene dispersion demonstrate expectedly stronger responses compare to ones dispersed in DCAA. This phenomenon is apparently stems from different dissolution activity of DCAA and CB on PANI phase, leading to redistribution of polymer phase on the surface of nanocomposite particles and/or PANI dissolution/loss (see section 4.2). As a result the target core-shell structure transforms to structure with separate organic and inorganic phases.

Summarizing the above, the negative influence of DCAA on nanocomposites sensing properties, manifested in polymer dissolution and thus destroying the core-shell structure was confirmed. This negative regarding to the sensing responses effect can be eliminated by change of used dispersing solvent, in particular with chlorobenzene. The best results were obtained with chemically synthesized nanocomposite containing 18.9 wt.% PANI-DBSA cast from chlorobenzene.

5.2.2 Nanoparticles influence on the hybrid materials sensing properties

The increased interest in development of new organic-inorganic hybrid materials is explained by their advanced properties implying a wide range of potential applications, such as electronics, optics, sensors etc. Very often such materials demonstrate synergetic effect due to complementary interactions between the polymer and a second component. The effect is more pronounced when the introduced phase is of nanometer scale, e.g. metal oxide nanoparticles. Obviously, the properties of resulted hybrid nanocomposite depend both on polymer initial characteristics and on the nanoparticles nature. Therefore, by using the same PANI polymer but changing a metal oxides type (TiO_2 in rutile and anatase forms, SnO_2) it is possible to see changes induced by their presence, which opens wide perspectives in designing of materials with predetermined properties.

According to the results on PANI content influence on sensing responses to ammonia, the anatase based nanocomposite containing 18.9 wt.% of PANI-DBSA and synthesized at the polymerization ratio $An:TiO_2$= 10:90 wt.%, demonstrated the best sensing properties. Thus, all the further syntheses with other type nanoparticles were carried out using the same monomer to nanoparticles ratio. The comparison of parameters of typical nanocomposites responses to ammonia is shown in figure 5.7. As one can see, the high adsorption potential of synthesized materials does not allow reaching the saturation state during the tested 5 min time interval, which makes the

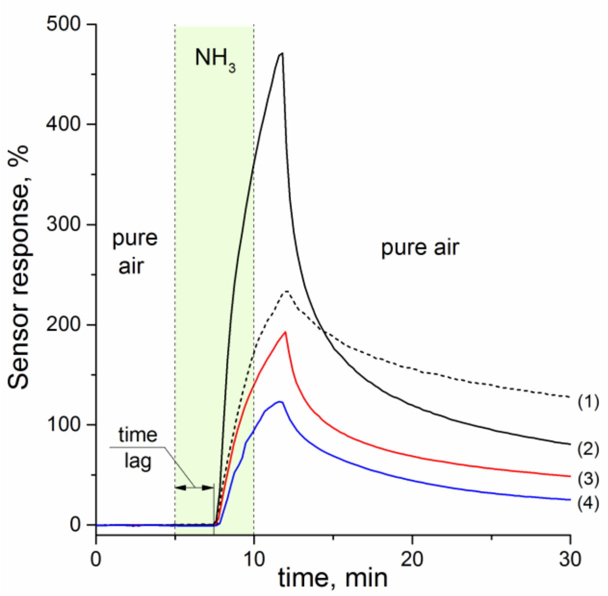

Figure 5.7 – The influence used nanoparticles type: (1) pure PANI-DBSA, nanocomposites with (2) TiO_2 anatase (10 nm, 18.9 wt.% PANI-DBSA), (3) TiO_2 anatase (20 nm, 12.3 wt.% PANI-DBSA), (4) SnO_2 (50 nm, 15.7 wt.% PANI-DBSA) on sensors response kinetics to 100 ppm of ammonia.

sensors response time calculation meaningless. Nevertheless, the comparison of other parameters of sensors kinetic curves revealed that the highest response magnitudes (471%) and fastest regeneration (1.3 min for 50% regeneration) were obtained when the anatase nanoparticles were used. The pure PANI-DBSA and nanocomposite with rutile nanoparticles have close maximum response values: 233 and 193% respectively (figure 5.7, curves 1 and 3). However, the regeneration process is significantly faster in the nanocomposite case than in case of PANI-DBSA (2.7 vs. 24.8 min), which can be assigned to more developed surface of hybrid material. The worst results were obtained with the hybrid nanocomposite based on SnO_2 nanoparticles: response maximum value (122%) was significantly lower even compared to pure PANI-DBSA, while the regeneration occurred quite fast (4.1 min). The results on sensitivity and signal repeatability of synthesized materials to ammonia are presented in figure 5.8.

It was found that nanocomposite materials sensitivities are generally higher than in case of pure PANI with same dopants. The observable amplification of the TiO_2 based nanocomposites sensitivity in ~2.1 times, compared to the most sensitive pure PANI-DBSA, is probably due to high nanocomposites porosity as well as owing to the use of chlorobenzene as a solvent. The latter allows keeping the original nanocomposite materials structure (see section 4.2).

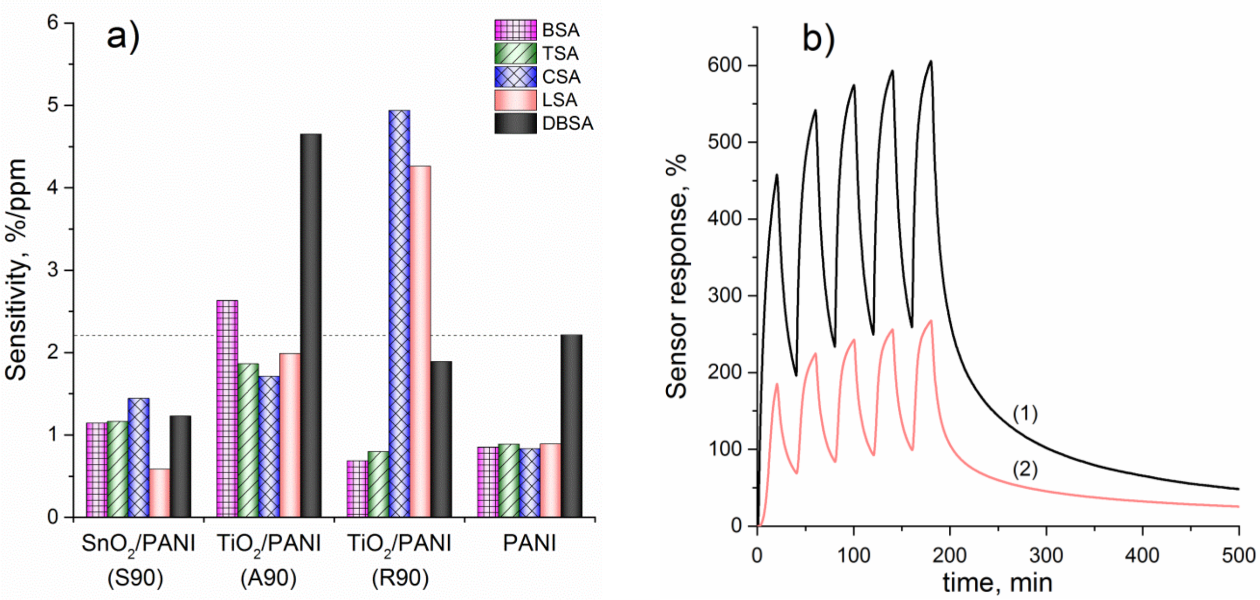

Figure 5.8 – Sensing properties of synthesized materials **(a)** sensitivity to 5 – 100 ppm of ammonia, **(b)** typical nanocomposites repeatability curves: (1) TiO_2/PANI-DBSA, (2) TiO_2/PANI-LSA.

Expectedly, while using TiO_2 nanoparticles with smaller size (10 nm for anatase and 20 nm for rutile) compared to SnO_2 ones (50 nm) with comparable doped polymer content (18.9 and 12.3 vs. 15.7 wt.% respectively), TiO_2 based nanocomposites have higher sensitivity. This is due to a lower specific surface of SnO_2 nanoparticles and, therefore, bigger polymer thickness on their surface, resulting in lower sensing layer porosity.

However, the rutile based nanocomposite R90-CSA has unexpectedly high sensitivity. This deviation from general trend probably can be associated with higher content of PANI-CSA in the nanocomposite or with higher doping degree compared to other composites obtained in the presence of “small” dopants. The comparison of sensing properties of the best PANI based nanocomposites synthesized in this work with literature data is presented in table 5.2.

Considering the high sensitivity to ammonia of nanocomposites A90-DBSA, R90-CSA and R90-LSA, further investigations were conducted with these materials.

Table 5.2 The comparison of PANI nanocomposites sensing properties with literature data

Material / [dopant]	Sensitivity to ammonia, %/ppm for 5 min exposure	Lowest tested concentration	Ref.
anatase TiO_2/PANI [DBSA]	4.65	1 ppm	This work
rutile TiO_2/PANI [CSA]	4.94		
rutile TiO_2/PANI [LSA]	4.26		
SnO_2/PANI [DBSA]	0.72*	10 ppm	[167]
anatase TiO_2/PANI [HCl]	3.63*	5 ppm	[288]
TiO_2/PANI [DBSA]	0.64*	1.5 ppm	[306]
anatase TiO_2/PANI [HCl]	4.29**	23 ppm	[307]
CeO_2/PANI [phytic acid]	0.09**	2 ppm	[308]
TiO_2/PANI [PSSA]	0.245*	10 ppm	[309]

*Published data after conversion to units used in this work, using formula 2.2. Sensors response values were taken from given in literature kinetic curves at time 5 min.

**Sensor reached saturation less than in 5 min.

5.2.3 The influence of UV exposure on the nanocomposites sensing properties

As was shown, the properties of synthesized nanocomposite materials could significantly change under use in light conditions (see section 4.6). Taking into account the possible influence of this factor also on materials sensing properties, we studied the impact of near UV irradiation on synthesized nanocomposites sensitivity to analytes of basic nature, on the example of ammonia (figure 5.9).

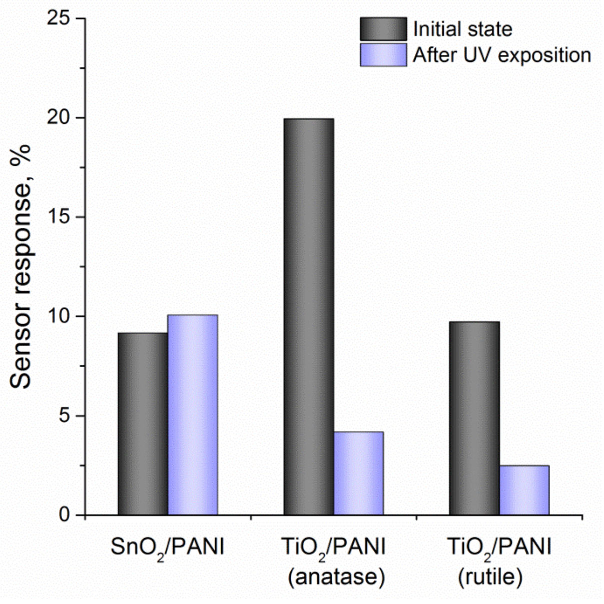

Figure 5.9 – The influence of UV light exposure on sensors responses to 10 ppm ammonia.

All investigated materials had the maximum doping degree in order to exclude the influence of dopant content. The SnO_2 based nanocomposite demonstrates the partial improvement of sensing properties, which can be both connected to the UV induced partial increase of polymer phase oxidation degree (see table 4.5) and thus establishing of closer to ideal quinoid to benzenoid units ratio, or to specific interactions of both components.

However, TiO_2 based nanocomposites demonstrate a significant attenuation of sensors response, which weakly correlates with OD changes in PANI phase (see table 4.5). The similarity of changes in both TiO_2 based nanocomposites under UV irradiation, suggests that in this case the main factor determining the sensors response magnitude is not a PANI OD value, but probably the amount of change in photo-induced dedoping. This assumption is consistent with the fact that nanocomposites based on nanoparticles of both allotropic modifications of TiO_2 (rutile and anatase) have more developed surface and, consequently, greater contact area of PANI phase with TiO_2 nanoparticles compared to nanocomposites based on SnO_2. Therefore, the weakening of their sensing properties can be associated with easier oxidation of a thinner polymer layer with oxygen (superoxide anion) activated by UV irradiation.

Summarizing the above, the polymer oxidation degree value strongly influences synthesized materials sensing properties to ammonia. However, in all cases there is no evident dependence between PANI phase oxidation degree and sensors response magnitude, which may indicate an additional impact of other factors, in particular of a partial dopant degradation.

5.2.4 Humidity and temperature effects on the nanocomposites sensing properties

It was found that temperature and humidity factors have a significant influence on pure PANI sensors responses to ammonia. In this regard, the investigation of influence of these parameters also on nanocomposites responses is of great interest (figure 5.10).

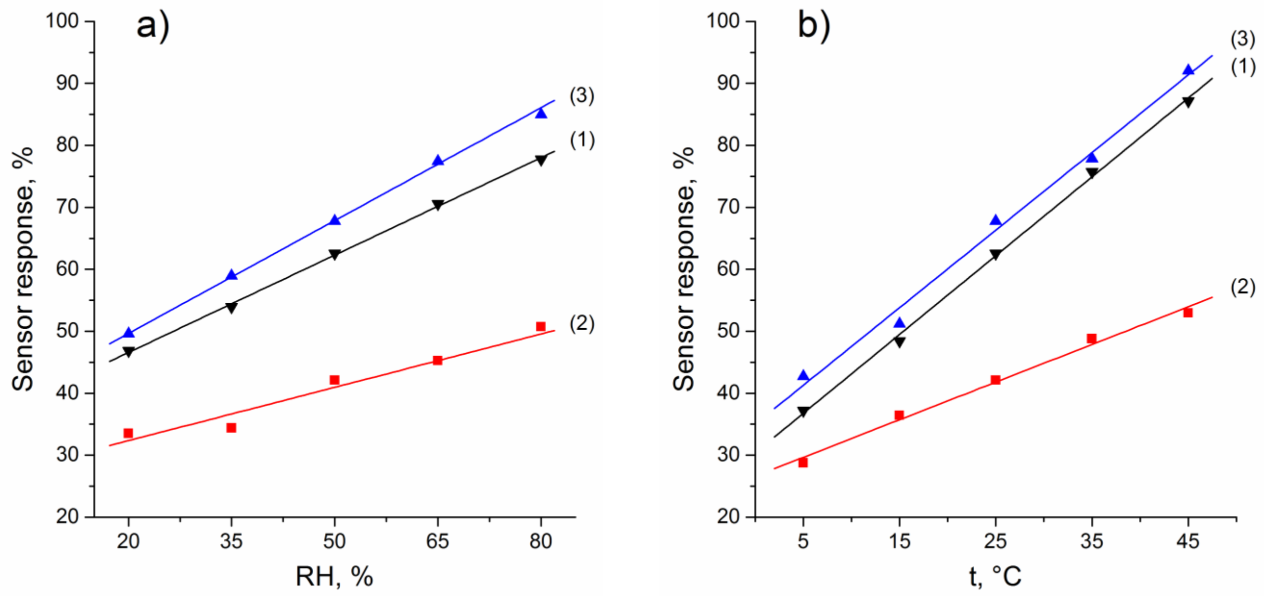

Figure 5.10 – The influence of (**a**) relative humidity and (**b**) temperature on sensing properties of PANI nanocomposites: (1) A90-DBSA, (2) R90-LSA, (3) R90-CSA to 10 ppm of ammonia.

In spite of pure PANIs, nanocomposite materials with anatase and rutile nanoparticles demonstrate linear dependence of sensor responses on humidity level along with significantly higher sensitivity. The latter can be attributed to the formation of highly developed surface facilitating the analyte and moisture contacts with PANI sensing clusters, while the proportionality of signal growth is probably connected with impact of interaction effects in system “water – PANI – ammonia”.

“Response – temperature” dependences of synthesized materials also have linear character (figure 5.10b); however, the slope of these dependences is steeper, which probably can be explained by the difference in absolute humidity at different temperature, while maintaining the same relative humidity.

5.2.5 Nanocomposites sensitivity to amines

Amines are more hazardous alkyl- or aryl-substituted derivatives of ammonia [33]. Depending on chemical structure they can have carcinogenic [37, 38], mutagenic and/or hemotoxicant effects [39, 40]. Their wide industrial use increases the potential for occupational exposure [48]. Nevertheless, the similarity of their chemical structure to ammonia allows their detection with the synthesized PANI based hybrid materials. The results on methylamine (MA) and trimethylamine (TMA) influence on sensitivity of nanocomposites with the best sensing properties, namely A90-DBSA, R90-LSA and R90-CSA are presented in figure 5.11a.

Anatase and rutile based nanocomposites A90-DBSA and R90-CSA demonstrate responses decrease in the row MA> TMA> NH_3 while the basicity of analytes reduces in the row TMA> MA> NH_3. The moderate sensitivity in case of most basic TMA can be explained by large dimensions of TMA molecules compared to other analytes, and thus to hindered penetration deep into polymer shell of the nanocomposite.

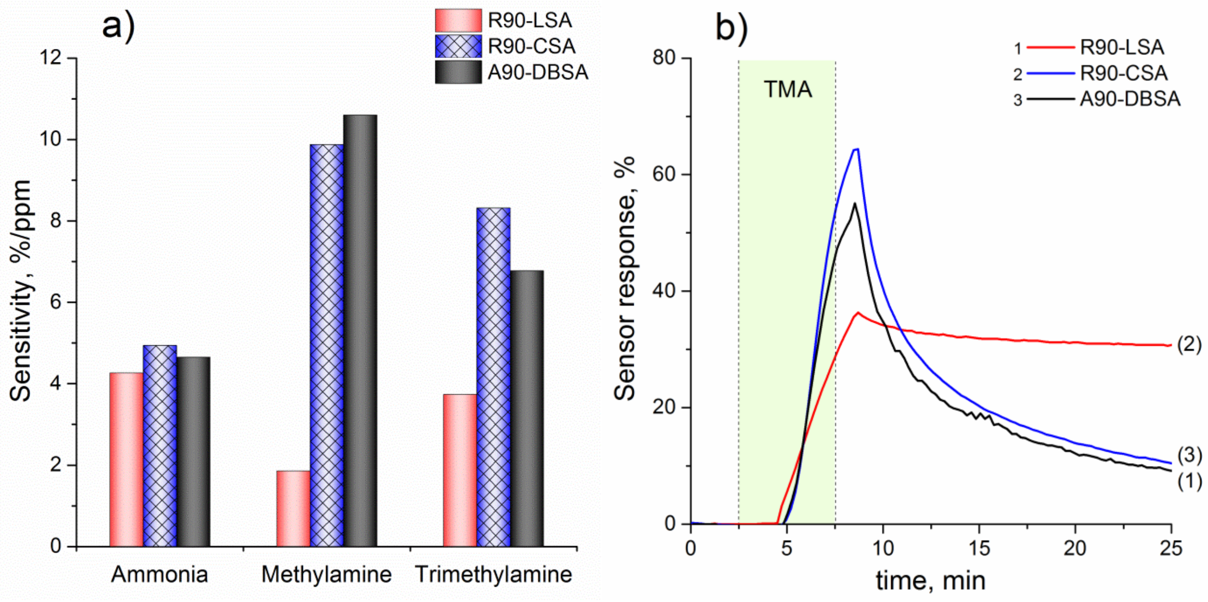

Figure 5.11 – Comparison of PANI nanocomposites (**a**) sensitivity to ammonia and amines and (**b**) regeneration after interaction with 10 ppm of TMA

At the same time the R90-CSA nanocomposite demonstrates a sensitivity decrease in the row NH_3> TMA> MA. Such behavior probably can be explained by its lower porosity. In this case the penetration of smallest ammonia molecules with lowest basicity appears almost with the same speed as interaction with most basic large TMA molecules. This suggestion partially confirms by the shape of sensors response kinetic curves (figure 5.11b).

5.3 Sensing properties of hybrid materials prepared in alternative ways

The unique properties of conducting polymers gave rise to a large number of studies directed on further improvement of their characteristics, in particular by creation of ICP based composites materials. It was shown that variation of preparation conditions and techniques proposed by different research groups [88, 118, 126, 167, 169, 173, 294, 296, 301, 306, 310, 311] allows obtaining materials with different properties. In this regard, the comparison of hybrid materials prepared in alternative (to proposed in this work chemical route) ways can help to understand better the influence of different factors on resulting sensing properties.

5.3.1 Sensing responses of PANI-metal oxide mechanical mixture

The different dissolving activities of DCAA and chlorobenzene on doped PANI, obviously, should reflect on quality and structure of the formed sensing layers and thus, on response magnitudes to ammonia. It was found recently [197, 312] that in hybrid composite materials with low PANI content the main part of polymer is localized in a form of thin shell covering nanoparticles. The crystallinity, molecular weight, oxidation degree as well as solubility of such layer differ considerably from the bulk PANI. Therefore, changes of original nanocomposites structure, followed by partial metal oxide nanoparticles denuding and polymer redistribution may occur in different degree, depending on used solvent.

In this regard, the question concerning reasonability of nanocomposites chemical synthesis compared with a simple mechanical mixing of components into the solvent. To clarify this point the mechanical mixture containing 10 wt.% PANI-DBSA with TiO_2 (anatase) nanoparticles was prepared. Results of the study of solvent and preparation method influence on hybrid composite materials sensing properties are presented in figure 5.12.

As one can see from the chemically synthesized anatase based nanocomposite TiO_2/PANI-DBSA (18.9 wt.% PANI-DBSA) cast from chlorobenzene has higher sensitivity than mechanically mixed analog. This fact suggests a much better accessibility of PANI-DBSA sensing clusters, which are more uniformly distributed in thin shell on nanoparticles surface than in case of mechanical mixture. Indeed, due to poor solubility of PANI-DBSA in chlorobenzene, the mixed analog obviously consists of TiO_2 nanoparticles (major component) randomly intermixed with the

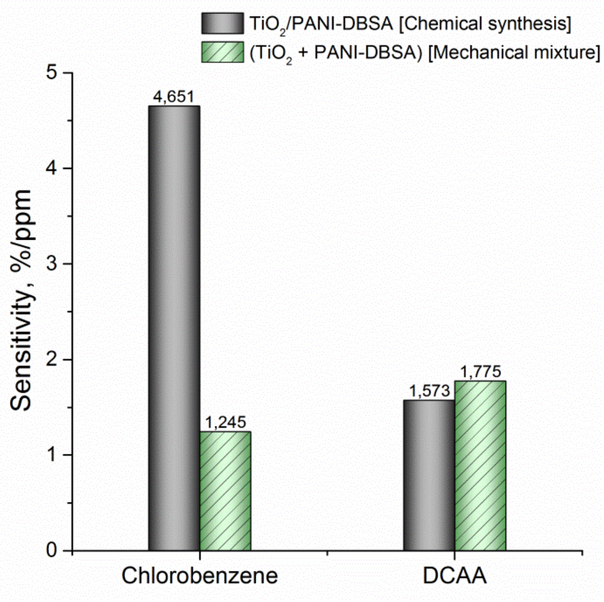

Figure 5.12 – The influence of solvent and preparation method on PANI hybrid materials sensitivity to 1 – 100 ppm of ammonia

doped PANI lumps. The latter contributes to the emergence of point electrical junctions resulting in high resistance of their percolation network and, therefore, can suppress sensor responses. Moreover, while ammonia molecules easily interact with the surface of polymer particles, their access to majority of sensing clusters localized in the mechanical mixture bulk probably has diffusion limitations. In turn it results in attenuation of observed sensors signal amplitude compared to chemically synthesized nanocomposites.

It should be noted, that situation with layers cast from DCAA has opposite character. The mechanical mixture shows slightly better responses than chemically synthesized nanocomposite. This phenomenon can be explained on the basis of data on polymer phase solubility in different solvents (see section 4.2.2). The use of DCAA contributes to polymer dissolution with its subsequent precipitation in a form of thin layer on bare TiO_2 nanoparticles after solvent evaporation. This new two-layer morphology has small thickness of doped PANI shell, which probably facilitates analytes accessibility to PANI sensing clusters.

Thus, the high efficiency of a core-shell structure and the particular PANI state in this shell were confirmed by significantly higher sensitivity (in 1.8 – 4.5 times) to ammonia of chemically synthesized anatase based nanocomposites TiO_2/PANI-

DBSA with different polymer phase content (8.7 – 36.1 wt.%), compared to the one obtained by simple mechanical mixing and containing 10 wt.%. of PANI-DBSA.

5.3.2 Sensing properties of polyaniline-polycarbonate composites.

The results on synthesized polyaniline-polycarbonate hybrid materials sensitivity to ammonia are presented in figure 5.13. For their sensing layers fabrication we used chloroform. It should be noted that obtained composite layers had a quite dense structure, due to slight dissolution of a polycarbonate (PC) component. This probably can be a one of the reasons for low sensor responses.

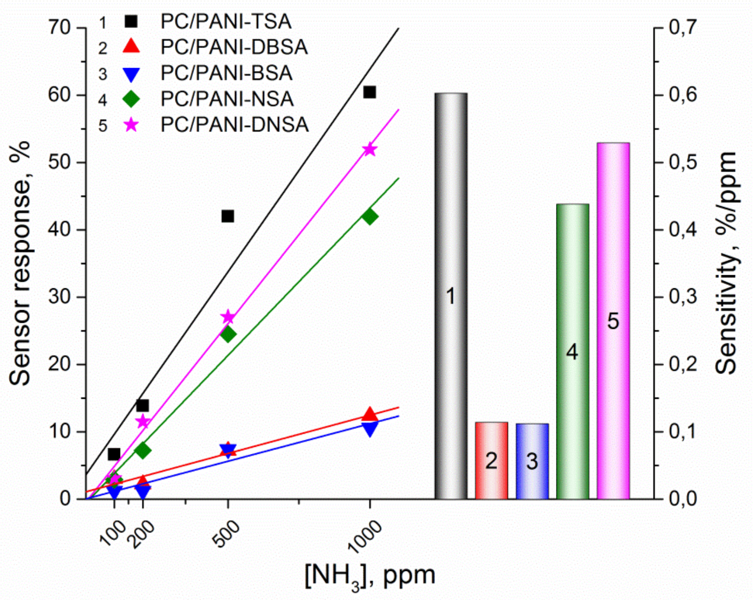

Figure 5.13 – The sensitivity of polyaniline-polycarbonate hybrid composites to 100 – 1000 ppm of ammonia: (1) PC/PANI-TSA, (2) PC/PANI-DBSA, (3) PC/PANI-BSA, (4) PC/PANI-NSA, (5) PC/PANI-NDSA.

Obtained data indicates no specific influence of dopants type and structure (small or large anions) on the sensors response magnitudes. The possible explanation is the strong acidic nature of used sulfonic acids-dopants ($pK_a < -1$) [221-224] facilitating the formation of PANI salts with the practically similar strength of acid-base interactions between acid-dopant and PANI emeraldine base. Therefore, composites sensor responses to basic substances, in particular to ammonia, should be also quite similar. Nevertheless, the difference in sensitivity between the PC/PANI-DBSA (PC/PANI-BSA) and PC/PANI-TSA (PC/PANI-NSA and PC/PANI-DNSA) indicates the interference of additional effects, influencing the interaction in system “PANI salt – ammonia”. In particular, it can be the manifestation of hydrophobic-hydrophilic interactions effect, occurring due to embedding of the doped PANI clusters in the hydrophobic PC matrix during casting the formed mixture onto electrodes.

Summarizing the above, despite the linear character of the obtained materials sensor responses on pollutant concentrations, their low sensitivity suggests only partial applicability of such materials for gas sensors production.

5.3.3 Sensing responses of electrodeposited ZnO/polypyrrole heterostructure

The main disadvantage of hybrid nanostructures chemical synthesis is the requirement of additional separate stage of obtained materials deposition onto electrodes. The common drop-casting and spin-coating methods have drawbacks connected with difficulties in control of layers uniformity and thickness reproducibility. In addition, according to received data, dispersing solvents can change the structure of the synthesized nanocomposite, which plays crucial role when evaluating sensing properties.

In this regard, the electrochemical formation of hybrid inorganic-organic heterostructures looks very attractive from the viewpoint of the sensors production easiness. This approach allows direct synthesis on electrodes with facile creation of structures with p-n junctions and strict control of layers properties. Nevertheless, this method also has some limitations. Firstly, the direct electrodeposition of TiO_2 layer onto used gold electrodes is impossible due to oxidative passivation of titanium electrode. Therefore, the best candidate for TiO_2 replacement is the ZnO, which has the same band gap (figure 2.1) and can be synthesized by simple procedures [195, 196]. However, zinc oxide is unstable under typical aniline electropolymerization conditions [158, 313] due to high acidity of used solutions. Moreover, the electropolymerized PANI has such problems as lower conductivity and crystallinity, higher solubility (that implies lower molecular weight), non-optimal quinoid to benzenoid structures ratio and noticeably bigger particles size compared to chemically synthesized ones [198]. Taking into account all these factors, the PANI polymer was changed to polypyrrole. The latter is also used for ammonia detection [314-316] and typically synthesized from solutions with close to neutral pH [67, 92]. The results on electrochemically synthesized pure polypyrrole and its hybrid material sensitivity to ammonia and amines are presented in figure 5.14.

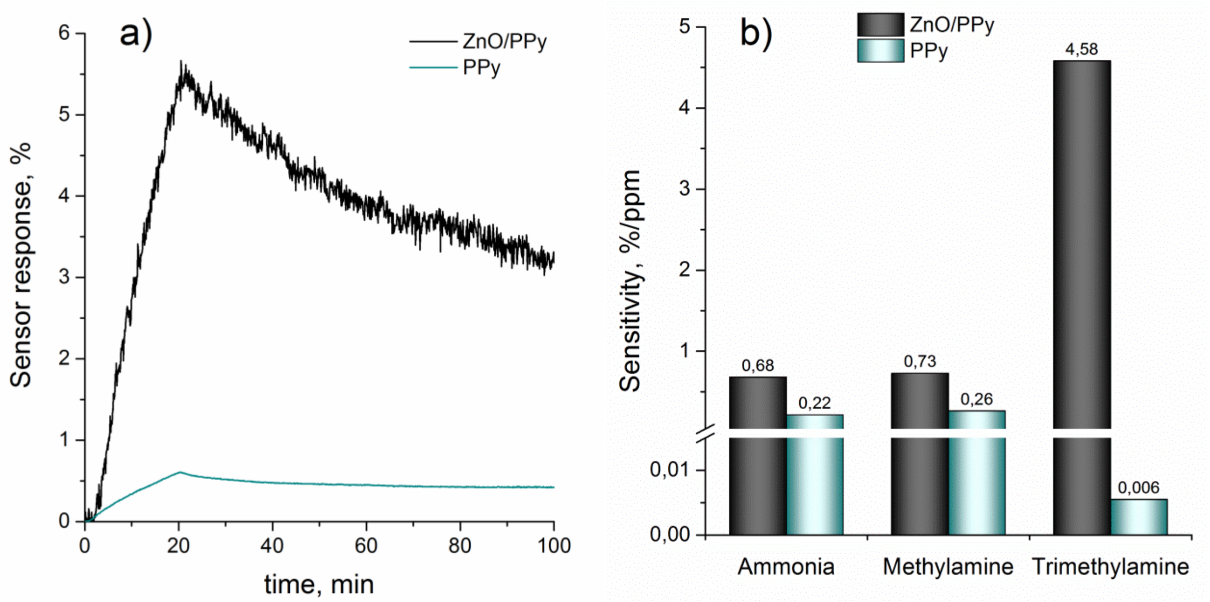

Figure 5.14 – The electrochemically synthesized pure polypyrrole and its heterostructure ZnO/PPy **(a)** sensors responses to 1 ppm ammonia and **(b)** sensitivity to ammonia and amines

Both pure polymer and heterostructure with ZnO demonstrate weak responses with poor regeneration of sensing layer (figure 5.14a). Such behavior also persists during measurements of materials sensitivity to amines. The figure 5.14b demonstrates the sensitivity of electrochemically synthesized polypyrrole materials to different analytes. For the convenience of sensitivity comparison with chemically synthesized PANI materials, PPy materials' responses were taken from the figure 5.14a at time 5 minutes.

Pure polypyrrole demonstrates a sensitivity decrease in a raw MA> NH_3> TMA. Such behavior can be explained by low porosity of the formed polypyrrole layer (figure 4.11), which is similarly to observed responses decrease in PANI case originates from hindered penetration into the active sensing layer of larger TMA molecules (compared to MA and ammonia). At the same time the ZnO/PPy heterostructure demonstrates responses decrease in the row TMA> MA> NH_3 in full accordance with the reduction of analytes basicity, which probably due to formation of more porous structure during synthesis. The comparison of sensing properties of the best PPy based materials synthesized in this work with literature data is presented in table 5.3.

Table 5.3 The comparison of PPy based materials sensing properties with literature data

Material / [dopant]	Sensitivity to ammonia, %/ppm for 5 min exposure	Lowest tested concentration	Ref.
PPy [HCl]	0.22	200 ppb	This work
ZnO/PPy [HCl]	0.68		
PPy [PVS]	0.07*	50 ppm	[314]
PPy [$HClO_4$]	0.24*	1 ppm	[317]
sCoPc/PPy [$HClO_4$]	0.36*	1 ppm	[318]
TiO_2/PPy [Graphene]	1.37**	1 ppm	[319]
PPy nanotubes	0.075**	10 ppb	[320]

*Published data after “sensitivity” parameter conversion to units used in this work, using formula 2.2. Sensors response values were taken from given in literature kinetic curves at time 5 min.
**Sensor reached saturation less than in 5 min.

Therefore, polypyrrole heterostructure shows better results than pure polypyrrole, but still worse than polyaniline based nanocomposite materials.

* * *

Thus, the use DCAA as dispersing solvent significantly changes nanocomposites morphology and reduces the active layers sensitivity to analytes. Chemically synthesized PANI based nanocomposites obtained by aniline polymerization in the presence of metal oxides demonstrate better sensing characteristics compared to simple mechanical mixture of PANI with TiO_2 nanoparticles. Active layers of PANI-PC nanocomposites cast from chloroform have very low sensor responses, comparable with those obtained for pure PANI cast from

DCAA. The sensitivities of both electrodeposited heterostructure ZnO/PP and pure PPy are lower compared to PANI based nanocomposites.

The best sensing results were obtained using PANI nanocomposites synthesized at a weight ratio of An:TiO_2= 10:90 and cast from chlorobenzene. These materials have in 1.92 – 2.23 times higher sensitivity compared to the best samples of pure PANI. In addition, nanocomposites demonstrate linear increase of response magnitude to analytes with temperature and humidity increase. The deterioration of synthesized materials sensing properties is observed after the UV light exposure. Nevertheless, high response magnitudes to amines confirm the applicability of synthesized hybrid materials for their detection.

CONCLUSIONS AND PERSPECTIVES

In this work a new approach to control polyaniline synthesis parameters by simultaneous monitoring of pH and redox profiles of aniline polymerization process was proposed. The approach to systematize ideas about the impact of a content and type of inorganic components and dopant structure on sensing and other properties of nanocomposite materials was made. The most important results are as follows:

1. It was found that that chemical oxidative polymerization of aniline in the presence of TiO_2 (rutile and anatase), SnO_2 nanoparticles leads to the formation of nanocomposites with core-shell morphology and improved characteristics of polymer phase compared to pure PANI, particularly with 1.6 – 2.4 times higher molecular weight and 1.9 – 2.3 times lower polydispersity, higher oxidation degree, better thermal stability, improved electrical conductivity and ~2 times higher sensing responses.
2. The results on kinetic analysis of changes in physicochemical parameters of polymerization medium (RedOx potential, pH) revealed that aniline polymerization rate linearly accelerates in 2 – 6 times with the growth of TiO_2 nanoparticles content from 50 to 95 wt.% in the polymerization medium.
3. It was found that UV exposure leads to photodegradation and changes in PANI materials characteristics. These changes are more evident in case of nanocomposites with TiO_2 nanoparticles compared to nanocomposites with SnO_2 nanoparticles.
4. It was shown that the use of surface active acids-dopants (DBSA) for the synthesis of nanocomposites with polymer phase content less than 79.2 wt.% is optimal for the “core-shell” structure formation. The highest sensitivity to analytes and stability are achieved for the nanocomposites with TiO_2 nanoparticles and doped PANI phase content of 18.9 wt.%.
5. It was shown that used for sensing layers formation dispersing solvents significantly affect the synthesized nanocomposites morphology and sensing

response magnitudes. In particular, the use of chlorobenzene 3.6 times increases nanocomposites sensitivity to ammonia in comparison with DCAA.

6. It was found that sensitivity of PANI nanocomposites is practically indifferent to used nanoparticles nature and mainly determined by their size, which affects the covering polymer shell thickness and thus active layer porosity.
7. It was shown that sensing responses of polypyrrole based hybrid materials to ammonia and amines are 1.5 – 14.5 times weaker (depending on the analyte) compared to PANI nanocomposites. Such behavior probably explained by much lower specific surface of electrodeposited polypyrrole layer.

Proposed in this work approaches to the formation of ICPs based nanostructured composites with “core-shell” structure open wide perspectives for the production of materials with predetermined properties. Moreover, obtained results testify the applicability of developed new hybrid materials as active layers for the manufacturing of chemoresistive ammonia/amines gas sensors. However, for the practical application of synthesized materials, additional investigations are desirable.

In particular, the study on PANI doping degree in synthesized nanocomposite materials would be useful for the better understanding of the interrelation of protonated sites number and sensors response magnitudes to analytes.

It is worth mentioning that fabricated sensors are notable for great adsorption potential of active layers, which leads to continuous growth of signal without reaching the saturation state. In this regard, the estimation of such important sensor characteristic as “response time”, defined as time corresponding to 90% of saturation level is impossible. Therefore, the further development directed on active layer thickness decrease is needed.

At the same time, the used in this work drop-coating technique for sensors active layers formation has problems with layers uniformity and thickness reproducibility. To solve these problems the use of more advanced inkjet printing technique is suggested. This technique allows controlled layers formation with predetermined geometrical parameters (shape and thickness), as well as more suitable for sensor devices mass production.

Also, it is worth to note that all sensing results were obtained in laboratory conditions. Thus, in order to validate these results field-tests are required. In addition, the increase of measurement system mobility by the development of compact integral electronic component (hardware) with the possibility of simple reproduction is desirable.

REFERENCES

1. Stejskal, J., et al., *The effect of polymerization temperature on molecular weight, crystallinity, and electrical conductivity of polyaniline.* Synthetic Metals, 1998. **96**(1): p. 55-61.
2. Stejskal, J., et al., *In-situ polymerized polyaniline films.* Synthetic Metals, 1999. **105**(3): p. 195-202.
3. Ćirić-Marjanović, G., et al., *Chemical oxidative polymerization of anilinium sulfate versus aniline: Theory and experiment.* Synthetic Metals, 2008. **158**(5): p. 200-211.
4. Ćirić-Marjanović, G., M. Trchová, and J. Stejskal, *Theoretical study of the oxidative polymerization of aniline with peroxydisulfate: Tetramer formation.* International Journal of Quantum Chemistry, 2008. **108**(2): p. 318-333.
5. Sapurina, I.Y. and J. Stejskal, *The effect of pH on the oxidative polymerization of aniline and the morphology and properties of products.* Russian Chemical Reviews, 2010. **79**(12): p. 1123.
6. Sapurina, I.Y. and J. Stejskal, *Oxidation of aniline with strong and weak oxidants.* Russian Journal of General Chemistry, 2012. **82**(2): p. 256-275.
7. Nino Künzli, Laura Perez, and R. Rapp, *Air Quality and Health*. 2010, European Respiratory Society (ERS).
8. Hellén, H., A.J. Kieloaho, and H. Hakola, *Gas-phase alkyl amines in urban air; comparison with a boreal forest site and importance for local atmospheric chemistry.* Atmospheric Environment, 2014. **94**(0): p. 192-197.
9. Heard, D.E., *Analytical Techniques for Atmospheric Measurement*. 2006: Blackwell Publishing Ltd. 534.
10. *Ammonia (NH3) emissions (APE 003)*. 2012, European Environment Agency (EEA).
11. Agency, E.E., *Ammonia (NH3) emissions (APE 003)*. 2012, European Environment Agency.
12. Susan W. Gay and K.F. Knowlton, *Ammonia Emissions and Animal Agriculture*. 2005, Virginia State University: Viriginia.
13. NRC, *Air Emissions from Animal Feeding Operations: Current Knowledge, Future Needs*. 2003, Washington, DC: The National Academies Press. 286.
14. van der Eerden, L.J.M., P.H.B. de Visser, and C.J. van Dijk, *Risk of damage to crops in the direct neighbourhood of ammonia sources.* Environmental Pollution, 1998. **102**(1, Supplement 1): p. 49-53.
15. Stokstad, E., *Ammonia Pollution From Farming May Exact Hefty Health Costs.* Science, 2014. **343**(6168): p. 238.
16. Meng, Z.-Y., et al., *Ambient sulfur dioxide, nitrogen dioxide, and ammonia at ten background and rural sites in China during 2007–2008.* Atmospheric Environment, 2010. **44**(21–22): p. 2625-2631.
17. Carmichael, G.R., et al., *Measurements of sulfur dioxide, ozone and ammonia concentrations in Asia, Africa, and South America using passive samplers.* Atmospheric Environment, 2003. **37**(9–10): p. 1293-1308.
18. Roney, N., et al., *Toxicological profile for ammonia*. 2004: Department of Health & Human Services, Public Health Service, Agency for Toxic Substances and Disease Registry.
19. Wetselaar, R., J.B. Passioura, and B.R. Singh, *Consequences of banding nitrogen fertilizers in soil.* Plant and Soil, 1972. **36**(1-3): p. 159-175.
20. Sweeten, J., et al. *Detecting and reducing ammonia emissions from cattle feedlots and dairies: A review*. in *International workshop on atmospheric nitrogen compounds II: Emissions, Transport, Transformation, Deposition, and Assessment*. 1999. NC State University, Raleigh.
21. INRS, *Fiche toxicologique n° 16. Ammoniac et solutions aqueuses*, INRS, Editor. 2007.

22. *ПРЕДЕЛЬНО ДОПУСТИМЫЕ КОНЦЕНТРАЦИИ (ПДК) ВРЕДНЫХ ВЕЩЕСТВ В ВОЗДУХЕ РАБОЧЕЙ ЗОНЫ*. 2003, Минздрав России: Москва. p. 609.
23. Troy Hibbard, K. Crowley, and A.J. Killard, *Direct measurement of ammonia in simulated human breath using an inkjet-printed polyaniline nanoparticle sensor.* Analytica Chimica Acta, 2013. **779**(0): p. 56-63.
24. L. R. Narasimhan, et al., *Correlation of breath ammonia with blood urea nitrogen and creatinine during hemodialysis.* Proceedings of the National Academy of Sciences, 2001. **98**(8): p. 4617-4621.
25. Javier Vaquero and R.F. Butterworth, *The brain glutamate system in liver failure.* Journal of Neurochemistry, 2006. **98**(3): p. 661-669.
26. Hiroyuki Wakabayashi, et al., *Measurement of the expiratory ammonia concentration and its clinical significance.* Metabolic Brain Disease, 1997. **12**(2): p. 161-169.
27. Di Francesco, F., et al., *Breath analysis: trends in techniques and clinical applications.* Microchemical Journal, 2005. **79**(1–2): p. 405-410.
28. Hibbard, T. and A.J. Killard, *Breath ammonia levels in a normal human population study as determined by photoacoustic laser spectroscopy.* Journal of Breath Research, 2011. **5**(3): p. 037101.
29. Wenqing Cao and Y. Duan, *Current Status of Methods and Techniques for Breath Analysis.* Critical Reviews in Analytical Chemistry, 2007. **37**(1): p. 3-13.
30. Miekisch, W., J.K. Schubert, and G.F.E. Noeldge-Schomburg, *Diagnostic potential of breath analysis—focus on volatile organic compounds.* Clinica Chimica Acta, 2004. **347**(1–2): p. 25-39.
31. Buszewski, B., et al., *Human exhaled air analytics: biomarkers of diseases.* Biomedical Chromatography, 2007. **21**(6): p. 553-566.
32. Simenhoff, M.L., et al., *Biochemical Profile of Uremic Breath.* New England Journal of Medicine, 1977. **297**(3): p. 132-135.
33. Greim, H., et al., *Toxicity of aliphatic amines: Structure-activity relationship.* Chemosphere, 1998. **36**(2): p. 271-295.
34. Goossens, A., T. Detienne, and M. Bruze, *Occupational allergic contact dermatitis caused by isocyanates.* Contact Dermatitis, 2002. **47**(5): p. 304-308.
35. Epstein, E. and H.I. Maibach, *Ethylenediamine: allergic contact dermatitis.* Archives of dermatology, 1968. **98**(5): p. 476-477.
36. Pigatto, P.D., A.S. Bigardi, and F. Cusano, *Contact Dermatitis to Cocamidopropylbetaine Is Caused by Residual Amines: Relevance, Clinical Characteristics, and Review of the Literature.* Dermatitis, 1995. **6**(1): p. 13-16.
37. Vineis, P. and R. Pirastu, *Aromatic amines and cancer.* Cancer Causes & Control, 1997. **8**(3): p. 346-355.
38. Johansson, S.L. and S.M. Cohen, *Epidemiology and etiology of bladder cancer.* Seminars in Surgical Oncology, 1997. **13**(5): p. 291-298.
39. Benigni, R., *Structure-activity relationship studies of chemical mutagens and carcinogens: mechanistic investigations and prediction approaches.* Chemical reviews, 2005. **105**(5): p. 1767-1800.
40. Benigni, R., et al., *QSARs for the mutagenicity and carcinogenicity of the aromatic amines*. 2003: CRC Press, Boca Raton, FL.
41. Benigni, R. and L. Passerini, *Carcinogenicity of the aromatic amines: from structure–activity relationships to mechanisms of action and risk assessment.* Mutation Research/Reviews in Mutation Research, 2002. **511**(3): p. 191-206.
42. Fournier, M., et al., *Sampling and analytical methodology development for the determination of primary and secondary low molecular weight amines in ambient air.* Journal of Environmental Monitoring, 2008. **10**(3): p. 379-386.
43. Woo, Y.-T. and D.Y. Lai, *Aromatic Amino and Nitro–Amino Compounds and Their Halogenated Derivatives*, in *Patty's Toxicology*. 2001, John Wiley & Sons, Inc.

44. Winder, C. and N.H. Stacey, *Occupational toxicology*. 2004: CRC Press.
45. Kuehn, B.M., *WHO: More than 7 million air pollution deaths each year*. JAMA, 2014. **311**(15): p. 1486-1486.
46. Zhang, C., *Environmental Sampling Techniques*, in *Fundamentals of Environmental Sampling and Analysis*. 2006, John Wiley & Sons, Inc. p. 69-96.
47. Namieśnik, J., A. Jastrzębska, and B. Zygmunt, *Determination of volatile aliphatic amines in air by solid-phase microextraction coupled with gas chromatography with flame ionization detection.* Journal of Chromatography A, 2003. **1016**(1): p. 1-9.
48. Chien, Y.-C., et al., *Analytical method for monitoring airborne trimethylamine using solid phase micro-extraction and gas chromatography-flame ionization detection.* Analytica Chimica Acta, 2000. **419**(1): p. 73-79.
49. Moffat, A.C., et al., *Perfluorobenzene derivatives as derivatising agents for the gas chromatography of primary and secondary amines using electron capture detection.* Journal of Chromatography A, 1972. **66**(2): p. 255-260.
50. Chen, G., et al., *Sensitive, accurate and rapid detection of trace aliphatic amines in environmental samples with ultrasonic-assisted derivatization microextraction using a new fluorescent reagent for high performance liquid chromatography.* Journal of Chromatography A, 2014. **1352**(0): p. 8-19.
51. Sellegri, K., et al., *Measurements of organic gases during aerosol formation events in the boreal forest atmosphere during QUEST.* Atmos. Chem. Phys., 2005. **5**(2): p. 373-384.
52. Sowell, R., et al., *Nanoflow LC/IMS-MS and LC/IMS-CID/MS of protein mixtures.* Journal of the American Society for Mass Spectrometry, 2004. **15**(9): p. 1341-1353.
53. Ruzsanyi, V., et al., *Detection of human metabolites using multi-capillary columns coupled to ion mobility spectrometers.* Journal of Chromatography A, 2005. **1084**(1–2): p. 145-151.
54. Fiddes, L.K., J. Chang, and N. Yan, *Electrochemical detection of biogenic amines during food spoilage using an integrated sensing RFID tag.* Sensors and Actuators B: Chemical, 2014. **202**(0): p. 1298-1304.
55. Rakow, N.A. and K.S. Suslick, *A colorimetric sensor array for odour visualization.* Nature, 2000. **406**(6797): p. 710-713.
56. Suslick, K.S., N.A. Rakow, and A. Sen, *Colorimetric sensor arrays for molecular recognition.* Tetrahedron, 2004. **60**(49): p. 11133-11138.
57. Guillermo, O., et al., *The Interplay of Indicator, Support and Analyte in Optical Sensor Layers*, in *Frontiers in Chemical Sensors*, G. Orellana and M. Moreno-Bondi, Editors. 2005, Springer Berlin Heidelberg. p. 189-225.
58. Filippini, D., et al., *Chemical Sensing with Familiar Devices.* Angewandte Chemie International Edition, 2006. **45**(23): p. 3800-3803.
59. Rakow, N.A., et al., *Molecular Recognition and Discrimination of Amines with a Colorimetric Array.* Angewandte Chemie International Edition, 2005. **44**(29): p. 4528-4532.
60. LaGasse, M.K., et al., *Colorimetric sensor arrays: Interplay of geometry, substrate and immobilization.* Sensors and Actuators B: Chemical, 2014. **197**(0): p. 116-122.
61. Diehl, K.L. and E.V. Anslyn, *Array sensing using optical methods for detection of chemical and biological hazards.* Chemical Society Reviews, 2013. **42**(22): p. 8596-8611.
62. Pushkarsky, M.B., et al., *Laser-based photoacoustic ammonia sensors for industrial applications.* Applied Physics B, 2002. **75**(2-3): p. 391-396.
63. Harren, F.J.M., et al., *Photoacoustic Spectroscopy in Trace Gas Monitoring*, in *Encyclopedia of Analytical Chemistry*. 2006, John Wiley & Sons, Ltd.
64. Elia, A., et al., *Photoacoustic techniques for trace gas sensing based on semiconductor laser sources.* Sensors, 2009. **9**(12): p. 9616-9628.
65. Wang, J., et al., *Breath ammonia detection based on tunable fiber laser photoacoustic spectroscopy.* Applied Physics B, 2011. **103**(2): p. 263-269.

66. Trojanowicz, M., et al., *Amperometric sensing of ammonia in aqueous solutions using a polyaniline-modified electrode in flow injection systems.* Electroanalysis, 1997. **9**(14): p. 1062-1066.
67. Dall'Antonia, L.H., et al., *A New Sensor for Ammonia Determination Based on Polypyrrole Films Doped with Dodecylbenzenesulfonate (DBSA) Ions.* Electroanalysis, 2002. **14**(22): p. 1577-1586.
68. Ji, X., et al., *Electrochemical Ammonia Gas Sensing in Nonaqueous Systems: A Comparison of Propylene Carbonate with Room Temperature Ionic Liquids.* Electroanalysis, 2007. **19**(21): p. 2194-2201.
69. David R. Walt, et al., *Optical sensor arrays for odor recognition.* Biosensors and Bioelectronics, 1998. **13**(6): p. 697-699.
70. Zhe Jin, Y. Su, and Y. Duan, *Development of a polyaniline-based optical ammonia sensor.* Sensors and Actuators B: Chemical, 2001. **72**(1): p. 75-79.
71. Z. P. Khlebarov, A.I. Stoyanova, and D.I. Topalova, *Surface acoustic wave gas sensors.* Sensors and Actuators B: Chemical, 1992. **8**(1): p. 33-40.
72. Keith J. Albert, et al., *Cross-Reactive Chemical Sensor Arrays.* Chemical Reviews, 2000. **100**(7): p. 2595-2626.
73. William A. Groves and E.T. Zellers, *Analysis of solvent vapors in breath and ambient air with a surface acoustic wave sensor array.* The Annals of Occupational Hygiene, 2001. **45**(8): p. 609-623.
74. N. M. White and J.D. Turner, *Thick-film sensors: past, present and future.* Measurement Science and Technology, 1997. **8**(1): p. 1.
75. Hua Bai and G. Shi, *Gas Sensors Based on Conducting Polymers.* Sensors, 2007. **7**: p. 267-307.
76. Penzes, M., et al. *Iodine doped polyaniline and cobalt-phthalocyanine as sensitive layers for ammonia detection via surface acoustic wave sensor*. in *General Assembly and Scientific Symposium (URSI GASS), 2014 XXXIth URSI*. 2014.
77. Eva-Lotta Kalman, et al., *Classification of complex gas mixtures from automotive leather using an electronic nose.* Analytica Chimica Acta, 2000. **403**(1–2): p. 31-38.
78. I. Eisele, T. Doll, and M. Burgmair, *Low power gas detection with FET sensors.* Sensors and Actuators B: Chemical, 2001. **78**(1–3): p. 19-25.
79. T. Eklöv, H. Sundgren, and I. Lundström, *Distributed chemical sensing.* Sensors and Actuators B: Chemical, 1997. **45**(1): p. 71-77.
80. Janata, J., *Electrochemical microsensors.* Proceedings of the IEEE, 2003. **91**(6): p. 864-869.
81. Todd A. Dickinson, et al., *Current trends in `artificial-nose' technology.* Trends in Biotechnology, 1998. **16**(6): p. 250-258.
82. Emmanuelle Schaller, J.O. Bosset, and F. Escher, *‘Electronic Noses’ and Their Application to Food.* LWT - Food Science and Technology, 1998. **31**(4): p. 305-316.
83. Dhivya, P. and M. Sridharan, *Expeditious detection of ammonia using sputtered TiO2 films.* Journal of Materials Science: Materials in Electronics, 2015. **26**(10): p. 7595-7606.
84. Wojkiewicz, J.L., et al., *Nanostructured polyaniline-based composites for ppb range ammonia sensing.* Sensors and Actuators B: Chemical, 2011. **160**(1): p. 1394-1403.
85. Valle, M.A.D., et al., *Polythiophene, polyaniline and polypyrrole electrodes modified by electrodeposition of Pt and Pt+Pb for formic acid electrooxidation.* Journal of Applied Electrochemistry, 1998. **28**(9): p. 943-946.
86. Pron, A. and P. Rannou, *Processible conjugated polymers: from organic semiconductors to organic metals and superconductors.* Progress in Polymer Science, 2002. **27**(1): p. 135-190.
87. Nicolas-Debarnot, D. and F. Poncin-Epaillard, *Polyaniline as a new sensitive layer for gas sensors.* Analytica Chimica Acta, 2003. **475**(1–2): p. 1-15.
88. Mérian, T., et al., *Ultra sensitive ammonia sensors based on microwave synthesized nanofibrillar polyanilines.* Sensors and Actuators B: Chemical, 2014. **203**(0): p. 626-634.

89. Pud, A., et al., *Some aspects of preparation methods and properties of polyaniline blends and composites with organic polymers.* Progress in Polymer Science, 2003. **28**(12): p. 1701-1753.
90. Sengupta, P.P. and B. Adhikari, *Influence of polymerization condition on the electrical conductivity and gas sensing properties of polyaniline.* Materials Science and Engineering: A, 2007. **459**(1–2): p. 278-285.
91. Huang, W.-S., B.D. Humphrey, and A.G. MacDiarmid, *Polyaniline, a novel conducting polymer. Morphology and chemistry of its oxidation and reduction in aqueous electrolytes.* Journal of the Chemical Society, Faraday Transactions 1: Physical Chemistry in Condensed Phases, 1986. **82**(8): p. 2385-2400.
92. Waltman, R.J. and J. Bargon, *Electrically conducting polymers: a review of the electropolymerization reaction, of the effects of chemical structure on polymer film properties, and of applications towards technology.* Canadian Journal of Chemistry, 1986. **64**(1): p. 76-95.
93. Cao, Y., et al., *Influence of chemical polymerization conditions on the properties of polyaniline.* Polymer, 1989. **30**(12): p. 2305-2311.
94. Wei, Y., et al., *A study of the mechanism of aniline polymerization.* Journal of Polymer Science Part A: Polymer Chemistry, 1989. **27**(7): p. 2385-2396.
95. Gospodinova, N. and L. Terlemezyan, *Conducting polymers prepared by oxidative polymerization: polyaniline.* Progress in Polymer Science, 1998. **23**(8): p. 1443-1484.
96. Liao, C. and M. Gu, *Electroless deposition of polyaniline film via autocatalytic polymerization of aniline.* Thin Solid Films, 2002. **408**(1–2): p. 37-42.
97. Stejskal, J. and R. Gilbert, *Polyaniline. Preparation of a conducting polymer (IUPAC technical report).* Pure and Applied Chemistry, 2002. **74**(5): p. 857-867.
98. Pud, A.A., et al., *Formation and properties of nano- and micro-structured conducting polymer host–guest composites.* Synthetic Metals, 2009. **159**(21–22): p. 2253-2258.
99. Ćirić-Marjanović, G., M. Trchová, and J. Stejskal, *MNDO-PM3 study of the early stages of the chemical oxidative polymerization of aniline.* Collection of Czechoslovak Chemical Communications, 2006. **71**(10): p. 1407-1426.
100. Ćirić-Marjanović, G., *Recent advances in polyaniline research: Polymerization mechanisms, structural aspects, properties and applications.* Synthetic Metals, 2013. **177**: p. 1-47.
101. Manohar, S.K., A.G. Macdiarmid, and A.J. Epstein, *Proceedings of the International Conference on Science and Technology of Synthetic Metals Polyaniline: Pernigranile, an isolable intermediate in teh conventional chemical synthesis of emeraldine.* Synthetic Metals, 1991. **41**(1): p. 711-714.
102. Wei, Y., K.F. Hsueh, and G.-W. Jang, *Monitoring the chemical polymerization of aniline by open-circuit-potential measurements.* Polymer, 1994. **35**(16): p. 3572-3575.
103. Pud, A.A., et al., *New Aspects of the Low-Concentrated Aniline Polymerization in the Solution and in SiC Nanocrystals Dispersion.* The Journal of Physical Chemistry B, 2007. **111**(9): p. 2174-2180.
104. Tran, H.D., D. Li, and R.B. Kaner, *One-Dimensional Conducting Polymer Nanostructures: Bulk Synthesis and Applications.* Advanced Materials, 2009. **21**(14-15): p. 1487-1499.
105. Yunus, S., A. Attout, and P. Bertrand, *Controlled Aniline Polymerization Strategies for Polyaniline Micro- and Nano Self-Assembling into Practical Electronic Devices.* Langmuir, 2009. **25**(3): p. 1851-1854.
106. Tian, Z., et al., *Recent progress in the preparation of polyaniline nanostructures and their applications in anticorrosive coatings.* RSC Advances, 2014. **4**(54): p. 28195-28208.
107. Wu, W., et al., *Facile fabrication of polyaniline nanotubes using the self-assembly behavior based on the hydrogen bonding: a mechanistic study and application in high-performance electrochemical supercapacitor electrode.* Electrochimica Acta, 2015. **152**(0): p. 126-134.

108. Zhang, L. and M. Wan, *Self-Assembly of Polyaniline—From Nanotubes to Hollow Microspheres.* Advanced Functional Materials, 2003. **13**(10): p. 815-820.
109. Trchová, M. and J. Stejskal, *Polyaniline: The infrared spectroscopy of conducting polymer nanotubes (IUPAC Technical Report).* Pure and Applied Chemistry, 2011. **83**(10): p. 1803-1817.
110. Trchová, M., et al., *Spectroscopy of thin polyaniline films deposited during chemical oxidation of aniline.* Chemical Papers, 2012. **66**(5): p. 415-445.
111. Ding, H., et al., *Formation Mechanism of Polyaniline Nanotubes by a Simplified Template-Free Method.* Macromolecular Chemistry and Physics, 2008. **209**(8): p. 864-871.
112. Zhang, L., L. Zhang, and M. Wan, *Molybdic acid doped polyaniline micro/nanostructures via a self-assembly process.* European Polymer Journal, 2008. **44**(7): p. 2040-2045.
113. Bhadra, J. and D. Sarkar, *Self-assembled polyaniline nanorods synthesized by facile route of dispersion polymerization.* Materials Letters, 2009. **63**(1): p. 69-71.
114. Stejskal, J., I. Sapurina, and M. Trchová, *Polyaniline nanostructures and the role of aniline oligomers in their formation.* Progress in Polymer Science, 2010. **35**(12): p. 1420-1481.
115. Shishov, M., V. Moshnikov, and I. Sapurina, *Self-organization of polyaniline during oxidative polymerization: formation of granular structure.* Chemical Papers, 2013. **67**(8): p. 909-918.
116. Laslau, C., Z. Zujovic, and J. Travas-Sejdic, *Theories of polyaniline nanostructure self-assembly: Towards an expanded, comprehensive Multi-Layer Theory (MLT).* Progress in Polymer Science, 2010. **35**(12): p. 1403-1419.
117. Xia, H. and Q. Wang, *Ultrasonic Irradiation: A Novel Approach To Prepare Conductive Polyaniline/Nanocrystalline Titanium Oxide Composites.* Chemistry of Materials, 2002. **14**(5): p. 2158-2165.
118. Nasirian, S. and H. Milani Moghaddam, *Effect of different titania phases on the hydrogen gas sensing features of polyaniline/TiO2 nanocomposite.* Polymer, 2014. **55**(7): p. 1866-1874.
119. Zheng, W., et al., *Experimental Evidence for Hydrogen Bonding in Polyaniline: Mechanism of Aggregate Formation and Dependency on Oxidation State.* Macromolecules, 1997. **30**(10): p. 2953-2955.
120. Malinauskas, A., *Chemical deposition of conducting polymers.* Polymer, 2001. **42**(9): p. 3957-3972.
121. Bhattacharya, A. and A. De, *Conducting Polymers in Solution—Progress Toward Processibility.* Journal of Macromolecular Science, Part C, 1999. **39**(1): p. 17-56.
122. Mattoso, L.H.C., A.G. MacDiarmid, and A.J. Epstein, *Controlled synthesis of high molecular weight polyaniline and poly(o-methoxyaniline).* Synthetic Metals, 1994. **68**(1): p. 1-11.
123. MacDiarmid, A.G. and A.J. Epstein, *The concept of secondary doping as applied to polyaniline.* Synthetic Metals, 1994. **65**(2–3): p. 103-116.
124. J Heeger, A., *Polyaniline with surfactant counterions: Conducting polymer materials which are processible in the conducting form.* Synthetic metals, 1993. **57**(1): p. 3471-3482.
125. Cao, Y., P. Smith, and A.J. Heeger, *Counter-ion induced processibility of conducting polyaniline and of conducting polyblends of polyaniline in bulk polymers.* Synthetic Metals, 1992. **48**(1): p. 91-97.
126. Deshpande N. G., et al., *Studies on tin oxide-intercalated polyaniline nanocomposite for ammonia gas sensing applications.* Sensors and Actuators B: Chemical, 2009. **138**(1): p. 76-84.
127. Dhingra Mansi, et al., *Polyaniline mediated enhancement in band gap emission of Zinc Oxide.* Composites Part B: Engineering, 2013. **45**(1): p. 1515-1520.
128. Vikki, T., et al., *Molecular recognition solvents for electrically conductive polyaniline.* Macromolecules, 1996. **29**(8): p. 2945-2953.

129. Malmonge, L.F. and L.H.C. Mattoso, *Electroactive blends of poly(vinylidene fluoride) and polyaniline derivatives.* Polymer, 1995. **36**(2): p. 245-249.
130. Dawn, A. and A.K. Nandi, *Nanostructured Self-Assembly of Double-Stranded DNA/Poly(o-methoxyaniline) Hybrid.* The Journal of Physical Chemistry C, 2007. **111**(17): p. 6268-6274.
131. Gregorio, R., et al., *Dielectric behavior of PVDF/POMA blends that have a low doped POMA content.* Journal of Applied Polymer Science, 2003. **87**(5): p. 752-758.
132. Yavuz, A.G., A. Uygun, and V.R. Bhethanabotla, *Substituted polyaniline/chitosan composites: Synthesis and characterization.* Carbohydrate Polymers, 2009. **75**(3): p. 448-453.
133. Pron, A., et al., *Processable conducting polyaniline.* Synthetic metals, 1993. **57**(1): p. 3520-3525.
134. Roeder, J., et al., *Mixed conductive blends of SPEEK/PANI.* Solid State Ionics, 2005. **176**(15–16): p. 1411-1417.
135. Thanpitcha, T., et al., *Preparation and characterization of polyaniline/chitosan blend film.* Carbohydrate Polymers, 2006. **64**(4): p. 560-568.
136. Zhao, S., et al., *PSf/PANI nanocomposite membrane prepared by in situ blending of PSf and PANI/NMP.* Journal of Membrane Science, 2011. **376**(1–2): p. 83-95.
137. Bhadra, S., et al., *Progress in preparation, processing and applications of polyaniline.* Progress in Polymer Science, 2009. **34**(8): p. 783-810.
138. Paul, R.K. and C.K.S. Pillai, *Melt/solution processable conducting polyaniline with novel sulfonic acid dopants and its thermoplastic blends.* Synthetic Metals, 2000. **114**(1): p. 27-35.
139. Shacklette, L.W., C.C. Han, and M.H. Luly, *Polyaniline blends in thermoplastics.* Synthetic Metals, 1993. **57**(1): p. 3532-3537.
140. Morgan, H., P.J.S. Foot, and N.W. Brooks, *The effects of composition and processing variables on the properties of thermoplastic polyaniline blends and composites.* Journal of Materials Science, 2001. **36**(22): p. 5369-5377.
141. Lindfors, T. and A. Ivaska, *pH sensitivity of polyaniline and its substituted derivatives.* Journal of Electroanalytical Chemistry, 2002. **531**(1): p. 43-52.
142. Pinto, N., et al., *Charge transport and electron localization in polyaniline derivatives.* Physical Review B, 1994. **49**(19): p. 13983.
143. Chen, T., et al., *Thermal degradation mechanism of dodecylbenzene sulfonic acid-hydrochloric acid co-doped polyaniline.* Polymer Degradation and Stability, 2009. **94**(10): p. 1788-1794.
144. Rannou, P., et al., *Ageing of PANI: chemical, structural and transport consequences.* Synthetic metals, 1999. **101**(1): p. 734-737.
145. Trchová, M., et al., *FTIR spectroscopic and conductivity study of the thermal degradation of polyaniline films.* Polymer Degradation and Stability, 2004. **86**(1): p. 179-185.
146. Bhattacharya, A. and B.N. Misra, *Grafting: a versatile means to modify polymers: Techniques, factors and applications.* Progress in Polymer Science, 2004. **29**(8): p. 767-814.
147. Lee, I.S., M.S. Cho, and H.J. Choi, *Preparation of polyaniline coated poly(methyl methacrylate) microsphere by graft polymerization and its electrorheology.* Polymer, 2005. **46**(4): p. 1317-1321.
148. Ruckenstein, E. and Z.F. Li, *Surface modification and functionalization through the self-assembled monolayer and graft polymerization.* Advances in Colloid and Interface Science, 2005. **113**(1): p. 43-63.
149. Sharma, A.L., et al., *Synthesis and characterization of a copolymer: Poly(aniline-co-fluoroaniline).* Journal of Applied Polymer Science, 2001. **81**(6): p. 1460-1466.
150. Asawapirom, U., et al., *Semiconducting block copolymers—synthesis and nanostructure formation.* Thin Solid Films, 2005. **477**(1–2): p. 48-52.
151. Wang, Z., et al., *One-step synthesis of gold–polyaniline core–shell particles.* Nanotechnology, 2007. **18**(11): p. 115610.

152. Deng, J., et al., *Magnetic and conducting Fe3O4–cross-linked polyaniline nanoparticles with core–shell structure.* Polymer, 2002. **43**(8): p. 2179-2184.
153. Chen, S., et al., *Nanostructured Polyaniline-Decorated Pt/C@PANI Core–Shell Catalyst with Enhanced Durability and Activity.* Journal of the American Chemical Society, 2012. **134**(32): p. 13252-13255.
154. Jang, J., J. Ha, and B. Lim, *Synthesis and characterization of monodisperse silica-polyaniline core-shell nanoparticles.* Chemical Communications, 2006(15): p. 1622-1624.
155. Yu, Y., et al., *Carbon nanotube/polyaniline core-shell nanowires prepared by in situ inverse microemulsion.* Synthetic Metals, 2005. **150**(3): p. 271-277.
156. Fusalba, F. and D. Bélanger, *Electropolymerization of Polypyrrole and Polyaniline−Polypyrrole from Organic Acidic Medium.* The Journal of Physical Chemistry B, 1999. **103**(42): p. 9044-9054.
157. Pournaghi-Azar, M.H. and B. Habibi, *Electropolymerization of aniline in acid media on the bare and chemically pre-treated aluminum electrodes: A comparative characterization of the polyaniline deposited electrodes.* Electrochimica Acta, 2007. **52**(12): p. 4222-4230.
158. Mujawar, S.H., et al., *Electropolymerization of polyaniline on titanium oxide nanotubes for supercapacitor application.* Electrochimica Acta, 2011. **56**(12): p. 4462-4466.
159. Li, Y., et al., *I–V characteristics of the p–n junction between vertically aligned ZnO nanorods and polyaniline thin film.* Synthetic Metals, 2010. **160**(5–6): p. 499-503.
160. Shi, G., et al., *Electrochemical fabrication of a P-type silicon–polythiophene p–n junction diode.* J. Chem. Soc., Chem. Commun., 1994(22): p. 2549-2550.
161. Kaya, M., et al., *Temperature dependence of the current–voltage characteristics of Sn/PANI/p-Si/Al heterojunctions.* Journal of Physics: Condensed Matter, 2007. **19**(40): p. 406205.
162. Córdova, R., et al., *Effect of anions on the nucleation and growth mechanism of polyaniline.* Journal of Electroanalytical Chemistry, 1994. **377**(1–2): p. 75-83.
163. Bhadra, S., et al., *Improvement of conductivity of electrochemically synthesized polyaniline.* Journal of Applied Polymer Science, 2008. **108**(1): p. 57-64.
164. Sengupta, P.P., P. Kar, and B. Adhikari, *Influence of dopant in the synthesis, characteristics and ammonia sensing behavior of processable polyaniline.* Thin Solid Films, 2009. **517**(13): p. 3770-3775.
165. Chatterjee, K., et al., *Morphology dependent ammonia sensing with 5-sulfosalicylic acid doped nanostructured polyaniline synthesized by several routes.* Sensors and Actuators B: Chemical, 2013. **181**(0): p. 544-550.
166. Izzuddin, I., et al. *Development of gas sensor system based on the TiO_2/Pani composite thin film*. in *Semiconductor Electronics, 2008. ICSE 2008. IEEE International Conference on*. 2008.
167. Khuspe, G.D., et al., *SnO2 nanoparticles-modified polyaniline films as highly selective, sensitive, reproducible and stable ammonia sensors.* Electronic Materials Letters, 2014. **10**(1): p. 191-197.
168. Khuspe, G.D., et al., *Ammonia gas sensing properties of CSA doped PANi-SnO_2 nanohybrid thin films.* Synthetic Metals, 2013. **185–186**(0): p. 1-8.
169. Talwar, V., O. Singh, and R.C. Singh, *ZnO assisted polyaniline nanofibers and its application as ammonia gas sensor.* Sensors and Actuators B: Chemical, 2014. **191**(0): p. 276-282.
170. Patil, S.L., et al., *Measurements on room temperature gas sensing properties of CSA doped polyaniline–ZnO nanocomposites.* Measurement, 2012. **45**(3): p. 243-249.
171. Pawar S. G., et al., *New Method for Fabrication of CSA Doped PANi-TiO_2 Thin-Film Ammonia Sensor.* Sensors Journal, IEEE, 2011. **11**(11): p. 2980-2985.
172. Pawar S. G., et al., *Room Temperature Ammonia Gas Sensor Based on Polyaniline-TiO_2 Nanocomposite.* Sensors Journal, IEEE, 2011. **11**(12): p. 3417-3423.

173. Gong Jian, et al., *Ultrasensitive NH3 Gas Sensor from Polyaniline Nanograin Enchased TiO2 Fibers.* The Journal of Physical Chemistry C, 2010. **114**(21): p. 9970-9974.
174. MacDiarmid, A.G., *Synthetic metals: a novel role for organic polymers.* Synthetic Metals, 2001. **125**(1): p. 11-22.
175. Kumar, D. and R.C. Sharma, *Advances in conductive polymers.* European Polymer Journal, 1998. **34**(8): p. 1053-1060.
176. Heeger, A.J., *Semiconducting and Metallic Polymers: The Fourth Generation of Polymeric Materials (Nobel Lecture).* Angewandte Chemie International Edition, 2001. **40**(14): p. 2591-2611.
177. Zuo, F., et al., *AC conductivity of emeraldine polymer.* Physical Review B, 1989. **39**(6): p. 3570.
178. Wolter, A., et al., *Model for aging in HCl-protonated polyaniline: structure, conductivity, and composition studies.* Physical Review B, 1998. **58**(12): p. 7637.
179. Luthra, V., et al., *Mechanism of dc conduction in polyaniline doped with sulfuric acid.* Current Applied Physics, 2003. **3**(2–3): p. 219-222.
180. Shimano, J.Y. and A.G. MacDiarmid, *Polyaniline, a dynamic block copolymer: key to attaining its intrinsic conductivity?* Synthetic Metals, 2001. **123**(2): p. 251-262.
181. Ivanov, V.F., et al., *Redox heterogeneity in polyaniline films: from molecular to macroscopic scale.* Synthetic Metals, 2005. **152**(1–3): p. 153-156.
182. Ivanov, V.F., O.L. Gribkova, and A.V. Vannikov, *Wide-range regulation of polyaniline conduction by interphase doping of a polyaniline film.* Russian Journal of Electrochemistry, 2006. **42**(3): p. 263-267.
183. Epstein, A.J., W.P. Lee, and V.N. Prigodin, *Low-dimensional variable range hopping in conducting polymers.* Synthetic Metals, 2001. **117**(1–3): p. 9-13.
184. Prigodin, V.N. and A.J. Epstein, *Nature of insulator–metal transition and novel mechanism of charge transport in the metallic state of highly doped electronic polymers.* Synthetic Metals, 2001. **125**(1): p. 43-53.
185. Travers, J.P., et al., *Is granularity the determining feature for electron transport in conducting polymers ?* Synthetic Metals, 1999. **101**(1–3): p. 359-362.
186. Ivanov, V.F., et al., *Multilevel redox heterogeneity in polyaniline films: from molecular to macroscopic scale.* Materials Science and Engineering: C, 2003. **23**(6–8): p. 953-957.
187. K. Arshak, E.M., G.M. Lyons, J. Harris, S. Clifford, *A review of gas sensors employed in electronic nose applications.* Sensor Review, 2004. **24**(2): p. 181-198.
188. Mikhaylov, S., et al., *Ammonia/amine electronic gas sensors based on hybrid polyaniline-TiO2 nanocomposites. The effects of titania and the surface active doping acid.* RSC Advances, 2015. **5**(26): p. 20218-20226.
189. H. T. Nagle, R. Gutierrez-Osuna, and S.S. Schiffman, *The how and why of electronic noses.* Spectrum, IEEE, 1998. **35**(9): p. 22-31.
190. Senadeera, G.K.R., et al., *Deposition of polyaniline via molecular self-assembly on TiO2 and its uses as a sensitiser in solid-state solar cells.* Journal of Photochemistry and Photobiology A: Chemistry, 2004. **164**(1–3): p. 61-66.
191. Kohtani, S., E. Yoshioka, and H. Miyabe, *Photocatalytic hydrogenation on semiconductor particles*. 2012: INTECH Open Access Publisher.
192. Sheng, H., L. Wenjun, and Z. Zhigang, *Band positions and photoelectrochemical properties of Cu 2 ZnSnS 4 thin films by the ultrasonic spray pyrolysis method.* Journal of Physics D: Applied Physics, 2013. **46**(23): p. 235108.
193. Memming, R., *Solar energy conversion by photoelectrochemical processes.* Electrochimica Acta, 1980. **25**(1): p. 77-88.
194. Gratzel, M., *Photoelectrochemical cells.* Nature, 2001. **414**(6861): p. 338-344.
195. Yoshida, T., et al., *Mechanism of cathodic electrodeposition of zinc oxide thin films from aqueous zinc nitrate baths.* Thin Solid Films, 2004. **451–452**: p. 166-169.

196. Izaki, M. and T. Omi, *Transparent zinc oxide films prepared by electrochemical reaction.* Applied Physics Letters, 1996. **68**(17): p. 2439-2440.
197. Ogurtsov, N.A., et al., *Deep Impact of the Template on Molecular Weight, Structure, and Oxidation State of the Formed Polyaniline.* The Journal of Physical Chemistry B, 2013. **117**(17): p. 5306-5314.
198. Bhadra, S., N.K. Singha, and D. Khastgir, *Electrochemical synthesis of polyaniline and its comparison with chemically synthesized polyaniline.* Journal of Applied Polymer Science, 2007. **104**(3): p. 1900-1904.
199. Trchová, M., J. Stejskal, and J. Prokeš, *Infrared spectroscopic study of solid-state protonation and oxidation of polyaniline.* Synthetic Metals, 1999. **101**(1–3): p. 840-841.
200. Wudl, F., et al., *Poly-p-phenyleneamineimine: synthesis and comparison to polyaniline.* Journal of the American Chemical Society, 1987. **109**(12): p. 3677-3684.
201. Epstein A. J., et al., *Spectroscopy and Photoexcitation Spectroscopies of Polyaniline: A Model System for New Phenomena*. 1991, Ft. Belvoir: Defense Technical Information Center.
202. Abdiryim, T., Z. Xiao-Gang, and R. Jamal, *Comparative studies of solid-state synthesized polyaniline doped with inorganic acids.* Materials Chemistry and Physics, 2005. **90**(2–3): p. 367-372.
203. Hatchett, D.W., M. Josowicz, and J. Janata, *Acid Doping of Polyaniline: Spectroscopic and Electrochemical Studies.* The Journal of Physical Chemistry B, 1999. **103**(50): p. 10992-10998.
204. Abell, L., et al., *Thermal studies of doped polyaniline.* Synthetic Metals, 1997. **84**(1–3): p. 127-128.
205. Wang, X.H., et al., *Thermal behaviors of doped polyaniline.* Synthetic Metals, 1995. **69**(1–3): p. 265-266.
206. Zhang, L., P. Liu, and Z. Su, *Preparation of PANI–TiO2 nanocomposites and their solid-phase photocatalytic degradation.* Polymer Degradation and Stability, 2006. **91**(9): p. 2213-2219.
207. Kang, E.T., K.G. Neoh, and K.L. Tan, *Polyaniline: A polymer with many interesting intrinsic redox states.* Progress in Polymer Science, 1998. **23**(2): p. 277-324.
208. Tzou, K. and R.V. Gregory, *Kinetic study of the chemical polymerization of aniline in aqueous solutions.* Synthetic Metals, 1992. **47**(3): p. 267-277.
209. Fu, Y. and R.L. Elsenbaumer, *Thermochemistry and Kinetics of Chemical Polymerization of Aniline Determined by Solution Calorimetry.* Chemistry of Materials, 1994. **6**(5): p. 671-677.
210. Bodalia, R.R. and R.S. Duran, *Polymerization of 2-pentadecylaniline monolayers at fluid surfaces: kinetics, thermodynamics, and mechanism.* Journal of the American Chemical Society, 1993. **115**(24): p. 11467-11474.
211. Gill, M.T., et al., *A study of the kinetics of polymerization of aniline using proton NMR spectroscopy.* Synthetic Metals, 1998. **93**(3): p. 227-233.
212. Chakraborty, M., D.C. Mukherjee, and B.M. Mandal, *Dispersion Polymerization of Aniline in Different Media: A UV−Visible Spectroscopic and Kinetic Study.* Langmuir, 2000. **16**(6): p. 2482-2488.
213. Sivakumar, C., et al., *Chemical Oxidative Polymerization and in situ Spectroelectrochemical Studies of a Sulfonated Aniline Derivative by UV−Visible Spectroscopy.* Industrial & Engineering Chemistry Research, 2001. **40**(1): p. 40-51.
214. Ayad, M.M., et al., *The kinetics and spectral studies of the in situ polyaniline film formation.* Journal of Colloid and Interface Science, 2003. **263**(1): p. 196-201.
215. Ogurtsov, N.A., Y.V. Noskov, and A.A. Pud, *Effect of Multiwalled Carbon Nanotubes on the Kinetics of the Aniline Polymerization: The Semi-Quantitative OCP Approach.* The Journal of Physical Chemistry B, 2015. **119**(15): p. 5055-5061.

216. Mattoso, L.H.C., et al., *Synthesis of polyaniline/polytoluidine block copolymer via the pernigraniline oxidation state.* Polymer International, 1994. **35**(1): p. 89-93.
217. Kolla, H.S., et al., *Absolute Molecular Weight of Polyaniline.* Journal of the American Chemical Society, 2005. **127**(48): p. 16770-16771.
218. Mattoso, L.H.C., et al., *Studies on the chemical syntheses and on the characteristics of polyaniline derivatives.* Journal of Polymer Science Part A: Polymer Chemistry, 1995. **33**(8): p. 1227-1234.
219. Wei, Y., Y. Sun, and X. Tang, *Autoacceleration and kinetics of electrochemical polymerization of aniline.* The Journal of Physical Chemistry, 1989. **93**(12): p. 4878-4881.
220. Noskov, Y., et al., *Acid-dopant effects in the formation and properties of polycarbonate-polyaniline composites.* Synthetic Metals, 2016. **217**: p. 266-275.
221. Lüning, U., *Acid—Base Behaviour in Macrocycles and Other Concave Structures*, in *Advances in Physical Organic Chemistry*, D. Bethell, Editor. 1995, Academic Press. p. 63-116.
222. Guthrie, J.P., *Hydrolysis of esters of oxy acids: pKa values for strong acids; Brønsted relationship for attack of water at methyl; free energies of hydrolysis of esters of oxy acids; and a linear relationship between free energy of hydrolysis and pKa holding over a range of 20 pK units.* Canadian Journal of Chemistry, 1978. **56**(17): p. 2342-2354.
223. Clark, M.D., S. Subramanian, and R. Krishnamoorti, *Understanding surfactant aided aqueous dispersion of multi-walled carbon nanotubes.* Journal of Colloid and Interface Science, 2011. **354**(1): p. 144-151.
224. Namani, T. and P. Walde, *From Decanoate Micelles to Decanoic Acid/Dodecylbenzenesulfonate Vesicles.* Langmuir, 2005. **21**(14): p. 6210-6219.
225. Kohut-Svelko, N., S. Reynaud, and J. François, *Synthesis and characterization of polyaniline prepared in the presence of nonionic surfactants in an aqueous dispersion.* Synthetic Metals, 2005. **150**(2): p. 107-114.
226. Holmberg, K., et al., *Surfactants and polymers in aqueous solution*. Hardcover ed. 2002: Wiley.
227. Samuelson, L., S. Tripathy, and F. Bruno, *Enzymatic polymerization of anilines or phenols around a template. vol US 6.569. 651 B1.* The United States of America as represented by the secretary of the army, lowell, Massachusetts, 2003.
228. Xu, J., et al., *Hierarchical Nanocomposites of Polyaniline Nanowire Arrays on Graphene Oxide Sheets with Synergistic Effect for Energy Storage.* ACS Nano, 2010. **4**(9): p. 5019-5026.
229. Wang, A.-L., et al., *Design of Pd/PANI/Pd Sandwich-Structured Nanotube Array Catalysts with Special Shape Effects and Synergistic Effects for Ethanol Electrooxidation.* Journal of the American Chemical Society, 2013. **135**(29): p. 10703-10709.
230. Zhang, H., et al., *Dramatic Visible Photocatalytic Degradation Performances Due to Synergetic Effect of TiO2 with PANI.* Environmental Science & Technology, 2008. **42**(10): p. 3803-3807.
231. Raza, M., et al., *Interaction and UV-Stability of Various Organic Capping Agents on the Surface of Anatase Nanoparticles.* Materials, 2014. **7**(4): p. 2890-2912.
232. Bremer, L.G.B., et al., *Preparation of core-shell dispersions with a low tg polymer core and a polyaniline shell.* Synthetic Metals, 1997. **84**(1–3): p. 355-356.
233. Schaub, R., et al., *Oxygen vacancies as active sites for water dissociation on rutile TiO 2 (110).* Physical Review Letters, 2001. **87**(26): p. 266104.
234. Ramis, G., et al., *Fourier transform infrared study of the adsorption and coadsorption of nitric oxide, nitrogen dioxide and ammonia on TiO2 anatase.* Applied Catalysis, 1990. **64**: p. 243-257.
235. Primet, M., P. Pichat, and M.V. Mathieu, *Infrared study of the surface of titanium dioxides. I. Hydroxyl groups.* The Journal of Physical Chemistry, 1971. **75**(9): p. 1216-1220.

236. Mathieu, M.V., M. Primet, and P. Pichat, *Infrared study of the surface of titanium dioxides. II. Acidic and basic properties.* The Journal of Physical Chemistry, 1971. **75**(9): p. 1221-1226.
237. Xu, J.-C., W.-M. Liu, and H.-L. Li, *Titanium dioxide doped polyaniline.* Materials Science and Engineering: C, 2005. **25**(4): p. 444-447.
238. Yang, R.T., W.B. Li, and N. Chen, *Reversible chemisorption of nitric oxide in the presence of oxygen on titania and titania modified with surface sulfate.* Applied Catalysis A: General, 1998. **169**(2): p. 215-225.
239. Guerrero, G., P.H. Mutin, and A. Vioux, *Anchoring of Phosphonate and Phosphinate Coupling Molecules on Titania Particles.* Chemistry of Materials, 2001. **13**(11): p. 4367-4373.
240. Dobson, K.D. and A.J. McQuillan, *In situ infrared spectroscopic analysis of the adsorption of aromatic carboxylic acids to TiO2, ZrO2, Al2O3, and Ta2O5 from aqueous solutions.* Spectrochimica Acta Part A: Molecular and Biomolecular Spectroscopy, 2000. **56**(3): p. 557-565.
241. Dobson, K.D. and A.J. McQuillan, *In situ infrared spectroscopic analysis of the adsorption of aliphatic carboxylic acids to TiO2, ZrO2, Al2O3, and Ta2O5 from aqueous solutions.* Spectrochimica Acta Part A: Molecular and Biomolecular Spectroscopy, 1999. **55**(7–8): p. 1395-1405.
242. Milton, A.J. and A.P. Monkman, *A comparative study of polyaniline films using thermal analyses and IR spectroscopy.* Journal of Physics D: Applied Physics, 1993. **26**(9): p. 1468.
243. Wei, Y., R. Hariharan, and S.A. Patel, *Chemical and electrochemical copolymerization of aniline with alkyl ring-substituted anilines.* Macromolecules, 1990. **23**(3): p. 758-764.
244. Geniès, E.M. and P. Noël, *Study of polyanilines and substituted polyanilines molecular weights by gel permeation chromatography.* Synthetic Metals, 1992. **46**(3): p. 285-292.
245. Tang, X., Y. Sun, and Y. Wei, *Molecular weight of chemically polymerized polyaniline.* Die Makromolekulare Chemie, Rapid Communications, 1988. **9**(12): p. 829-834.
246. Huang, J. and R.B. Kaner, *A General Chemical Route to Polyaniline Nanofibers.* Journal of the American Chemical Society, 2004. **126**(3): p. 851-855.
247. Stejskal, J., et al., *The genesis of polyaniline nanotubes.* Polymer, 2006. **47**(25): p. 8253-8262.
248. Li, X., et al., *Surface modification of titanium dioxide nanoparticles by polyaniline via an in situ method.* Journal of Chemical Technology & Biotechnology, 2008. **83**(11): p. 1558-1564.
249. Sun, Y., et al., *Preparation and electromagnetic wave absorption properties of core-shell structured Fe3O4-polyaniline nanoparticles.* RSC Advances, 2013. **3**(44): p. 22554-22559.
250. Watanabe, A., et al., *Polyanilines prepared by electrochemical polymerization: Molecular weight of polyaniline films.* Journal of Polymer Science Part A: Polymer Chemistry, 1989. **27**(13): p. 4431-4437.
251. Pouget J. P., et al., *X-ray structure of polyaniline.* Macromolecules, 1991. **24**(3): p. 779-789.
252. Privalko, V.P., et al., *Structure/Property Relationships for Poly(Vinylidene Fluoride)/Doped Polyaniline Blends.* Journal of Macromolecular Science, Part B, 2005. **44**(5): p. 749-759.
253. Olinga, T.E., et al., *Highly Conducting and Solution-Processable Polyaniline Obtained via Protonation with a New Sulfonic Acid Containing Plasticizing Functional Groups.* Macromolecules, 2000. **33**(6): p. 2107-2113.
254. Li, D. and R.B. Kaner, *Shape and Aggregation Control of Nanoparticles: Not Shaken, Not Stirred.* Journal of the American Chemical Society, 2006. **128**(3): p. 968-975.
255. Ping, Z., *In situ FTIR-attenuated total reflection spectroscopic investigations on the base-acid transitions of polyaniline. Base-acid transition in the emeraldine form of polyaniline.* Journal of the Chemical Society, Faraday Transactions, 1996. **92**(17): p. 3063-3067.
256. Neoh, K.G., et al., *Polyaniline treated with organic acids: doping characteristics and stability.* Synthetic Metals, 1995. **73**(3): p. 209-215.

257. Macdiarmid, A.G., et al., *Proceedings of the International Conference of Science and Technology of Synthetic Metals Polyaniline: a new concept in conducting polymers.* Synthetic Metals, 1987. **18**(1): p. 285-290.
258. Lin, Y.-C., F.-H. Hsu, and T.-M. Wu, *Enhanced conductivity and thermal stability of conductive polyaniline/graphene composite synthesized by in situ chemical oxidation polymerization with sodium dodecyl sulfate.* Synthetic Metals, 2013. **184**(0): p. 29-34.
259. Macdiarmid, A.G., et al., *Polyaniline: a new concept in conducting polymers.* Synthetic Metals, 1987. **18**(1–3): p. 285-290.
260. Wan, M., *Absorption spectra of thin film of polyaniline.* Journal of Polymer Science Part A: Polymer Chemistry, 1992. **30**(4): p. 543-549.
261. Wei, Y., K.F. Hsueh, and G.W. Jang, *A study of leucoemeraldine and effect of redox reactions on molecular weight of chemically prepared polyaniline.* Macromolecules, 1994. **27**(2): p. 518-525.
262. Liu, L. and X. Chen, *Titanium Dioxide Nanomaterials: Self-Structural Modifications.* Chemical Reviews, 2014. **114**(19): p. 9890-9918.
263. Yang, C.Y., et al., *Electron diffraction studies of the structure of polyaniline-dodecylbenzenesulfonate.* Polymer, 1994. **35**(6): p. 1142-1147.
264. Aharony, A. and D. Stauffer, *Introduction to percolation theory*. 2003: Taylor & Francis.
265. Brook, I., et al., *A novel approach for preparation of conductive hybrid elastomeric nano-composites.* Polymers for Advanced Technologies, 2013. **24**(8): p. 758-763.
266. Han, M.G. and S.S. Im, *Electrical and structural analysis of conductive polyaniline / polyimide blends.* Journal of Applied Polymer Science, 1999. **71**(13): p. 2169-2178.
267. Cooper, E.C. and B. Vincent, *Electrically conducting organic films and beads based on conducting latex particles.* Journal of Physics D: Applied Physics, 1989. **22**(11): p. 1580.
268. Beadle, P., et al., *Electrically conductive polyaniline-copolymer latex composites.* Macromolecules, 1992. **25**(9): p. 2526-2530.
269. Zallen, R., *The percolation model.* The Physics of Amorphous Solids, 1983: p. 135-204.
270. Pohanish, R.P. and S.A. Greene, *Wiley guide to chemical incompatibilities*. 2009: John Wiley & Sons.
271. Šeděnková, I., M. Trchová, and J. Stejskal, *Thermal degradation of polyaniline films prepared in solutions of strong and weak acids and in water – FTIR and Raman spectroscopic studies.* Polymer Degradation and Stability, 2008. **93**(12): p. 2147-2157.
272. Trchová, M., et al., *Structural and conductivity changes during the pyrolysis of polyaniline base.* Polymer Degradation and Stability, 2006. **91**(1): p. 114-121.
273. Shaheen, S.E., et al., *2.5% efficient organic plastic solar cells.* Applied Physics Letters, 2001. **78**(6): p. 841-843.
274. Min, S., F. Wang, and Y. Han, *An investigation on synthesis and photocatalytic activity of polyaniline sensitized nanocrystalline TiO2 composites.* Journal of Materials Science, 2007. **42**(24): p. 9966-9972.
275. Hurum, D.C., et al., *Explaining the Enhanced Photocatalytic Activity of Degussa P25 Mixed-Phase TiO2 Using EPR.* The Journal of Physical Chemistry B, 2003. **107**(19): p. 4545-4549.
276. Li, S.-C. and U. Diebold, *Reactivity of TiO2 Rutile and Anatase Surfaces toward Nitroaromatics.* Journal of the American Chemical Society, 2010. **132**(1): p. 64-66.
277. Uddin, M.T., et al., *Nanostructured SnO2–ZnO Heterojunction Photocatalysts Showing Enhanced Photocatalytic Activity for the Degradation of Organic Dyes.* Inorganic Chemistry, 2012. **51**(14): p. 7764-7773.
278. Zheng, L., et al., *Network Structured SnO2/ZnO Heterojunction Nanocatalyst with High Photocatalytic Activity.* Inorganic Chemistry, 2009. **48**(5): p. 1819-1825.
279. Geniès, E.M., et al., *Polyaniline: A historical survey.* Synthetic Metals, 1990. **36**(2): p. 139-182.

280. Albuquerque, J.E., et al., *A simple method to estimate the oxidation state of polyanilines.* Synthetic Metals, 2000. **113**(1–2): p. 19-22.

281. Cao, Y., et al., *Solution‐cast films of polyaniline: Optical‐quality transparent electrodes.* Applied Physics Letters, 1992. **60**(22): p. 2711-2713.

282. Beena Unni, A., et al., *Solvent Assisted Rinsing: Stability/Instability of Ultrathin Polymer Residual Layer.* Macromolecules, 2016. **49**(5): p. 1807-1815.

283. Ikkala, O.T., et al., *On the molecular recognition and associations between electrically conducting polyaniline and solvents.* The Journal of Chemical Physics, 1995. **103**(22): p. 9855-9863.

284. Trznadel, M. and P. Rannou, *Effect of solvent-dopant competition on the conductivity of polyaniline films.* Synthetic Metals, 1999. **101**(1–3): p. 842.

285. Kebiche, H., et al., *Relationship between ammonia sensing properties of polyaniline nanostructures and their deposition and synthesis methods.* Analytica Chimica Acta, 2012. **737**(0): p. 64-71.

286. Österholm, J.E., et al., *Proceedings of the International Conference on Science and Technology of Synthetic Metals Emulsion polymerization of aniline.* Synthetic Metals, 1993. **55**(2): p. 1034-1039.

287. Zheng, W.-Y., et al., *Self-assembly of the electroactive complexes of polyaniline and surfactant.* Macromolecular Chemistry and Physics, 1995. **196**(8): p. 2443-2462.

288. Kunzo, P., et al., *Nanocomposites of polyaniline and titania nanoparticles for gas sensors.* physica status solidi (a), 2013. **210**(11): p. 2341-2347.

289. Khuspe, G.D., et al., *Fussy nanofibrous network of polyaniline (PANi) for NH3 detection.* Synthetic Metals, 2012. **162**(21–22): p. 1822-1827.

290. Kumar, J., et al., *Highly Sensitive Chemo-Resistive Ammonia Sensor Based on Dodecyl Benzene Sulfonic Acid Doped Polyaniline Thin Film.* Science of Advanced Materials, 2015. **7**(3): p. 518-525.

291. Rizzo, G., et al., *Flexible, all-organic ammonia sensor based on dodecylbenzene sulfonic acid-doped polyaniline films.* Thin Solid Films, 2010. **518**(23): p. 7133-7137.

292. Harsányi, G., *Polymer films in sensor applications: a review of present uses and future possibilities.* Sensor Review, 2000. **20**(2): p. 98-105.

293. McGovern, S.T., G.M. Spinks, and G.G. Wallace, *Micro-humidity sensors based on a processable polyaniline blend.* Sensors and Actuators B: Chemical, 2005. **107**(2): p. 657-665.

294. Nohria, R., et al., *Humidity sensor based on ultrathin polyaniline film deposited using layer-by-layer nano-assembly.* Sensors and Actuators B: Chemical, 2006. **114**(1): p. 218-222.

295. Zeng, F.-W., et al., *Humidity sensors based on polyaniline nanofibres.* Sensors and Actuators B: Chemical, 2010. **143**(2): p. 530-534.

296. Jain, S., et al., *Humidity sensing with weak acid-doped polyaniline and its composites.* Sensors and Actuators B: Chemical, 2003. **96**(1–2): p. 124-129.

297. Danesh, E., et al., *Development of a New Generation of Ammonia Sensors on Printed Polymeric Hotplates.* Analytical Chemistry, 2014. **86**(18): p. 8951-8958.

298. Yang, Z., et al., *Proton conductivity of acid-doped meta-polyaniline.* Journal of Membrane Science, 2008. **313**(1–2): p. 86-90.

299. Hangarter, C.M., et al., *Conducting polymer nanowires for chemiresistive and FET-based bio/chemical sensors.* Journal of Materials Chemistry, 2010. **20**(16): p. 3131-3140.

300. Virji, S., et al., *Polyaniline Nanofiber Gas Sensors: Examination of Response Mechanisms.* Nano Letters, 2004. **4**(3): p. 491-496.

301. Parvatikar, N., et al., *Electrical and humidity sensing properties of polyaniline/WO3 composites.* Sensors and Actuators B: Chemical, 2006. **114**(2): p. 599-603.

302. Tai, H., et al., *Preparation, Characterization and Comparative NH3-sensing Characteristic Studies of PANI/inorganic Oxides Nanocomposite Thin Films.* Journal of Materials Science & Technology, 2010. **26**(7): p. 605-613.

303. Prokeš, J., et al., *Enhanced stability of polyaniline/inorganic salt composites during temperature cycling.* Polymer Degradation and Stability, 2000. **68**(2): p. 261-269.
304. Prokeš, J., et al., *Conductivity ageing in temperature-cycled polyaniline.* Polymer Degradation and Stability, 2002. **78**(2): p. 393-401.
305. Banica, F.-G., *Chemical Sensors and Biosensors: Fundamentals and Applications*. 2012: John Wiley & Sons.
306. Scandurra, G., et al. *Detection of ammonia at ppm levels using titanium dioxide/polyaniline films deposited on plastic sheets*. in *Instrumentation and Measurement Technology Conference (I2MTC), 2012 IEEE International*. 2012.
307. Tai, H., et al., *Fabrication and gas sensitivity of polyaniline–titanium dioxide nanocomposite thin film.* Sensors and Actuators B: Chemical, 2007. **125**(2): p. 644-650.
308. Wang, L., et al., *Enhanced Sensitivity and Stability of Room-Temperature NH3 Sensors Using Core–Shell CeO2 Nanoparticles@Cross-linked PANI with p–n Heterojunctions.* ACS Applied Materials & Interfaces, 2014. **6**(16): p. 14131-14140.
309. Lin, Q., Y. Li, and M. Yang, *Gas sensing properties of layer-by-layer self-assembled ultrathin film of polyaniline/titanium dioxide.* Synthetic Metals, 2012. **162**(24): p. 2242-2249.
310. Joubert, M., et al., *Conducting polyaniline composite: From syntheses in waterborne systems to chemical sensor devices.* Polymer, 2010. **51**(8): p. 1716-1722.
311. Duboriz, I. and A. Pud, *Polyaniline/poly(ethylene terephthalate) film as a new optical sensing material.* Sensors and Actuators B: Chemical, 2014. **190**(0): p. 398-407.
312. Ogurtsov, N.A., et al., *Evolution and Interdependence of Structure and Properties of Nanocomposites of Multiwall Carbon Nanotubes with Polyaniline.* The Journal of Physical Chemistry C, 2016. **120**(1): p. 230-242.
313. Wang, J., et al., *Electrochemically Fabricated Polyaniline Nanoframework Electrode Junctions that Function as Resistive Sensors.* Nano Letters, 2004. **4**(9): p. 1693-1697.
314. Kharat, H.J., et al., *Synthesis of polypyrrole films for the development of ammonia sensor.* Polymers for Advanced Technologies, 2007. **18**(5): p. 397-402.
315. Lähdesmäki, I., A. Lewenstam, and A. Ivaska, *A polypyrrole-based amperometric ammonia sensor.* Talanta, 1996. **43**(1): p. 125-134.
316. Zhang, J., et al., *Polypyrrole-Coated SnO2 Hollow Spheres and Their Application for Ammonia Sensor.* The Journal of Physical Chemistry C, 2009. **113**(5): p. 1662-1665.
317. Patois, T., et al., *Ammonia gas sensors based on polypyrrole films: Influence of electrodeposition parameters.* Sensors and Actuators B: Chemical, 2012. **171–172**: p. 431-439.
318. Patois, T., et al., *Elaboration of ammonia gas sensors based on electrodeposited polypyrrole—Cobalt phthalocyanine hybrid films.* Talanta, 2013. **117**: p. 45-54.
319. Xiang, C., et al., *Ammonia sensor based on polypyrrole–graphene nanocomposite decorated with titania nanoparticles.* Ceramics International, 2015. **41**(5, Part A): p. 6432-6438.
320. Kwon, O.S., et al., *Highly sensitive and selective chemiresistive sensors based on multidimensional polypyrrole nanotubes.* Chemical Communications, 2012. **48**(85): p. 10526-10528.

ABSTRACT

The thesis is devoted to the synthesis and investigation of properties of inorganic-organic polyaniline (PANI) and polypyrrole (PPy) based hybrid materials with TiO_2 (rutile and anatase) and SnO_2 nanoparticles applicable for ammonia and amines detection. The direct polymer growth on the surface of nanoparticles allowed obtaining of nanocomposite materials with a “core-shell” structure which differs from simple mechanical mixture by more uniform polymer distribution and stronger interaction between source components.

The object of research is the process of formation of polyaniline and polypyrrole nanocomposites with metal oxides. The research goal is to reveal formation peculiarities and properties of nanostructured composite materials based on conducting polymers and metal oxides nanoparticles that are sensitive to ammonia and amines. Research methods include RedOx and pH monitoring, FTIR and UV-spectroscopy, SEM, TEM, thermogravimetry, liquid chromatography, conductivity measurements and sensor tests.

The new approach to study kinetics of aniline polymerization process by simultaneous RedOx and pH monitoring of reaction medium was proposed. For the first time the influence of sulfonic acids and metal oxides on the aniline polymerization process and molecular characteristics of the obtained polymer was shown. For the first time a linear correlation between the nanoparticles content and reciprocal duration of separate stages of polymerization was shown. Formed "core-shell" nanocomposites have sensitivity to ammonia and amines of about 2 times higher than the pure polymer. Developed new materials can be used in the manufacturing of chemoresistive sensors' active layers.

Keywords: polyaniline, polypyrrole, nanocomposites, dispersing solvent, sensor, ammonia, amines.

RÉSUMÉ

La thèse est consacrée à la synthèse et à l’étude des propriétés des matériaux hybrides inorganique-organique à base de polyaniline (PANI) et de polypyrrole (PPy) avec des nanoparticules TiO_2 (rutile et anatase) et SnO_2 applicables à détection l'ammoniac et aux amines. La croissance directe du polymère sur la surface des nanoparticules a permis l’obtention de matériaux nanocomposites avec une structure “core-shell” qui diffère du mélange mécanique simple par une distribution plus uniforme des polymères et une interaction plus forte entre les composants source.

L’objet de la recherche est le processus de formation de nanocomposites de polyaniline et de polypyrrole avec des oxydes métalliques. L’objectif de la recherche est de révéler les particularités de la formation et les propriétés des matériaux composites nanostructurés à base de polymères conducteurs et nanoparticules d’oxydes métalliques sensibles à l’ammoniac et aux amines. Les méthodes de recherche incluent le RedOx et la surveillance du pH, FTIR et UV-spectroscopie, SEM, TEM, thermogravimétrie, chromatographie liquide, mesures de conductivité et tests de capteurs.

La nouvelle approche d’étude de la cinétique du processus de polymérisation de l'aniline par la surveillance simultané du RedOx et du pH du milieu réactionnel a été proposée. Pour la première fois, on a montré l’influence des acides sulfoniques et des oxydes métalliques sur le procédé de polymérisation de l’aniline et les caractéristiques moléculaires du polymère obtenu. En outre, une corrélation linéaire entre le contenu en nanoparticules et la durée réciproque des stades séparés de la polymérisation a été démontrée. Les nanocomposites “core-shell” formés ont une sensibilité à l’ammoniac et aux amines environ 2 fois supérieure à celle du polymère pur. Les nouveaux matériaux développés peuvent être utilisés dans la fabrication de couches actives des capteurs chimiorésistifs.

Mots-clés: polyaniline, polypyrrole, nanocomposites, solvant de dispersion, capteur, ammoniac, amines.